Tracking Structural Changes in the Spinal Cord and Brain as Biomarkers for Interventions after Spinal Cord Injury

Dissertation

zur

Erlangung der naturwissenschaftlichen Doktorwürde

(Dr. sc. nat.)

vorgelegt der

Mathematisch-naturwissenschaftlichen Fakultät

der

Universität Zürich

von

Eveline Huber

von

Zürich ZH

Promotionskommission

Prof. Dr. Dominik Bach (Vorsitz)

Prof. Dr. Armin Curt (Leitung der Dissertation)

Dr. Patrick Freund (Leitung der Dissertation)

Prof. Dr. Martin Schwab

Prof. Dr. Bogdan Draganski

Zürich, 2018

Table of content

Summary

Traumatic spinal cord injury (SCI) imposes major life changes affecting mostly the young and is more prevalent in men than in women. Worldwide, about 170'000 new cases occur annually. The majority of patients are left with profound and persistent functional impairments such as paralysis, sensory deficiencies, chronic pain, and bladder and bowel problems. At the injury site, the primary impact leads to tissue destruction including damage of blood vessels, neurons and glial cells, and disruption of axons. This creates an excitotoxic environment in the penumbra, which sets adjacent, non-injured cells, including neurons, at risk. A complex secondary cascade follows where astrocytes form a persistent dense scar to separate, and therefore also protect, the intact neurons from the toxic environment of the injury site. This physical barrier, together with the limited regenerative capability of injured axons, is one of the main reasons for the limited degree of recovery following SCI.

Experimental evidence suggests that these processes can be influenced by the application of targeted drugs. Therefore, several clinical trials have been undertaken during the last years. Although no standard treatment evolved worldwide from these trials, they have improved our understanding of the difficulties faced in such trials. In particular, they struggle in adequately identifying treatment effects vs. spontaneous improvements. This might be partly due to our current clinical assessments, which lack sensitivity to minimal changes in sensorimotor functions, making reliable stratification of homogenous sub-groups and prediction of outcome still challenging. To enable efficient translation from bench to bedside, these interventions require biomarkers that can be used as surrogate makers to early test safety and efficacy of new drugs applied within clinical trials.

Such biomarkers need to be able to capture biological processes of recovery like neuronal and myelin repair. Today, structural magnetic resonance imaging (MRI) is one of the few tools able to capture such structural changes *in-vivo* and might therefore be a promising method to close this knowledge gap. As a first step towards the development of neuroimaging biomarkers, recent studies have focused on characterizing spontaneous trauma-induced structural changes after SCI in the spinal cord and brain. At the spinal cord level, remote cervical atrophy of up to 30% was evident in chronic SCI patients. Supraspinally, degeneration and reorganization was present within the sensorimotor and limbic system. In this thesis, the main aim was to further improve our understanding of trauma-induced structural changes by applying conventional and advanced MRI protocols. This enabled us to quantitatively analyze changes at different levels of the neuraxis (at and above the level of injury). Further, this thesis explores the relationships between quantitative MRI readouts, and electrophysiological and functional outcome.

In the first study, we investigated the spatial and temporal evolution of the lesion and adjacent tissue bridges after SCI using a clinically established imaging protocol. At 1-month post injury, the lesion was well demarcated and allowed reliable identification of midsagittal lesion extent and tissue bridges. The lesion width decreased within the first year after injury, suggesting removal of axonal and myelin debris. In contrast, the size of total tissue bridges remained stable within the first year after injury, and these tissue bridges were transmissible for electrophysiological information flow. Importantly, the size of tissue bridges and the extent of damage are predictive of outcome at 1 year follow-up.

Next we moved on to explore underlying tissue-specific structural, microstructural and molecular changes within areas of cervical atrophy occurring in chronic SCI patients.

In the second study, we investigated whether grey matter pathology, alongside white matter changes, also contributes to clinical impairment. We therefore took advantage of recent improvements in diffusion-weighted imaging and spinal anatomical MRI sequences with higher in-plane resolution. Besides white matter atrophy and evidence for neurodegeneration and demyelination within the major sensorimotor tracts, we found marked atrophy within ventral and dorsal horns which related to lesion severity. Tissue-specific neurodegeneration was associated with appropriate clinical and neurophysiological impairment. Next to antero- and retrograde degeneration of sensorimotor tracts, this study provides evidence that neuronal circuits within the spinal cord undergo trans-synaptic neurodegeneration, leading to grey matter changes above the level of injury.

In the third study, we identified underlying molecular changes in areas of cervical atrophy by using a novel spinal magnetic resonance spectroscopy protocol. This study showed lesion level dependent metabolic alterations related to chronic neuroinflammation, neurodegeneration and demyelination above the level of injury. Lesion severity was driving the amount of metabolic changes relating to neuroinflammation. Greater signs of neuroinflammation were associated with more cervical atrophy and greater clinical impairment. Our data suggest that the SCI results in chronic neuroinflammation, in addition to ongoing neurodegeneration and demyelination, which might drive or contribute to cervical atrophy.

In the fourth and last study in this thesis, we investigated the temporal and spatial evolution of the extrapyramidal system after SCI. We analyzed surface area changes as well as underlying microstructural changes within the thalamus, striatum and globus pallidus. Whereas recent neuroimaging studies focused on changes within the sensorimotor and limbic system after SCI, the involvement of basal ganglia structures in recovery from a SCI has been suggested by animal studies. We revealed that within the first 2 years after SCI, patients showed contractions of surface area in the motor thalamus within regions representing lower limbs, within the pulvinar and the striatum

compared to controls. In addition, surface area expansions were evident in the sensorimotor thalamus within regions that represent the upper limbs, and in the striatum. In parallel, microstructural parameters also changed over time, suggesting degeneration, demyelination and probably inflammation in the sensorimotor thalamus, striatum and globus pallidus. At 1 month post injury, increased surface area changes within the motor striatum predicted lower extremity motor score at 2-year follow-up and increased signs of iron accumulation within the pulvinar nuclei were predictive of 2-year pin-prick score. This study provides evidence for progressive basal ganglia changes after SCI related to clinical readouts.

In conclusion, this thesis expands previous knowledge and shows transneuronal reorganization of primarily unaffected spinal and brain regions after SCI, in addition to degenerative changes occurring at the lesion site and in directly injured white matter tracts above the level of injury. Moreover next to degeneration and demyelination, the findings within this thesis indicate that chronic neuroinflammation might be present after SCI. This biological response might relate or contribute to degenerative changes within the central nervous system, and therefore is also possibly associated to clinical outcome. Thus, quantitatively analyzed conventional as well as innovative new multimodal MRI protocols allow for the quantification of trauma-induced spinal and supraspinal changes and might serve as biomarkers to assess the efficacy of new treatment interventions. Towards this goal, next steps involve the combination of structural and functional MRI in longitudinal multicenter assessments in acute SCI to simultaneously measure spinal and supraspinal changes and their impact on reorganization as SCI patients recover. This will not only increase our understanding of the temporal sequence of structural changes and their relationship to each other, but allow the identification of the most sensitive biomarkers for different experimental approaches focusing on the treatment of SCI patients.

Zusammenfassung

Eine traumatische Rückenmarksverletzung verändert das Leben der Betroffenen nachhaltig. Jedes Jahr treten weltweit ungefähr 23 neue Fälle pro Million Einwohner auf. Insgesamt handelt es sich also um jährlich mehr als 170'000 Fälle, was die grosse Bedeutung dieses Themas hervorhebt. In den meisten Fällen verbleiben die Patienten mit tiefgreifenden und persistierenden Einschränkungen wie motorischen Dysfunktionen, sensorischen Störungen, chronischen Schmerzen und Blasen- und Darmprobleme. Die primäre Verletzung im Rückenmark führt zum Untergang des betroffenen Gewebes, zur Unterbrechung von Axonen und zur Schädigung von Blutgefässen und Gliazellen. Dadurch entsteht eine toxische Umgebung für die angrenzenden, nicht verletzten Zellen in der Penumbra, welche dadurch sekundär auch zu Schaden kommen können. Um das zu verhindern, setzt eine komplexe, sekundäre Kaskade ein, in der Astrozyten aktiviert werden und eine dichte, bleibende Barriere bilden, um so die intakten Neuronen vor der toxischen Umgebung der primären Verletzung zu schützen. Zusammen mit der begrenzten Regenerationsfähigkeit von verletzten Neuronen ist diese physische Barriere eine der Hauptgründe für die limitierte Erholung von rückenmarksverletzten Patienten.

Tierstudien haben gezeigt, dass die limitierte Erholung mittels der Anwendung von Wirkstoffen beeinflusst werden kann, was zur Realisierung von verschiedenen klinischen Studien an Menschen geführt hat. Obwohl keine dieser Studien in neue Behandlungsstandards von rückenmarksverletzten Patienten resultierte, haben wir viel über die Planung und Durchführung solcher Studien gelernt. Eines der Hauptprobleme bleibt jedoch bestehen – nämlich die adäquate Identifizierung von Behandlungseffekten im Unterschied zu spontaner Erholung. Ein Grund dafür ist, dass unsere momentanen klinischen Messungen nicht sensitiv genug sind, um minimale Verbesserungen in sensomotorischen Funktionen zu erfassen. Dies macht die zuverlässige Stratifizierung von homogenen Subgruppen innerhalb von klinischen Studien und die Vorhersage von funktionellen Verbesserungen zu einer echten Herausforderung. Um einen effizienten Transfer von präklinischen zu klinischen Studien zu ermöglichen, sind Biomarker notwendig, welche als Surrogatmarker benutzt werden können, um Sicherheit und Wirksamkeit von neuen Medikamenten innerhalb klinischen Studien zu testen.

Solche Biomarker müssen im Stande sein, biologische Prozesse der Erholung zu erfassen, wie zum Beispiel Reymelinisierung oder neuronale Plastizität. Heutzutage ist Magnetresonanztomographie (MRT) eine der wenigen nicht-invaisven Methoden, welche in-vivo strukturelle Änderungen des Zentralnervensystems darstellen kann. Dies macht MRT zu einer vielversprechenden Technik, um als Biomarker dienen zu können. Um solche MRT Biomarker zu entwickeln, haben verschiedene Studien in einem ersten Schritt versucht, spontan auftretende strukturelle Änderungen im Rückenmark und

Hirn zu charakterisieren. Diese Studien haben gezeigt, dass eine Rückenmarksverletzung oberhalb der Läsion zu zervikaler Atrophie von bis zu 30% führt und dass degenerative und reorganisierende Prozesse im Hirn, vor allem innerhalb des sensomotorischen und limbischen Systems, auftreten. Ziel dieser Dissertation war es deshalb, unser Verständnis von trauma-induzierten, strukturellen Änderungen auf verschiedenen Ebenen der Neuroachse, das heisst auf und oberhalb der Läsion, besser zu verstehen. Dabei haben wir sowohl klinische MRT-Sequenzen als auch weiterentwickelte, hochmoderne Sequenzen und Post-Processing-Methoden verwendet, um Veränderungen quantitativ analysieren zu können. Ein weiteres Ziel dieser Arbeit umfasste ein besseres Verständnis von Zusammenhängen zwischen solchen quantitativen MRT Parametern und klinischer Erholung, um die bestehende Prognostik zu verbessern.

Innerhalb der ersten Studie haben wir die zeitliche und räumliche Entwicklung der Läsion sowie der angrenzenden Gewebebrücken mittels konventionellen MRT-Sequenzen charakterisiert. Nach einem Monat nach der Verletzung war die Läsion gut genug abgegrenzt, so dass eine zuverlässige Identifizierung des Läsionsausmasses und der Grösse von midsagittalen Gewebebrücken gemacht werden konnte. Die Läsionsbreite nahm innerhalb des ersten Jahres ab, was für eine Beseitigung von Axon- und Myelin-Fragmenten innerhalb der Läsion spricht. Die Gewebebrücken hingegen blieben unverändert, und ihre Grösse wiederspiegelte ihre Fähigkeit für elektrophysiologischen Informationsfluss. Grössere Gewebebrücken und kleinere Läsionen, gemessen einen Monat nach der Verletzung, korrelierten mit besserer Erholung nach einem Jahr.

Als nächstes haben wir die darunterliegenden strukturellen, mikrostrukturellen und molekularen Prozesse von zervikaler Atrophie oberhalb der Läsion nach einer traumatischen Rückenmarksverletzung untersucht.
In der zweiten Studie erforschten wir, ob die graue Substanz des Rückenmarks oberhalb der Läsion, neben Änderungen der weissen Substanz, auch zu Einschränkungen des Patienten beiträgt. Dabei machten wir uns neuste Verbesserungen in Diffusions-gewichteter Bildgebung und spinale, hochaufgelösten MRT-Sequenzen zu Nutze. Neben Atrophie der weissen Substanz und Evidenz für Neurodegeneration und Demyelinisierung der sensomotorischen Hauptleitungsbahnen, stellten wir auch eine ausgeprägte Atrophie der Vorder- und Hinterhörner der grauen Substanz oberhalb der Läsion fest, deren Grösse mit dem Läsionsausmass zusammenhing. Gewebsspezifische Neurodegeneration war mit entsprechender klinischer und neurophysiologischer Beeinträchtigung assoziiert. Diese Studie zeigt antero- und retrograde Degeneration der sensomotorischen Leitungsbahnen und liefert Hinweise dafür, dass neuronale Schaltkreise innerhalb des Rückenmarks von transsynaptischer Neurodegeneration betroffen sind, was zu Änderungen innerhalb der grauen Substanz oberhalb der Läsion führt.

In der dritten Studie untersuchten wir zelluläre Änderungen innerhalb der atrophierten Region oberhalb der Läsion mittels neuartiger, spinaler MR Spektroskopie. Diese Studie zeigt läsionhöhen-abhängige metabolische Veränderungen oberhalb der Läsion, welche mit chronischer Neuroinflammation, Neurodegeneration und Demyelinisierung zusammenhängen. Die Stärke der chronischen Neuroinflammation hing mit der Grösse der initialen Läsion, der Stärke der zervikalen Atrophie und dem klinischen Status des Patienten zusammen. Diese Studie suggeriert, dass eine Rückenmarksverletzung nicht nur zur Neurodegeneration und Demyelinisierung oberhalb der Läsion führt, sondern dass chronische Neuroinflammation zur zervikalen Atrophie und dadurch auch zum klinischen Status des Patienten beitragen könnte.

In der vierten und letzten Studie haben wir die zeitliche und räumliche Entwicklung der Basalganglien nach einer Rückenmarksverletzung untersucht, in dem wir Änderung der Oberfläche und der Mikrostruktur innerhalb des Thalamus, des Striatums und des Globus Pallidus analysierten. Die meisten neueren Studien in rückenmarksverletzten Patienten, welche strukturelle Bildgebung benutzten, zeigten kortikale Änderungen des sensomotorischen und limbischen Systems. Tierstudien deuten jedoch darauf hin, dass die Basalganglien eine wichtige Rolle in der Erholung nach einer Rückenmarkverletzung spielen. Im Vergleich zur Kontrollgruppe haben Patienten in dieser Studie innerhalb den ersten zwei Jahren nach der Verletzung im motorischen Thalamus sowie im pulvinaren Kern und im Striatum Abnahmen der Oberflächen gezeigt. Die Abnahmen innerhalb des motorischen Thalamus sind dabei in Regionen aufgetreten, welche die unteren Extremitäten abbilden. Im gleichen Zeitraum zeigten Patienten zudem kompensatorische Zunahmen der Oberflächen im sensomotorischen Thalamus in Regionen der oberen Extremitäten und im Striatum. Parallel dazu änderten auch die mikrostrukturellen Parameter, welche zeigen, dass im Thalamus, im Striatum und im Globus Pallidus Degeneration, Demyelinisierung und möglicherweise neuroinflammatorische Prozesse stattfinden. Einen Monat nach der Verletzung korrelierte die Grösse der Oberflächenänderungen innerhalb des motorischen Striatums mit dem motorischen Status der unteren Extremitäten nach zwei Jahren. Ebenfalls einen Monat nach der Verletzung waren Zeichen von erhöhter Eisenansammlung innerhalb des pulvinaren Kern mit dem sensorischen Status des spinothalamischen Trakts nach zwei Jahren assoziiert. Diese Studie zeigt als erstes, dass eine Rückenmarksverletzung zu progressiven Änderungen der Basalganglien führt, welche mit dem klinischen Status des Patienten zusammenhängen.

Zusammenfassend zeigt diese Dissertation, dass eine traumatische Rückenmarksverletzung zum einen zu degenerativen Veränderungen auf Höhe der Läsionsstelle und den direkt verletzten Leitungsbahnen führt, aber auch transneuronale Änderungen im grossen Umfang in primär nicht betroffenen Regionen im Rückenmark und Hirn stattfinden. Neben den bekannten Mechanismen wie

Demyelinisierung und Neurodegeneration deuten die Resultate innerhalb dieser Arbeit darauf hin, dass anhaltende Neuroinflammation ebenfalls eine wichtige Rolle spielen könnte, die mit den degenerativen Änderungen und dadurch auch mit der Erholung der Funktion des Patienten in Zusammenhang steht. Konventionelle und innovative, neue MRT-Sequenzen erlauben eine Quantifizierung von trauma-induzierten Veränderungen im Rückenmark und im Gehirn. Diese könnten deshalb in Zukunft als Biomarker in klinischen Studien gebraucht werden, um die Wirksamkeit neuer Interventionen zu testen. Um dies zu erreichen, braucht es weitere Schritte wie zum Beispiel die Kombination von funktionellem und strukturellem MRT in longitudinalen Multi-Center Studien in akuten aber auch chronischen Patienten mit Rückenmarksverletztung. Dies erlaubt das zeitgleiche Messen von Änderungen im Rückenmark und Hirn, sowie das Erfassen der Auswirkungen der Erholung auf die Reorganisation des Zentralnervensystems.

Zum einen wird dies unser Verständnis des zeitlichen Musters von strukturellen Änderungen und des Zusammenhangs von strukturellen Änderungen zueinander, verbessern. Zum anderen ermöglichen uns solche Studien, die sensitivsten Biomarker zu identifizieren, welche dann für unterschiedliche pharmakologische und neurorehabilitative Interventionen genutzt werden können, welche zum Ziel haben, den klinischen Status des Patienten zu verbessern.

1 General Introduction

My research is a response to the urgent need to improve the validation of new interventions after spinal cord injury (SCI). To date, the only effective treatment leading to a limited extent of functional recovery is by means of intensive neurorehabilitation, highlighting the need for new therapeutical approaches. Although many clinical trials have emerged within the last years trying to overcome the limited recovery present after SCI, they are often unable to prove adequate efficacy. This is because SCI is a heterogeneous disorder in terms of primary and secondary damage, neurological deficits and subsequent spontaneous recovery (Bracken and Holford , 2002, Fawcett *et al.* , 2006*).* Neuroimaging biomarkers possess the potential to improve treatment validation, as they are able to measure structural changes associated with biological processes of recovery. As the spinal cord is inherently connected with the brain via axons of major pathways, it is assumed that a focal damage to the spinal cord will lead to tract-specific widespread changes within the whole central nervous system (CNS), measurable by means of magnetic resonance imaging (MRI). Such biomarkers have the potential to provide novel insights into structural changes specifically where clinical assessments are insensitive to unravel small alterations. The scope of the present thesis is therefore to better understand trauma-induced structural changes at different levels of the neuraxis after traumatic SCI, and explore the predictive ability of such neuroimaging biomarkers.

To better understand the context of the findings presented in this thesis, I will first outline the structure of the healthy spinal cord and then elucidate on pathophysiological mechanisms present after SCI. Next, studies using advanced imaging techniques to visualize remote changes above the level of injury are briefly summarized. Last, starting points for future therapies and ways to improve the validation of such interventions are presented, together with the specific aims of this thesis.

1.1 The spinal cord in healthy humans

The spinal cord is part of the central nervous system (CNS), connecting the brain to the peripheral nervous system and vice versa. It consists of about 10 billion neurons (Kalat, 1998) and is approximately 1cm in diameter. The spinal cord comprises two functionally and anatomically distinct compartments, the white and grey matter (Goshgarian, 2010).

The white matter is somatotopically organized in functional distinct columns (Fig. 1), with descending tracts mainly specific for motor function and ascending tracts mainly transmitting sensory function. Descending tracts are grouped into the pyramidal system, compromising of the lateral and anterior corticospinal tract, and the extrapyramidal system, consisting of the rubrospinal, reticulospinal, vestibulospinal and olivospinal tracts (Kuypers, 1964, Lemon, 2008). The lateral corticospinal tract controls fine movement of the limbs, whereas the anterior corticospinal tract contributes to

movement control of axial and trunk muscles (Nathan *et al.* , 1990). The rubrospinal tract influences the tonus of distal muscles, whereas the reticulospinal, vestibulospinal and olivospinal tracts affect the tonus of motoneurons of proximal or trunk muscles (Orlovsky, 1972, Nathan *et al.* , 1982, Nathan *et al.* , 1990). Ascending tracts consist of the dorsal column (transmitting information of light-touch and proprioception), the anterior and lateral spinothalamic tract (transmitting pain and temperature), and of the anterior and posterior spinocerebellar tracts (transmitting proprioceptive information to coordinate movement) (Tracey, 2004).

The butterfly-shaped grey matter consists primarily of cell bodies of sensory, motor and interneurons, as well neuropil (dendrites, mainly unmyelinated axons and their terminals) (Brown, 2012). In addition, it is highly vascularized, and embedded with glial cells (Brown, 2012). Primarily, the grey matter serves as the site of transmission of neuronal impulses between neurons (Brown, 2012). Similar as Brodman areas in the brain, which are regions with identical cytoarchitecture (Brodmann, 1912), the grey matter is also organized in anatomically distinct cell layers, so called Rexed laminae (Rexed, 1952, Rexed, 1954). In addition, single nuclei can be delineated from each other, which are partially overlapping with the laminae. Laminae I-VII are located within the dorsal horns, which is present at all spinal levels, and receive and transmit incoming somatosensory information. In particular, laminae I and II contain cells responding mainly to noxious and thermal stimuli arising from the dorsal root ganglion or the Lissauer tract. Their axons join the contralateral spinothalamic tract. Laminae III and IV include Aβ fibers arising from the dorsal root ganglion. These cells either (1) connect to cells from laminae IV, V and VI, and serve as propriospinal neurons and interneurons, (2) project to the contra- and ipsilateral spinothalamic tract, or (3) respond to light touch (Rexed, 1952, Rexed 1954, Brown, 2012). Lamina V and VI receive proprioceptive afferents from muscle spindles, joint and tendon receptors, and send information of body and limb position to the posterior spinocerebellar tract (Rexed, 1952, Rexed, 1954, Brown, 2012). Lamina VII receives information from lamina II-VI, and from visceral fibers and project to (1) visceral motor neurons, (2) ipsilateral posterior spinocerebellar tract, (3) ipsilateral anterior spinocerebellar tract or (4) sympathetic (T1-L3) or parasympathetic fibers (S2-S4) (Rexed, 1952, Rexed, 1954, Brown, 2012). The ventral horns involve Lamina VIII and IX and are present throughout the cord. They comprise mainly α-motor neurons, but also smaller β- and γ-motor neurons are present projecting to skeletal muscle (α), respectively to muscle spindles (γ), or both (β). The ventral horns possess a somatotopic organization with proximal motoneurons located in the medial part of the horns, and distal motoneurons located in the lateral part of the horns (Lamb, 1976). Lamina X connects the left and right grey matter and contains decussating commisural axons.

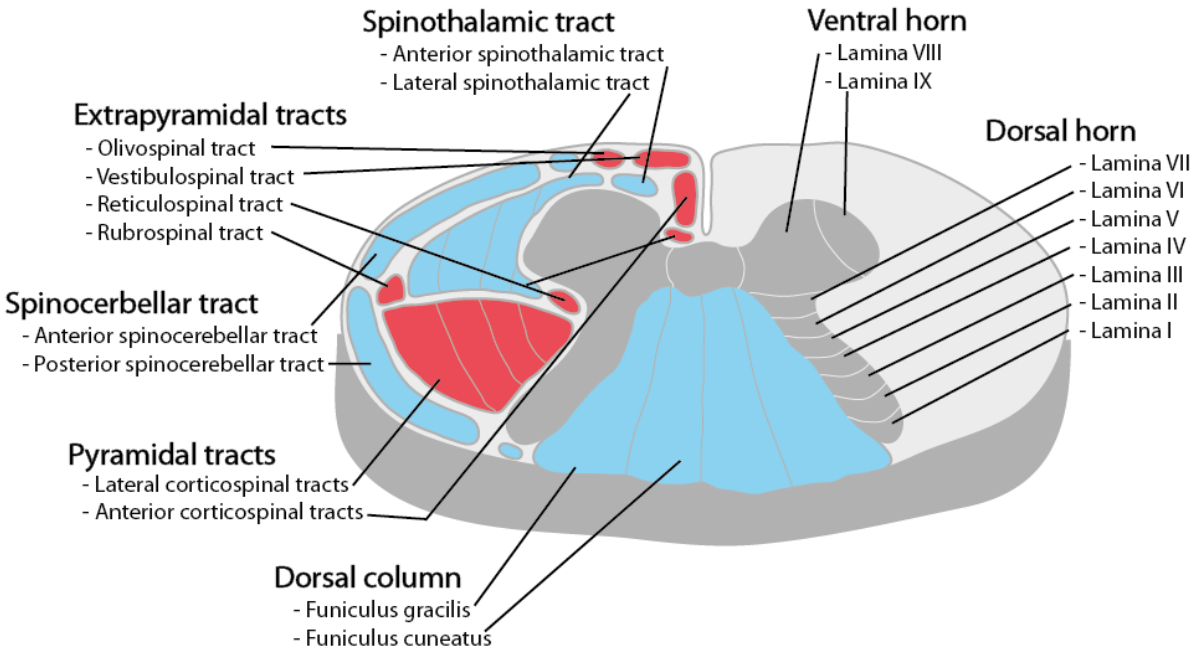

Figure 1: Cross-section of the spinal cord with whiter matter tracts (left) and grey matter columns (right).

1.2 Dysfunction of the spinal cord: Traumatic spinal cord injury

1.2.1 Epidemiology of spinal cord injury

SCI results from damage to the spinal cord and is a devastating event impacting the life of patients permanently. SCI is typically classified in traumatic and non-traumatic injuries. Causes of non-traumatic SCI include spinal ischemia, compression by tumors or degenerative diseases (e.g. osteoarthritis) (Kakulas, 1999). In contrast, causes of traumatic SCI vary depending on the country, but include motor vehicle accidents, falls, sports accidents and violence (Wyndaele and Wyndaele, 2006).

Worldwide, numbers of people suffering from SCI are estimated to be between 2 and 6 millions, mostly affecting young men (mean age: 33 years, prevalence: 3.8 times higher in men) (Wyndaele and Wyndaele, 2006). Although two thirds of all SCI are attributed to young people, the numbers of elderly people (> 60 years) suffering from a SCI has doubled in the last 10 years (Sekhon and Fehlings, 2001). Despite extensive rehabilitation programs, most patients are left with profound and persistent functional impairments such as motor deficits, sensory dysfunction, urological problems, and the emergence of neuropathic pain as a secondary complication (Siddall *et al.* , 1999, Siddall *et al.* , 2003, Cruz-Almeida *et al.* , 2005, Finnerup *et al.* , 2014). Patients being admitted without any function below the level of lesion usually show no or limited recovery, whereas patients with partially preserved sensorimotor function are able to undergo a more significant recovery like regaining hand

function or walking skills (Curt, 2008). Up to the present day, no treatment is available ameliorating neurological dysfunction. However, as the quality of emergency and primary care has improved over the last decades, life expectancy of SCI patients is similar to non-injured population (Fawcett *et al.* , 2006). Consequently, even after rehabilitation, most patients need regular medical checkups as they suffer from secondary health challenges, therapy to maintain their functional status, and/ or assistance in daily aspects of life (Kennedy *et al.* , 2006). Given the young average age of patients and the long-term consequences, SCI leads to a tremendous socio-economical impact with high costs arising from acute hospitalization, rehabilitation and on- going treatment and assistance (Dryden *et al.* , 2005). Novel therapeutical and pharmacological approaches are therefore highly needed to improve patients' quality of life and reduce health costs.

1.2.2 Classification and assessments of spinal cord injury

There are different ways to assess neurological and functional deficits after SCI. Here, the main methods are elucidated, which are routinely used in a clinical setting.

1.2.2.1 Clinical Assessments

International Standards for Neurological Classification of Spinal Cord Injury (ISNCSCI)

The International Standards for Neurological Classification of Spinal Cord Injury (ISNCSCI) is used as a gold standard for assessing motor and sensory deficits, the level injury and completeness as measured by the American Spinal Injury Association (ASIA) Impairment Scale (AIS) (Kirshblum *et al.* , 2011).

Crucially, to assess motor deficits, five key muscles representing spinal segments of the upper and lower extremities are tested and graded from zero (total paralysis) to five (active movement against full resistance). Sensory deficits are assessed by using light-touch and pin-prick on each dermatome to test dorsal column and spinothalamic tract function, graded from zero (absent sensation) to two (normal sensation). Depending on the extent of spared sensorimotor function below the level of lesion, the neurological completeness is classified in categories from A to E (Table 1).

Although this assessment is considered to be the gold standard, this clinical test depends on the patient's subjective perception, suffers from a rather high inter-rater variability and lacks sensitivity to minimal changes in motor and sensory functions (Ellaway *et al.* , 2011). The ISNCSCI classification and its associated scoring system is therefore insufficient to accurately predict a patient's outcome.

AIS	Functional completness of injury	Motor function below level of injury	Sensory function below level of injury
A	Complete	No	No
B	Incomplete	No	Yes
C	Incomplete	Yes, and more than half of the key muscles below the neurological level show a muscle grad less than 3 (grade 0-2)	Yes
D	Incomplete	Yes, and more than half of the key muscles below the neurological level show a muscle grad equal or greater than 3 (grade 3-5)	Yes
E	*Restutio ad integrum*	Yes	Yes

Table 1: Classification of spinal cord injury according to the American Spinal Injury Association (ASIA) Impairment Scale (AIS).

GRASSP

The Graded Redefined Assessment of Strength Sensibility and Prehension (GRASSP) was developed to reliably evaluate changes in upper limb impairment/function (Kalsi-Ryan *et al.* , 2012ab). In particular, this multimodal test includes (1) dorsal und (2) palmar sensation tested with Semmes-Weinstein monofilaments, graded from zero to two according to the ISNCSCI, (3) strength of 10 upper limb key muscles, graded from zero to five according to the ISNCSCI, (4) qualitative grasping, and (5) quantitative grasping involving different tasks of daily life.

SCIM

The Spinal Cord Independence Measure (SCIM) is a disability scale to define daily-life independence of patients after SCI. It involves questions about (1) self-care, (2) respiration and sphincter management, and (3) mobility (Itzkovich *et al.* , 2007).

1.2.2.2 Neurophysiological assessments

Neurophysiological assessments complement clinical assessments by supplementing them with information about the integrity of different tracts. This involves primarily the assessment of motor tracts by transcranial magnetic stimulation (TMS), somatosensory evoked potentials (SSEPs) to assess the integrity of large diameter fibers within the dorsal columns (Dawson, 1947, Kramer *et al.* , 2008), and contact heat evoked potentials (CHEPs) to assess integrity of small diameter fibers within the spinothalamic tracts (Chen *et al.* , 2001, Kramer *et al.* , 2012). In addition, nerve conduction

assessments provide information about the central and peripheral conduction of sensory and motor neurons (Kimura, 1984), and sympathetic skin assessments provide information about the autonomous nervous system (Kucera *et al.* , 2004).

1.2.2.3 Neuroimaging

After SCI, structural T1- and T2-weighted MRI is the gold standard to determine the level and extent of the injury. Standard clinical sequences provide insights into vertebral injury, ligamentous disruption, disc protrusion, site of maximal spinal cord compression and type of cord injury, and is clinically used to define whether decompressive or reconstructive surgery is needed (Chandra *et al.* , 2012). Additionally, such sequences can depict macro-structural intramedullary changes such as the evolution of hemorrhage, edema, cord swelling, and dynamics of lesions.

When applying spinal MRI in a clinical setting, an important criterion for feasibility of sequences is time. Unfortunately, advanced, time-saving imaging techniques rely on fast gradient-echo sequences such as echo-planar imaging, which come with major technical challenges. Specifically, the spinal cord is (1) surrounded by many different tissue types, resulting in susceptibility artefacts (Posse and Aue, 1990), (2) affected by physiological motion leading to the generation of artefacts (Zaitsev *et al.* , 2015), and (3) a small structure which needs high resolution to be properly imaged (Stroman *et al.* , 2014). Despite these challenges, novel innovative spinal structural sequences have recently advanced the neuroimaging field. This includes for example structural sequences providing higher in-plane resolution and optimized contrast (e.g. multiple echo data image combination (MEDIC) (Schmid *et al.* , 2005)) allowing disentangling effects within white and grey matter (Martin *et al.* , 2016). In addition, technical advances in spinal diffusion-weighted imaging (DWI) include a reduced field of view (FOV) which allows for higher in-plane resolution, and reduced acquisition time and artefacts. This enables improved mapping of diffusion processes capable of revealing changes within white matter tracts, which are related to axonal integrity and myelin content (Schmierer *et al.* , 2004, Schmierer *et al.* , 2008). Recent developments in spinal magnetic resonance spectroscopy (MRS) included the usage of saturation pulses (Edden *et al.* , 2006), higher order shimming (Hock *et al.* , 2013a) and non-water suppressed spectroscopy (Hock *et al.* , 2013b) with B0 frequency alignment, allowing to detect metabolic alterations within the tiny spinal cord.

At the brain level, clinically feasible quantitative imaging has recently become available and has the potential to measure neuronal changes at the microstructural level by applying physical models (Weiskopf *et al.* , 2013, Callaghan *et al.* , 2014). This is because the amount of myelination, iron content and neuronal microstructure is reflected in MR relaxation times, proton density and magnetization transfer (Stüber *et al.* , 2014). Quantitative imaging protocols usually consists of multiple images with varied acquisition parameters like magnetization transfer saturation (MT),

longitudinal relaxation rate (R1=1/T1) and effective transverse relaxation rate (R2*). In particular, it was shown that R1 relates to myelination/ demyelination (Mottershead et al. , 2003, Schmierer et al. , 2008 , Lutti et al. , 2014), proton density (Gelman et al. , 2001, Rooney et al. , 2007, Harkins et al., 2016), and lipid content (Stanisz et al. , 2005). MT is sensitive for myelination/ demyelination (Schmierer et al. , 2004, Dula et al. , 2010, Turati et al. , 2015) and R2* is sensitive to iron (Hankins et al. , 2009, Lemasson et al. , 2013). Such measures are unbiased and independent of the scanner used, which might facilitate multicenter studies (Weiskopf et al. , 2013).

1.3 Pathophysiology of traumatic spinal cord injury

The pathophysiology of acute traumatic SCI consists of a primary injury mechanism, which is caused by the initial trauma, and a secondary injury mechanism, followed with a time lag, which is characterized by additional processes further exacerbating and manifesting the initial functional deficits.

1.3.1 Primary injury

In traumatic SCI, the mechanical impact causes cell damage to neurons and glial cells, leads to blood vessel disruption and interruption of axons within the spinal cord (Dumon *et al.* , 2001). Additionally, SCI can also harm the surrounding structures resulting in bone fracture, ligamentous injuries and dislocation of fragments or disc material which can also harm the spinal cord (McDonald and Sadowsky, 2002). Depending on the injury morphology, neurons and their axons may only show signs of transection or in addition also be compressed, stretched and dislocated (Bunge *et al.* , 1993) . This primary injury largely determines the clinical status of the patient at admission (Dumont *et al.* , 2001).

At the molecular level, different cascades are triggered as a response to the mechanical insult that occur within minutes to days after injury. Within minutes, TNF-α gets upregulated and acts as a proinflammatory cytokine (Yang *et al.* , 2004). Together with the release of erythrocytes and serum constituents from damaged blood vessels, this leads to an edematous swelling of the spinal cord (Kakulas, 1984). Depending on the venous blood pressure, the swelling of the cord can result in secondary ischemia (McDonald and Sadowsky, 2002). Apart from TNF-α, many other inflammatory molecules get activated within the first 24 hours after injury which subsequently leads to the activation of neutrophils and macrophages. Neutrophils activation then primarily results in additional cord swelling (McDonald and Sadowsky, 2002), whereas macrophages are involved in coagulate necrosis with prominent ischemic cell change (Buss *et al.* , 2004). Later on, astrocytes invade the epicenter of the lesion (Nagamoto-Combs *et al.* , 2007), and eventually become reactive in the secondary injury cascade.

1.3.2 Secondary damage

The primary SCI is followed by a second phase which can exacerbate the primary damage and therefore additionally limit regeneration. In our current understanding, one of the main factors triggering the secondary injury cascade involves the local disturbance of blood supply (Schwab and Bartholdi , 1996; Lee *et al.* , 1999; Dumont *et al.* , 2001). Most important, the damage of cells, myelin and blood vessels leads to a toxic microenvironment, setting adjacent neurons in the penumbra at risk (for a review see Rolls *et al.* , 2009). To prevent further damage, reactive astrocytes form a persistent dense scar tissue around the lesion (Faulkner *et al.* , 2004). The downside of this process is that the glial scar itself acts as a physiological barrier, and in addition contains extracellular matrix molecules including chondroitin sulphate proteoglycans which inhibit axonal regrowth (Fawcett and Asher , 1999).

1.4 Using advanced structural MRI to track pathophysiological events after spinal cord injury

As described in chapter 1.2.2.3, several new MRI sequences emerged within the last years which are clinically applicable and provide information on tissue microstructure. Because the injury site contains the primary information about the recovery potential (chapter 1.3), most preclinical MR studies focused on identifying changes at the lesion site (Sundberg *et al.* , 2010, Li *et al.* , 2015). Unfortunately, the application of such sequences at the lesion site in humans is hampered by metal artefacts induced by vertebral fixations. Because the CNS is organized in hierarchical levels, which depend on each other (Freund *et al.* , 2016), it is assumed that a SCI leads to changes within damaged networks. Specifically, changes at the cord level can lead to appropriate spinal circuit remodeling (Filli *et al.* , 2015), which may also lead to changes in cortical networks, trackable by means of MRI. Based on this concept, MRI studies have started to elucidate remote changes above the level of injury by taking advantage of advanced imaging techniques. These studies are briefly summarized in this chapter.

1.4.1.1 Remote spinal changes

Two months after injury, decreases of spinal cord area above the level of injury are already evident in patients (Freund *et al.* , 2013a, Hou *et al.* , 2016). This decrease linearly progressed over the first year after injury, resulting in spinal atrophy of about 7% (Freund *et al.* , 2013a). In chronic SCI patients, spinal cord atrophy of up to 30% was observed (Cohen-Adad *et al.* , 2011, Freund *et al.* , 2011a, Lundell *et al.* , 2011) which presumably represents the endpoint of neurodegenerative events including demyelination and neuronal degeneration. In line, white matter integrity within the sensorimotor tracts were altered in chronic SCI patients, as assessed by means of diffusion and magnetization transfer imaging (Cohen-Adad *et al.* , 2011, Freund *et al.* , 2011a, Petersen *et al.* ,

2012, Koskinen *et al.* , 2013). Recent longitudinal MRI studies in animals showed that transected axons caused subsequent disintegration of the spinal cord, with demyelination spreading rostrally and caudally, resulting in spinal atrophy (Rao *et al.* , 2013). Crucially, the amount of atrophy was related to the sensorimotor outcome (Cohen-Adad *et al.* , 2011, Lundell *et al.* , 2011, Freund *et al.* , 2012ab, Freund *et al.* , 2013a, Grabher *et al.* , 2015, Ziegler *et al.* , 2018).

1.4.1.2 Remote supraspinal changes

Further upstream, chronic SCI patients exhibit atrophy of primary sensorimotor cortex (Freund *et al.* , 2011a, Jurkiewicz *et al.* , 2006, Wrigley *et al.* , 2009a, Jutzeler *et al.* , 2016), decreased volumes in the pyramids (Freund *et al.* , 2013, Jutzeler *et al.* , 2016), in sensorimotor brainstem pathways (Grabher *et al.* , 2017), and in the limbic system (Jutzeler *et al.* , 2016). In line, studies in rats showed altered tract integrity of the internal capsule and the pyramids (Guleria *et al.* , 2008, Jirjis *et al.* , 2016) suggestive of Wallerian degeneration and demyelination. In recent longitudinal studies, the temporal evolution of these changes was addressed in subacute SCI patients. Specifically, such changes occurred within the first month after SCI, and were paralleled by microstructural changes indicative of demyelination, iron accumulation and neuronal degeneration (Freund *et al.* , 2013a, Grabher *et al.* , 2015, Grabher *et al.* , 2017, Ziegler *et al.* , 2018). Importantly, the amount of structural brain changes were associated to sensorimotor outcome (Jurkiewicz *et al.* , 2006, Freund *et al.* , 2013a, Grabher *et al.* , 2015, Grabher *et al.* , 2017, Ziegler *et al.* , 2018).

1.5 Starting points for future therapies

To overcome the limited capacity for recovery, several new therapeutical approaches emerged within the last years, which can be attributed to four main mechanisms (Schwab, 2002). These approaches will be briefly explained, and the current status of such applications in humans will be discussed.

1.5.1 Enhancing regenerative sprouting

Although peripheral nerves are capable of reinitiating axonal growth after damage (Fawcett and Keynes, 1990), sprouting of transected axons in the CNS is limited as different inhibitory proteins block neurite outgrowth (Caroni and Schwab, 1988). The main neurite outgrowth inhibitor is Nogo-A, whose blocking with Anti-Nogo A antibody has been extensively investigated in different preclinical models over the last two decades (Merkler *et al.* , 2001, Foud *et al.* , 2004, Liebscher *et al.* , 2005, Freund *et al.* , 2007). Neutralizing Nogo-A leads to greater axonal sprouting which results in a meaningful rewiring and therefore enhances functional recovery (Liebscher *et al.* , 2005, Freund *et al.* , 2006). The first clinical trial in humans was conducted between 2006 and 2011 (NCT00406016 identified in clinicaltrials.gov), and showed that Anti-Nogo A antibodies are safe and well tolerable. Next steps include a placebo-controlled phase II clinical trial to proof efficacy of the drug.

1.5.2 Crossing the glial scar

The glial scar serves as a physical barrier to axonal regrowth, and in addition, contains neurite-growth inhibitory molecules like chondroitin sulphate proteoglycans (CSGPs) acting as a chemical barrier to the process of neuroregeneration (McKeon *et al.* , 1991, Fawcett and Asher, 1999, Roitbak and Syková, 1999). To enable fibers to cross the lesion site, different approaches have been suggested and tested in preclinical models: (1) inhibition of CSGP using chondroitinase ABC (Bradbury *et al.* , 2002), (2) applying neurite growth-promoting molecules by either a pump or modified gene (Bunge, 2001) and (3) implantation of scaffolds into the lesion site (Tsintou *et al.* , 2015). Of these, only scaffolds have so far made it to the application in human clinical trials (NCT02688049, NCT02510365, NCT02352077, NCT02138110, NCT02688062, NCT03105882, NCT02326662 identified in clinicaltrials.gov), which are partially seeded with stem cells (NCT02688049, NCT02352077, NCT02326662 identified in clinicaltrials.gov).

1.5.3 Repairing myelin

SCI does not only lead to demyelination of directly injured axons, also surviving bundles of nerve fibers often lose their myelin after injury (Schwab, 1996; Kakulas, 1999, Norenberg *et al.* , 2004, Guest *et al.* , 2005). This loss of myelin leads to an abnormal or absent conduction of action potentials, which is not restored in the adult nervous system (Schwab, 2002, Guest et al. , 2005). Therefore, strategies aiming at myelin repair, like the Schwann cell autotransplantation (Evercooren *et al.* , 1997), or the transplantation of embryonic stem cells which subsequently develop to myelin-producing oligodendrocytes (Liu *et al.* , 2000), have shown to be successful approaches for remyelination. Autologous human Schwann cells (NCT01739023, NCT02354625 identified in clinicaltrials.gov) and oligodendrocytes progenitor cells (NCT02302157 identified in clinicaltrials.gov) are currently being tested in phase I clinical trials.

1.5.4 Enhancing central neuroplasticity

The forth approach relies on central neuroplastictity, which might account for spontaneous recovery occurring in SCI patients. Such neuroplasticity includes the formation of new circuits through collateral sprouting of damaged and undamaged tracts, and synaptic plasticity in unaffected pathways (Raintenau and Schwab, 2001, Bareyre *et al.* , 2004, Ballermann and Fouad, 2006, Courtine *et al.* , 2008, Rosenzweig *et al.* , 2010). In contrast to regenerative sprouting, this mechanism presents not a “true” repair strategy, but the usage of alternative or detour pathways. Most therapeutical interventions aiming at regeneration are not specific to this process, and will likely also enhance compensatory growth (Schwab, 2002). Inter alia, such processes can be enhanced by applying neurotrophic factors (Bregman *et al.* 1997, Grill *et al.* , 1997, Bregman *et al.* , 2002). However, as such treatments have the highest chance to succeed in incomplete patients, who have anyway high rates of spontaneous recovery, it will be very challenging and difficult to detect

treatment effects (Blesch and Tuszynksi, 2009). So far, no clinical trial has started which specifically targets neuroplasticity.

1.5.5 Issues in validating future therapies

Due to the complexity of different mechanisms occurring after SCI, it is very likely that only a combination of treatment approaches will lead to the amelioration of functional impairments (Bunge, 2001). To identify most promising therapies or combination of therapies, the field urgently needs biomarkers to stratify patients into homogenous subgroups within clinical trials, and subsequently delineate treatment effects from spontaneous recovery.

1.6 Improving the validation of future therapies by the use of neuroimaging biomarkers

1.6.1 Motivation for biomarker development

Although several new clinical trials within the SCI field have emerged in recent years, it should be considered that less than 10% of all Phase I trials actually succeed to the make it on the market (CMR International, 2006), resulting in unsustainable increase in research and development cost. The main reason for this early drugs failure is the inability to show adequate efficacy or poor safety (Kola and Landis, 2004). As SCI is a heterogeneous disease, we need on one hand an increased understanding of SCI pathophysiology to identify potential responders to existing treatments; on the other hand it is essential to confirm drug pharmacology in initial human studies and terminate them if they show inadequate pharmacology (Peck, 2007). Unfortunately our current assessments, mostly rely on patient's subjective perception and are insensitive to minimal changes, making prediction of outcome still challenging (Wilson *et al.* , 2012; Tanadini *et al.* , 2014). Finding biomarkers, defined as markers of pharmacologic responses to a therapeutic intervention (Biomarkers Definitions Working Group, 2001), which are predictive of safety or efficacy in Phase I and II clinical trials would allow better determining potential success of a treatment. In addition, such biomarkers would drastically decrease persisting developmental, but also socio-economical costs.

1.6.2 Biomarkers as surrogate endpoints

In a clinical study, primary endpoints are defined to identify treatment effects and are characterized by measures which consider a patient's subjective feelings and functions (Biomarkers Definition Working Group, 2001). There is broad agreement that the patient's subjective perception of his or her current status is the most relevant goal, and therefore should be the primary endpoint in all biomedical research (De Gruttola, 2001). On the other hand, a biomarker is an objective, quantifiable characteristics of a biological process, but does not necessarily correlate with a patient's perception of his or her status (Strimbu and Tavel, 2010). Therefore, when biomarkers are used within clinical trials, they are considered as a substitute or "surrogate" for a clinical endpoint, which are expected

to predict clinical benefit or harm (Biomarkers Definitions Working Group, 2001). This means, that not all biomarkers are surrogate markers – they are rather a small subgroup of well-characterized biomarkers with well-defined clinical relevance and related to the pathophysiology of the disease (Strimbu and Tavel, 2010).

1.6.3 Biomarker identification: When a biomarker becomes a surrogate marker

Finding reliable surrogate markers usable within clinical trials is a time-consuming process, with phases comparable to a clinical trial itself (Fig. 2). Similar to preclinical phases in clinical trials, we first need to understand the natural history of SCI, the degree and time course of spontaneous recovery (Lammertse, 2007) and develop quantitative MRI sequences which are sensitive and comparable across different sites. Then, here called phase I, quantitative MRI sequences are applied in chronic and acute SCI patients and their proximity to clinical outcome (i.e. measures which serve as a primary endpoint in clinical trials) is examined. To reduce false positive results, it is important to base analysis on plausible biological hypotheses, which have the potential to pick up changes of the disease process (e.g. demyelination, degeneration). In phase II, the biomarker's effectiveness or utility as a surrogate marker is investigated. This is achieved by longitudinally assessing the sensitivity and specificity of the biomarker on interventions. Last, in phase III/IV, surrogate markers need to be evaluated in prospective cohort, which could be within a clinical trial. Please note that these stages are not stringently in order, they can and need to overlap with each other.

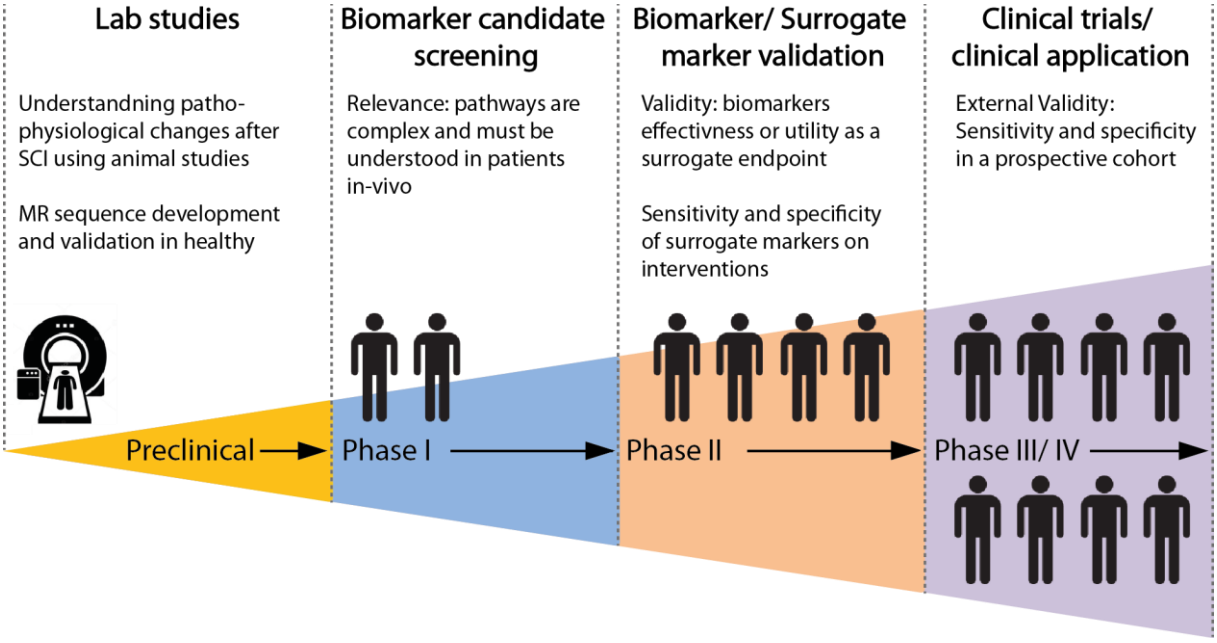

Figure 2: Stages of MR biomarker/ surrogate marker development

1.7 Aims

The overall objective of this thesis was to better understand trauma-induced structural changes at different levels of the neuraxis (at and above the level of injury), and to explore the relationships between MRI readouts, and electrophysiological and functional outcome. In particular, this thesis investigates new imaging methods which can assess microstructural changes not visible on conventional diagnostic imaging methods. For this goal, following aims were specifically addressed:

At the lesion site:

1) Treatments of the injured cord will likely depend on the existence of tissue bridges. We therefore wanted to characterize temporal changes at the lesion site and investigate their predictive capability of outcome after cervical SCI.

At the cervical cord above the level of lesion:

2) Previous studies have shown cervical cord atrophy of up to 30%. Here we assessed underlying tissue-specific grey and white matter changes using high-resolution structural and diffusion-weighted sequences, and investigated their relationship to lesion severity and outcome.
3) Following up on question 2), we investigated in a further study underlying molecular changes that may subtend the development of atrophy using spinal MRS, and investigated their relationship to atrophy, lesion severity and outcome.

At the brain level:

4) Structural changes of the pyramidal, sensory and limbic system have already been characterized after SCI. Animal models suggest that the extrapyramidal system, like the basal ganglia, plays a role in recovering motor function. We therefore investigated the spatial and temporal evolution of structural and microstructural changes and their association to outcome after SCI.

2 Study I

Are midsagittal tissue bridges predictive of outcome after cervical spinal cord injury?

Eveline Huber, Patrice Lachappelle, Reto Sutter, Armin Curt, Patrick Freund

This orginal article is published in Annals of Neurology.

The study was designed by P.F. and A.C.. Acquisition and analysis of data was performed by E.H., P.L., R.S., and P.F., E.H., and P.F. wrote the manuscript. All authors reviewed the manuscript.

2.1 Abstract

T_2-weighted scans provided data on the extent and dynamics of neuronal tissue damage and midsagittal tissue bridges at the epicenter of traumatic cervical spinal cord lesions in 24 subacute tetraplegic patients. At 1 month post injury, smaller lesion area and midsagittal tissue bridges identified those patients with lower extremity evoked potentials and better clinical recovery. Wider midsagittal tissue bridges and smaller lesions at 1 month post-injury were associated with neurological and functional recovery at 1-year follow-up. Neuroimaging biomarkers of lesion size and midsagittal tissue bridges are potential outcome predictors and patient stratifiers in both subacute and chronic clinical trials.

2.2 Introduction

In spinal cord injury (SCI), magnetic resonance imaging (MRI) is the most sensitive imaging modality to uncover the level and extent of spinal cord damage. Relationships exist between clinical impairment at admission (Miyanji *et al.* , 2007, Le *et al.* , 2015) and discharge (Mabray *et al.* , 2016) and acute (<48 hours) MRI biomarkers (hemorrhage (Miyanji *et al.* , 2007), lesion length (Le *et al.* , 2015), spinal canal compression (Miyanji *et al.* , 2007, Mabray *et al.* , 2016). However, these acute biomarkers have limited prognostic value for late outcome (Miyanji *et al.* , 2007). Signal alterations attributed to edema and hemorrhage, which resolve only after weeks (Shimada *et al. , 1999)*, hinder the accurate assessment of neuronal tissue damage and the amount of tissue sparing at the earliest stages post-injury.

Moreover, the sequela of tissue damage at the lesion epicenter and the optimal time points for characterization of neuronal tissue damage are unknown, because longitudinal MRI assessments are not standard care in SCI. Whereas post-traumatic cyst development is common in SCI (Wang *et al.* , 1996), its incidence and pathophysiology are incompletely understood. Residual tissue bridges spanning the lesion has been less studied, although these tissue bridges may be associated with improved recovery (Metz *et al.* , 2000). Treatments aiming at the repair of the injured spinal cord (Guest *et al.* , 1997, Silver and Miller , 2004, Freund *et al.* , 2006*)* will likely depend on such tissue bridges (Krishna *et al.* , 2014).

Identifying the extent of tissue damage and bridges post-SCI might be useful for prognostication, evaluating treatment efficacy, and stratifying patient cohorts in clinical trials (Wang *et al.* , 2011, Nagoshi *et al.* , 2015). Here, we report on detailed insights into structural cord damage using longitudinal MRI with specific emphasis on the presence and persistence of midsagittal tissue bridges, their electrophysiological conductivity, and predictive value for clinical recovery in sub-acute cervical SCI patients.

2.3 Materials and Methods

2.3.1 Experimental Design

Twenty-four patients with acute cervical traumatic SCI, admitted consecutively to University Hospital Balgrist (Zurich, Switzerland) between December 2005, and July 2014, were included in this study (Freund *et al.* , 2013a, Grabher *et al.* , 2015). The local ethics committee approved the study protocol and all patients gave informed, written consent.

In all patients, MRI data were acquired at approximately 1 month post-injury. Thirteen patients were additionally followed up with 100% compliance at 3, 6, and 12 months postinjury. At all time points, all patients were clinically assessed using the international standards for the neurological

classification of SCI protocol (ie, upper (UEMS) and lower (LEMS) extremity motor scores and light-touch and pin-prick scores), the Spinal Cord Independence Measure (SCIM) and the Graded Redefined Assessment of Strength, Sensibility and Prehension (GRASSP). SCIM data were missing for 2 patients (1 at 3 and 1 at 6 months) whereas GRASSP data were missing from 1 patient at 3 months. The GRASSP test was not available for 8 patients because their injuries date back before the introduction of this test.

2.3.2 Electrophysiological recordings

We obtained motor (MEPs) and sensory (SEPs) evoked potentials at 3 months post-injury according to standard protocols (Curt *et al.* , 2008). MEPs were recorded bilaterally over the tibialis anterior (TA) and abductor hallucis (AH). Bilateral tibialis nerves were stimulated for the SEP recordings. For MEPs and SEPs, amplitudes and latencies were calculated.

2.3.3 MRI

From the 24 patients, 14 were scanned with a 3 Tesla (T) MRI scanner and 10 with a 1.5T MRI scanner. From the 14 patients scanned at 3T, 8 were scanned with a 3T Magnetom Verio MRI scanner and 6 with the updated 3T Magnetom Skyra^{fit} scanner (Siemens Healthcare, Erlangen, Germany). From the 10 patients scanned at the 1.5T scanner system, 4 were scanned with a Magnetom Symphony, 3 with a Magnetom Espree, 2 with Magnetom Avanto (all Siemens Healthcare), and 1 with Signa HDx (GE Medical Systems, Waukesha, WI). All scanners were operated with a 16-channel receive head and neck coil. A standardized imaging protocol was used, based on product sequences including a sagittal T_1-weighted (for 1.5T: repetition time [TR] = 561ms; echo time [TE] = 11ms; flip angle = 150 degrees; for 3T: TR = 540ms; TE = 10ms; flip angle = 150 degrees), a sagittal T_2-weighted (T2w; for 1.5T: TR = 4,188ms; TE = 113ms; flip angle = 150 degrees; for 3T: TR = 3,430ms; TE = 90ms; flip angle = 150 degrees), and an axial T2w image (for 1.5T: TR = 5,170ms; TE = 100ms; flip angle = 150 degrees; for 3T: TR = 4,190ms; TE = 100ms; flip angle = 150 degrees). Axial and sagittal images were acquired using the same coordinate system in order to accurately identify the mid-sagittal slice. For the qualitative analysis, all sequences were considered. The sagittal T2-weighted images were used for quantitative analysis (for 1.5T: 0.55 × 0.55 × 2.75mm; for 3T: 0.57 × 0.57 × 2.75mm) of lesion size and midsagittal tissue bridges.

2.3.4 Image Analysis

Imaging at 1 month was used to classify whether a lesion (high-intense signal change on T2-weighted image), edema, and/or hemorrhage were present. Two raters, blinded to patient identity and scan time point, assessed the anterior-posterior width, rostrocaudal length, and total area of the lesion, and the width of tissue bridges on the midsagittal slice using Jim6.0 (Xinapse Systems, Aldwincle, UK) at all time points (Fig. 3). Inter- and intraobserver reliability was assessed for all quantitative MR

parameters in 10 randomly selected scans, by calculating the coefficient of variation (COV). Mean intra- and interobserver COV for all measures was remarkably low, with 4.3% and 5.2%, respectively.

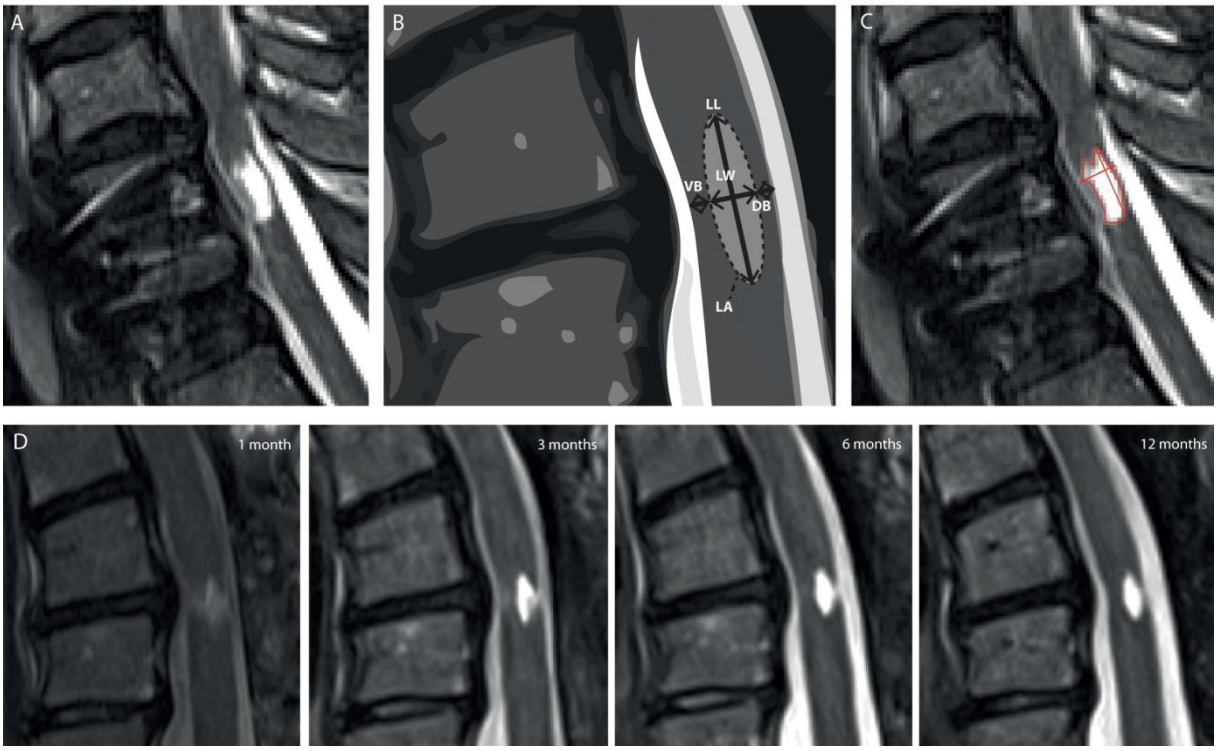

Figure 3: (A–C) Overview of quantitative magnetic resonance imaging (MRI) indices (LW, LL, LA, DB, and VB) assessed at the lesion site within the cervical cord using the midsagittal slice. (A) Typical T_2-weigthed MRI of the lesion epicenter from 1 spinal cord injury patient. (B) Schematic drawing of the MRI parameters analyzed. (C) T_2-weigthed midsagittal slice overlaid with the MRI lesion parameters in 1 patient. (D) Evolution of a post-traumatic cyst with persisting midsagittal tissue bridges shown over the course of the first year postinjury. DB = dorsal midsagittal tissue bridges; LA = lesion area; LL = lesion length; LW = lesion width; VB = ventral midsagittal tissue bridges.

2.3.5 Statistical Analysis

Stata software (version 13; StataCorp LP, College Station, TX) was used for statistical analysis. Rates of change of MRI readouts and clinical recovery were estimated with linear mixed-effects models with the MRI parameter or clinical measure as response variable and time as predictor. For clinical measures, time post-injury was modeled on a log scale to account for nonlinear recovery patterns, whereas a quadratic term in time was added to model nonlinear changes for all MRI measures (Freund *et al.* , 2013a). Linear regression models identified associations between the 1-month quantitative MRI parameters and clinical outcomes at 12 months, adjusted for age. For associations between midsagittal tissue bridges and clinical outcomes, only those patients with tissue bridges (mid- or parasagittal) entered the regression analysis.

2.4 Results

Twenty-four patients had acute traumatic cervical SCI (20 men, age [mean ± standard deviation] 46.58 ± 18.96 years). The interval between baseline and 1-month scan was 38.13 ± 16.71 days (n = 24), 3 months 95.1 ± 38.0 days (n = 13), 6 months 198.1 ± 39.3 (n = 13), and 12 months

390.2 ± 66.8 days (n = 13). Electrophysiological recordings were acquired at 87.92 ± 5.96 days post-injury (n = 24). After surgical decompression, 6 were classified as complete (American Spinal Injury Association Impairment Scale [AIS] A) and 18 as incomplete (AIS B–D; Table 2).

Within the first year, patients recovered, on average, 3.8 points/log-month on the UEMS ($p < 0.001$; 95% confidence interval [CI]: 2.620, 4.897; n = 24), 2.6 points/log-month on the LEMS ($p < 0.001$; CI: 1.339, 3.840; n = 24), 12.9 points/log-month in the SCIM (p < 0.001; CI: 8.218, 17.547; n = 24), 10.5 points/log-month in the GRASSP ($p = 0.001$; CI: 4.158, 16.872; n = 16), and 2.5 points/log-month in the light-touch score ($p = 0.030$; CI: 0.236, 4.661; n = 24). Pin-prick score showed no significant recovery over time ($p = 0.119$; CI: −0.64, 5.62; n = 24).

2.4.1 Lesion Characteristics and Changes Over Time

At 1 month, a lesion (ie, high-intense signal on the sagittal T2-weighted image) was visible in all patients and a subset of patients showed hemorrhage (n = 5) and edema (n = 15). In 23 of 24 patients, tissue bridges (midsagittal and/or parasagittal) were identified whereas the cord was completely transected in 1 patient who was classified as AIS A (Table 3). Of the 20 patients with midsagittal tissue bridges, 14 had both ventral and dorsal tissue bridges, whereas the remaining patients had only a dorsal (n = 3) or ventral (n = 3) tissue bridge.

In the 13 patients with serial MRI, lesion area declined by 6.73mm^2/month ($p = 0.027$; CI: –12.671, −0.781) over time. The rate of decline decelerated (ie, a negative quadratic term) by 0.39mm^2/month ($p = 0.035$; CI: 0.026, 0.742). Lesion width decreased by 0.40mm/month ($p = 0.001$; CI: −0.642, −0.159) with rate of decline decelerating at 0.02mm/month ($p = 0.014$; CI: 0.004, 0.034). Lesion length ($p = 0.779$) and the width of midsagittal tissue bridges ($p = 0.425$) remained essentially unchanged over time.

2.4.2 Electrophysiological Conductivity Across the Lesion

Lower extremity evoked potentials were abolished in all complete patients (AIS A; n = 6), although midsagittal tissue bridges were present in 2 of 6. Thickness of the midsaggital tissue bridges in the 2 AIS A patients was thinner than the overall average of those found in 18 incomplete patients (AIS B–E; Fig. 4AB). In these 18 incomplete patients, MEP and tibialis SEP latencies were recordable; the latencies prolonged (MEP: TA, 34.76 ± 6.84ms; AH, 44.22 ± 5.46ms; tibialis SEP: P40, 47.97 ± 4.44ms; N50, 56.06 ± 4.53ms) and the amplitudes reduced (MEP: TA, 0.45 ± 0.33mV; AH, 0.80 ± 0.90mV; tibialis SEP: 1.28 ± 1.09mV).

			ISNCSCI		Outcome measures at 12-month					
ID	Age at injury	sex	AIS at 1-/ 12-month	Initial site of impairment (motor/ sensory)	LEMS	UEMS	GRASSP	SCIM	Pin-prick	Light-Touch
1	41	m	A/A	C5/ C5	0	25	80	37	18	20
2	32	m	A/A	C5/ C3	0	35	137	26	29	32
3	30	m	A/A	C4/ C4	0	26	87	30	16	32
4	27	m	A/A	C2/ C3	0	14	20	19	13	16
5	17	m	A/A	C5/ C4	0	23	90	37	33	33
6	29	m	A/B	C5/ C5	0	23	77	34	26	53
7	30	m	B/B	C7/ C8	0	48	208	38	46	68
8	51	m	B/C	C6/ C6	12	32	116	31	44	67
9	70	m	C/C	C7/ C8	41	48	188	36	41	112
10	65	m	C/C	C4/C3	23	16	NA	10	61	61
11	53	f	C/D	C4/ C5	49	42	177	84	94	62
12	22	m	C/D	C7/ C6	19	48	205	70	37	72
13	59	m	C/D	C4/C4	32	38	NA	73	60	60
14	41	m	D/D	C5/C6	47	44	NA	100	70	95
15	30	m	D/D	C6/C6	46	45	NA	100	84	94
16	65	m	D/D	C4/C3	40	34	NA	32	64	60
17	63	f	D/D	C5/C5	49	47	NA	91	108	111
18	65	f	D/D	C4/C5	50	36	172	99	58	64
19	21	m	D/D	C5/C3	49	42	219	99	95	96
20	62	m	D/D	C4/C4	47	41	NA	92	112	112
21	66	f	D/D	C4/C4	50	45	129	98	70	60
22	75	m	D/D	C4/C2	49	43	NA	79	112	112
23	47	m	D/D	C5/ C4	47	35	130	98	97	98
24	67	m	D/E	C3/ C3	50	50	227	100	102	107

Table 2: Clinical and epidemiological data for all patients included in the study.
Abbreviations: AIS = American Spinal Injury Association Impairment Scale, GRASSP = Graded and Redefined Assessment of Strength, Sensibility and Prehension; ISNCSCI = International Standards for Neurological Classification of Spinal Cord Injury; LEMS = *Lower Extremity Motor Score*; NA= not available; SCIM = Spinal Cord Independence Measure; UEMS = *Upper Extremity Motor Score.*

			Electro-physiology	MRI parameters			
ID	Age at injury	sex	Evoked potentials	Magnetic field strength	Size of midsagittal tissue bridges [mm]	Para-sagittal tissue bridges	Lesion size (area [mm^2]/ length [mm])
1	41	m	No	3T	0	No	33/ 18.6
2	32	m	No	3T	0	Yes	54.3/ 10.4
3	30	m	No	3T	0	Yes	123.9/ 18.4
4	27	m	No	3T	0	Yes	131.6/ 20.4
5	17	m	No	3T	1.5	Yes	256.4/ 32.3
6	29	m	No	3T	1.5	Yes	156.4/ 28.9
7	30	m	Yes	3T	0.6	Yes	35.5/ 7.2
8	51	m	Yes	3T	1.3	Yes	50.7/ 11.7
9	70	m	Yes	3T	0.5	Yes	55/ 10.5
10	65	m	Yes	1.5T	2.5	Yes	21.5/ 9.4
11	53	f	Yes	3T	2.2	Yes	18.6/ 8.1
12	22	m	Yes	3T	3.2	Yes	30.2/ 11.7
13	59	m	Yes	1.5T	3.4	Yes	4.5/ 3.3
14	41	m	Yes	1.5T	1.5	Yes	15.0/ 6.2
15	30	m	Yes	1.5T	2.1	Yes	11.3/ 4.7
16	65	m	Yes	1.5T	2.7	Yes	34.4/ 7.8
17	63	f	Yes	1.5T	2.8	Yes	30.5/ 7.8
18	65	f	Yes	3T	3.2	Yes	18.2/ 6.4
19	21	m	Yes	1.5T	3.3	Yes	21.0/ 5.3
20	62	m	Yes	1.5T	3.5	Yes	9.7/ 3.5
21	66	f	Yes	1.5T	3.7	Yes	21.3/ 8.7
22	75	m	Yes	1.5T	5.6	Yes	63.7/ 18.6
23	47	m	Yes	3T	5.9	Yes	4.5/ 3.3
24	67	m	Yes	3T	1.5	Yes	21.5/ 9.4

Table 3: Electrophysiological and MRI data for all patients included in the study.

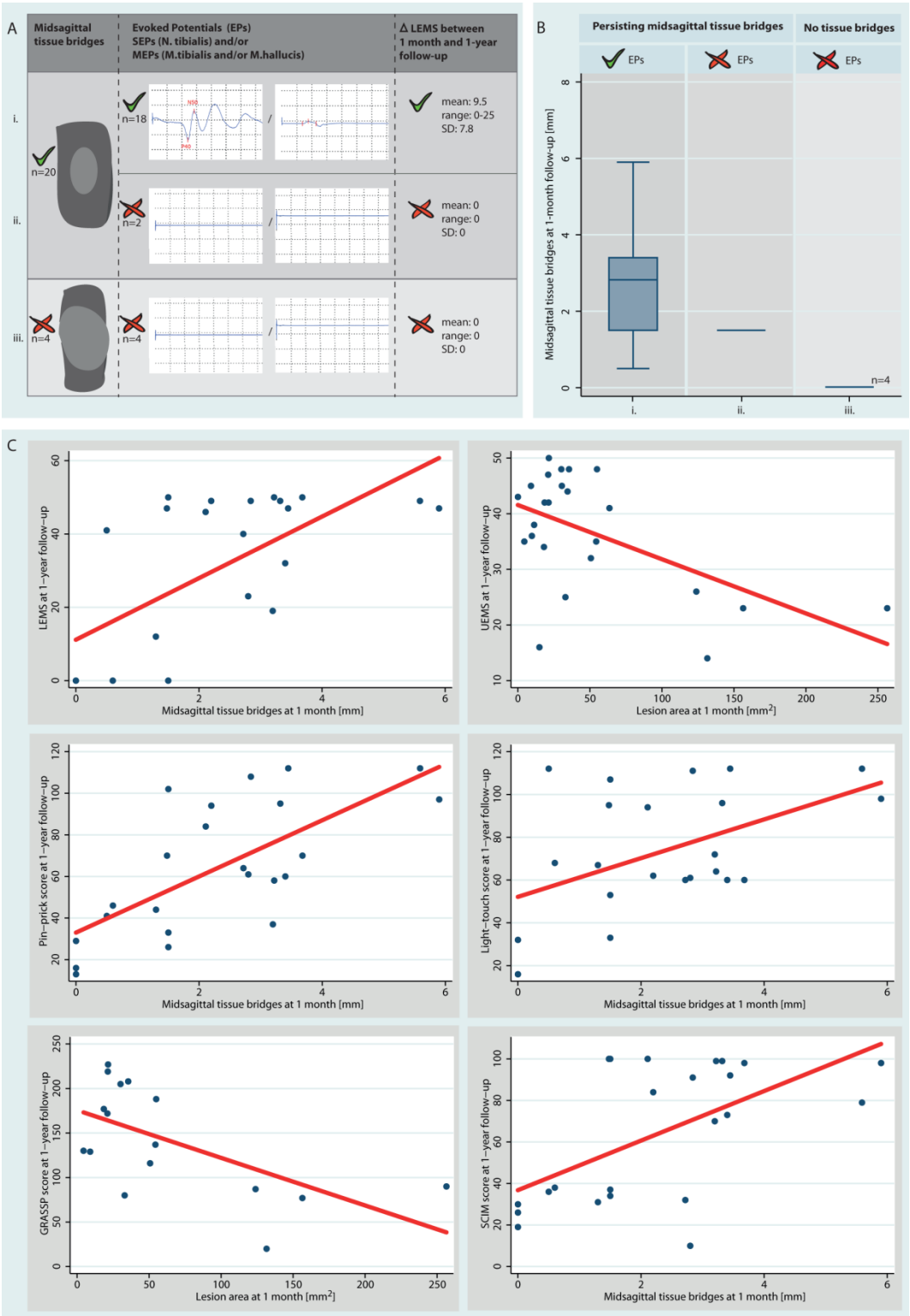

Figure 4: (A,B) Electrophysiological recordings across the tissue bridges. (A) Patients were grouped into two cohorts with (i./ ii.) and without (iii.) persisting tissue bridges. From most patients with tissue bridges, electrophysiological transmission was crossing the lesion and these patients showed better recovery of motor function below the level of lesion (i.). In patients without tissue bridges, no EPs and no recovery of motor function below the level of lesion was present (iii.). (B) Patients with midsagittal tissue bridges and recordable EPs (i.) showed a tendency toward wider tissue bridges than those with tissue bridges but without recordable EPs (ii.). (C) Correlations illustrating the relationship between magnetic resonance imaging (MRI) indices at 1 month and clinical recovery at 1 year.

EP = Evoked Potentials; GRASSP = Graded Redefined Assessment of Strength, Sensibility and Prehension; LEMS = Lower Extremity Motor Score; MEPs = Motor-evoked Potentials; SCIM = Spinal Cord Independence Measure; SEPs = Sensory-evoked Potentials; UEMS = Upper Extremity Motor Score.

2.4.3 Clinical Associations

Wider midsagittal tissue bridges at 1 month were associated with better LEMS ($p = 0.008$; $R^2 = 0.593$), SCIM scores ($p = 0.002$; $R^2 = 0.365$), pin-prick ($p < 0.001$; $R^2 = 0.475$) and light-touch scores ($p = 0.014$; $R^2 = 0.255$) at 1 year (Table 4). Smaller lesion area at 1 month was associated with better LEMS ($p = 0.001$; $R^2 = 0.408$), UEMS ($p = 0.005$; $R^2 = 0.305$), SCIM score ($p = 0.019$; $R^2 = 0.227$), GRASSP ($p = 0.013$; $R^2 = 0.367$), pin-prick ($p = 0.005$; $R^2 = 0.301$), and light-touch scores ($p = 0.016$; $R^2 = 0.237$) at 1 year. Smaller lesion length at 1 month was associated with better LEMS ($p < 0.001$; $R^2 = 0.448$), UEMS ($p = 0.005$; $R^2 = 0.311$), SCIM score ($p = 0.020$; $R^2 = 0.222$), GRASSP ($p = 0.009$; $R^2 = 0.400$), pin-prick ($p = 0.004$; R^2=0.321), and light-touch scores ($p = 0.013$; R^2 = ;0.249) at 1 year. Smaller lesion width at 1 month was related to higher pin-prick score ($p = 0.013$; $R^2 = 0.247$) at 1 year (Fig. 4C).

2.5 Discussion

This study characterizes the natural history of structural changes at the lesion site during the first year after traumatic cervical SCI. We uncovered the relationship between early MRI measures of lesion extent and midsagittal tissue bridges, and presence of evoked potentials and clinical recovery. In all patients, lesions were well demarcated at 1 month. The midsagittal tissue bridges that were identified in the majority of patients at 1 month were permissive for electrophysiological information flow. In the 13 patients with serial MRI, lesion area and width declined nonlinearly over time, whereas the size of midsagittal tissue bridges did not change significantly. Crucially, wider midsagittal tissue bridges and smaller lesions at 1 month post-injury were associated with enhanced clinical recovery at 1 year.

Acute spinal MRI (<48 hours) is limited in its prognostic usefulness (Miyanji *et al.* , 2007); however, at 1 month (i.e., subacute), lesion borders were clearly identifiable (Shimada *et al.* ,1999), allowing precise characterization of morphometric changes. Interestingly, already at 1 month, a post-traumatic cyst had formed in all patients with relevant cord damage. Over 1 year, both lesion area and width declined at a decreasing rate, whereas lesion length remained essentially unchanged. The removal of granular debris and axon/myelin fragments at the lesion epicenter by cerebrospinal fluid circulation (Noble and Wrathall, 1985) may explain decreasing lesion size. Recovery of upper limb function at 1 year was associated with lesion area (i.e., intramedullary damage) at 1 month post-injury. Because biological changes at the lesion site are complex and include death of motor neurons (Grumbles and Thomas, 2017) as well as axonal degeneration (Buss *et al.* , 2005), larger lesions might represent greater loss of motoneurons and axons. It is therefore possible that better recovery of upper extremity function was attributed to smaller lesions in which motor neuron pools innervating arm and hand muscles were less affected by trauma (Grumbles and Thomas, 2017).

Clinical measure at 1-year follow-up (dependent variable)	MR parameter at 1 month (independent variable)	n	p	R^2	Standardized regression coefficient (95% CI)
LEMS	Midsagittal tissue bridges	23	0.008	0.593	6.034 (1.751 10.317)
	Lesion area	24	0.001	0.408	-0.230 (-0.353 -0.108)
	Lesion length	24	<0.001	0.448	-1.797 (-2.679 -0.916)
UEMS	Lesion area	24	0.005	0.305	-0.097 (-0.163 -0.033)
	Lesion length	24	0.005	0.311	-0.733 (-1.215 -0.251)
GRASSP	Lesion area	16	0.013	0.367	-0.535 (-0.937 -0.132)
	Lesion length	16	0.009	0.400	-4.504 (-7.670 -1.338)
SCIM score	Midsagittal tissue bridges	23	0.002	0.365	12.293 (4.927 19.658)
	Lesion area	24	0.019	0.227	-0.258 (-0.469 -0.048)
	Lesion length	24	0.020	0.222	-1.900 (-3.475 -0.326)
Pin-prick score	Midsagittal tissue bridges	23	<0.001	0.475	13.499 (7.054 19.944)
	Lesion area	24	0.005	0.301	-0.296 (-0.495 -0.097)
	Lesion length	24	0.004	0.321	-2.271 (-3.731 -0.810)
	Lesion width	24	0.013	0.247	-5.886 (-10.427 -1.345)
Light-touch	Midsagittal tissue bridges	23	0.014	0.255	9.151 (2.045 16.258)
	Lesion area	24	0.016	0.237	-0.248 (-0.444 -0.051)
	Lesion length	24	0.013	0.249	-1.891 (-3.343 -0.440)

Table 4: Regression models predicting outcome at 1-year follow-up with quantitative MR measures at 1 month. N indicates number of subjects included in the regression models. All models are adjusted for age. Please note that for all correlations with tissue bridges, only those patients without complete cord transection were included.

Abbreviations: GRASSP = Graded Redefined Assessment of Strength, Sensibility and Prehension; LEMS = Lower Extremity Motor Score; UEMS = Upper Extremity Motor Score; SCIM = Spinal Cord Independence Measure.

All incomplete patients (AIS B–D) showed midsagittal tissue bridges, the size and location of which remained stable over time. The presence and size of midsagittal tissue bridges was paralleled by recordable electrophysiological information flow across the lesion and clinical recovery below the lesion (eg, LEMS). Interestingly, only in 2 of 20 patients with thinner tissue bridges were evoked potentials not recordable. This suggests that a crucial amount of fibers permissive for electrophysiological information flow is necessary to drive the complex processes of recovery of function below the lesion level (Kakulas *et al.* , 1998, Courtine *et al.* , 2009). This structure-function relationship indicates that neuronal tissue within the tissue bridges contain fibers that conduct afferent and efferent information of ascending and descending pathways. Plastic changes, such as regenerative sprouting (Freund *et al.* , 2006) and formation of detour circuits (Davies *et al.* , 1997, Filli *et al.* , 2014), likely contributed to the (re-)occurrence of information flow fostering functional recovery.

2.5.1 Limitations

This study has some limitations. First, the ratio of males to females was not balanced and therefore might be a limitation to its generalizability. However, the high male/female ratio is indeed representative in SCI and therefore our cohort reflects the inhomogeneity observed in SCI (Curt *et al.* , 2008). Second, because we intended to find a simple, clinically feasible measurement, midsagittal tissue bridges might not best assess tissue bridges of descending white matter tracts given that these would be located more laterally. Future studies should attempt to quantify also parasagittal tissue bridges, which, however, require more sophisticated MRI protocols with higher in-plane resolution and better signal-to-noise ratio. All findings should be validated with a larger sample size before entering clinical trials and clinical practice for stratification of study cohorts and prediction of individual recovery of function.

2.6 Conclusion

Preserved midsagittal tissue bridges may be an important diagnostic criterion for cohort selection and stratification for regenerative treatment trials in acute and chronic SCI (Guest *et al.* , 1997, Silver and Miller, 2004, Freund *et al.* , 2006) and for supraspinal control during epidural stimulation (Harkema *et al.* , 2011). This study characterized the changes occurring at the lesion epicenter in the first year post SCI and identified in vivo tissue bridges as a vital substrate for clinical recovery in cervical SCI. As early biomarkers, midsagittal tissue bridges appear to be sensitive and accurate predictors of clinical outcome and hold significant potential, next to clinical measures, for use in clinical practice and clinical trials. Directions of future studies include addressing our limited understanding of the importance of location and integrity of tissue bridges by using high-resolution sequences of the spinal cord.

3 Study II

Dorsal and ventral horn atrophy is associated with clinical outcome after spinal cord injury

Eveline Huber, Gergely David, Alan Thompson, Nikolas Weiskopf, Siawoosh Mohammadi, Patrick Freund

This orginal article is in press in Neurology.

EH, NW, SM and PF were involved in the concept and design of the study. Acquisition and analysis of data was conducted by EH and DG. EH, AT, and PF wrote the manuscript. All authors reviewed the manuscript.

3.1 Abstract

Objective: This study investigates whether grey matter pathology above the level of injury, alongside white matter changes, also contributes to sensorimotor impairments following spinal cord injury (SCI).

Methods: A 3T MRI protocol was acquired in 17 tetraplegic patients and 21 controls. A sagittal T2-weigthed sequence was used to characterize lesion severity. At the level C2/C3, a high-resolution T2*-weighted sequence was used to assess cross-sectional areas of grey and white matter including their sub-compartments; a diffusion weighted sequence was used to compute voxel-based diffusion indices. Regression models determined associations between lesion severity, tissue-specific neurodegeneration and associations of the latter with neurophysiological and clinical outcome.

Results: Neurodegeneration was evident within the dorsal and ventral horns and white matter above the level of injury. Tract-specific neurodegeneration was associated with prolonged conduction of appropriate electrophysiological recordings. Dorsal horn atrophy was associated with sensory outcome, while ventral horn atrophy was associated with motor outcome. White matter integrity of dorsal columns and corticospinal tracts was associated with daily-life independence.

Conclusion: Our results suggest that, next to antero- and retrograde degeneration of white matter tracts, neuronal circuits within the spinal cord far above the level of injury undergo trans-synaptic neurodegeneration, resulting in specific grey matter changes. Such improved understanding of tissue-specific cord pathology offers potential biomarkers with more efficient targeting and monitoring of neuroregenerative (i.e. white matter) and neuroprotective (i.e. grey matter) agents.

3.2 Introduction

Spinal cord injury (SCI) usually leads to sensorimotor dysfunction resulting from damage at the level of injury. However, a complex cascade of secondary neurodegenerative processes occurs across the spinal cord and brain (Huber *et al.* , 2015). In chronic SCI, cervical cord atrophy of up to 30% has been reported above the level of injury; its magnitude relating to the degree of clinical impairment (Freund *et al.* , 2011a). Recent improvements in diffusion-weighted imaging and anatomical sequences with higher in-plane resolution (Martin *et al.* , 2016), combined with advanced post-processing techniques (Mohammadi *et al.* , 2013a, David *et al.* , 2017) now allow assessing grey and white matter changes in the cervical spinal cord occurring after SCI.

Although white matter pathology within the spinal cord contributes to sensorimotor impairments, the functional effects of grey matter pathology above the level of injury are uncertain. Improved understanding of tissue-specific cord pathology may allow more efficient targeting and monitoring of neuroregenerative and neuroprotective agents. This study therefore addresses (i) to what extent cord atrophy above the level of injury is driven by pathophysiological processes occurring in grey and white matter, (ii) whether lesion severity is associated with the magnitude of neurodegeneration above the level of injury, and (iii) whether the tissue-specific neurodegeneration is associated with neurophysiological and clinical outcome.

Based on structural and diffusion MRI data we assessed tissue-specific cord pathology above the level of injury in chronic SCI patients when compared to healthy controls. These measures included the assessment of dorsal and ventral horn areas (Grabher *et al.* , 2017), diffusivity changes within the major spinal pathways, and associations between lesion severity (Huber *et al.* , 2017), tissue-specific pathology and neurophysiological changes.

3.3 Materials and Methods

3.3.1 Standard Protocol Approvals, Registrations, and Patient Consents

Our study protocol was designed in accordance with the Declaration of Helsinki and was approved by the local Ethics Committee of Zurich (KEK-ZH-Nr. 2012-0343, PB_2016-00623). All participants gave their written informed consent prior to participation.

3.3.2 Participants

We recruited 17 SCI patients (mean age: 48.7±14.1 years, three females) between November 2014 and May 2016, who were preciously admitted to the University Hospital Balgrist (Zurich, Switzerland). Twenty-one healthy controls (mean age: 41.7±11.3 years, seven females) from the local neighborhood served as a control data set which was acquired and used in a previous study (Grabher *et al.* , 2016).

Inclusion criteria for SCI patients were 1) traumatic cervical SCI, 2) no other neurological or mental disorders affecting clinical outcome, 2) age between 18 to 70 years, 3) MRI compatible, and 4) no pregnancy.

3.3.3 Clinical Assessments

All patients were examined with comprehensive clinical protocols to assess neurological and functional impairment. These included 1) the International Standards for Neurological Classification of Spinal Cord Injury protocol for motor, light-touch and pin-prick score and completeness of injury (Kirshblum *et al.* , 2011), 2) the Spinal Cord Independence Measure (SCIM) to measure daily life independence (Itzkovich *et al.* , 2007), 3) Graded Redefined Assessment of Strength, Sensibility and Prehension (GRASSP) for assessing upper limb function (Kalsi-Ryan *et al.* , 2012ab), and 4) the Walking Index for Spinal Cord Injury (WISCI) (Dittuno *et al.* , 2001). All patients completed the full protocol, except GRASSP score was not available for 1 patient.

3.3.4 Neurophysiological Assessments

Contact heat evoked potentials (CHEPs) and somatosensory evoked potentials (SSEPs) were acquired bilaterally in patients at the dermatomes C4, C6 and C8 to measure the integrity of the spinothalamic tract (i.e. CHEPs) and the dorsal column (i.e. SSEPs). For the acquisition of CHEPs (Kramer *et al.* , 2013) and SSEPs (Kramer *et al.* , 2008), the same protocols were applied as previously described.

3.3.4.1 Contact heat evoked potentials

A contact heat stimulator (PATHWAY Pain & Sensory Evaluation System, Medoc, Israel) was used to deliver contact heat stimuli from a baseline temperature of 35°C to a peak temperature of 52°C with a heating rate of 70°C/s and a cooling rate of 40°C/s. For each dermatome, we first assessed heat perception and pain thresholds within two consecutive trials. For the CHEPs recording, scalp recording sites were prepared with Nuprep (D.O. Weaver & Co, Aurora, CO) and alcohol. Three 9mm Ag/AgCl surface disc electrodes were positioned according to the international 10-20 system with the active electrode at the Cz position and referenced to linked earlobes (A1-A2); impedances were kept below 5kΩ. Ten to 15 contact heat stimuli were applied (interstimulus interval=8-12seconds). Two seconds after each stimulus, an audio cue appeared and patients rated their perceived intensity according to numerical rating scale. All signals were sampled from 100ms pre-trigger to 1500ms post-trigger at a sampling rate of 2000Hz using a preamplifier (20 000×, bandpass filter=0.25-300Hz, ALEA Solutions, Switzerland). Data were recorded in a LabView-based program (V1.43 CHEP, ALEA Solutions, Switzerland) with a 100-millisecond period pretrigger and 1-second posttrigger. Raw data was bandpass filtered from 0.5-30Hz.

3.3.4.2 Somatosensory evoked potentials

For dermatomal SSEPs, Key Point (Medtronic, Mississauga, Canada) was used to record and deliver electrical stimulation of 3Hz. Stimuli were elicited by single 0.2-msec, repetitive, square wave electrical stimulation. We first assessed electrical perception and pain thresholds for each dermatome (not exceeding 40mA) within two consecutive trials. For the recording of SSEPs, surface gel electrodes (10mm) were used on each dermatome after having the skin prepared with Nuprep (D.O. Weaver & Co, Aurora, CO) and alcohol. Disposable needle electrodes (Spes Medica, S.r.l., Italy) were positioned according to the international 10-20 system with the active electrode positioned at the contralateral side for the stimulated dermatome (C3-C4) referenced to Fz; impedances were kept below 5kΩ. The stimulation intensity was individually set as threefold electrical perception threshold. Averages of two traces of 300 cortical responses were obtained for each dermatome. Raw data was bandpass filtered from 2-2000Hz.

3.3.4.3 Neurophysiological Classification

We determined amplitudes and latencies of each dermatome for each patient after averaging all single trial waveforms for CHEPs (i.e. N2P2, N2, P2) and SSEPs (i.e. N1P1, N1, P1).

Furthermore, CHEPs and SSEPs were classified as normal (onset latency ≤ 2 standard deviations from control dermatome recording), pathological (onset latency > 2 standard deviations from control dermatome recording) or absent (not recordable) (Kramer *et al.* , 2008). The full CHEPs protocol was acquired in 14 patients and partially in 1 patient. For SSEPs, 12 patients received the full protocol and 2 patients participated in part of the protocol.

3.3.5 Image Acquisition

All imaging was performed on a clinical 3T Skyra^{Fit} scanner (Siemens Healthcare, Erlangen, Germany) equipped with a 16-channel radio-frequency receive-only head and neck coil and a radio-frequency body transmit coil. A stiff neck (Laerdal Medicals, Stavanger, Norway) was used in all participants to minimize motion artefacts. Due to motion artefacts, one patient was excluded from macrostructural analysis, and three patients had to be excluded from microstructural analysis.

At the lesion epicenter a sagittal T1-weighted (TR=600ms, TE=9.9ms, flip angle=150°, in-plane resolution=0.57mm×0.57mm, slice thickness=3.3mm), a sagittal T2-weighted (TR=3500ms, TE=84ms, flip angle=160°, in-plane resolution=0.34mm×0.34mm, slice thickness=2.75mm) and an axial T2-weighted image (TR=5510ms, TE=93ms, flip angle=150°, in-plane resolution=0.5mm×0.5mm, slice thickness=3.6mm) were acquired to assess the lesion size.

At the cervical cord above the level of injury (centered at C2/C3), five volumes were acquired with a T2*-weighted 3D multi-echo GRE sequence (multiple echo data image combination (Schmid *et al.* ,

2005)) in the oblique axial plane (i.e. perpendicular to the cord) to assess grey and white matter atrophy. Each of the five volumes acquired, consisted of 20 partitions with a resolution of 0.5×0.5mm^2 (FOV=192×162mm^2, slice thickness=2.50mm (10% gap), TR=44ms, TE=19ms, flip angle = 11°, readout bandwidth=260 Hz/pixel). Each volume took 2.13 minutes to acquire. Application of zero filling interpolation doubled the nominal in-plane resolution (0.25×0.25mm^2).

At the identical level, a high-resolution DTI dataset was acquired using a cardiac-gated reduced-FOV single-shot spin-echo EPI sequence with outer volume suppression (Morelli *et al.* , 2010) to assess microstructural changes of the whole spinal cord. Four measurements of 6 b=0 (T2-weighted) and 30 500s/mm^2 (diffusion-weighted) volumes were acquired, resulting in 144 images per participant and a nominal acquisition time of 6.17 minutes. The following parameters were applied: TR=350ms; TE=71ms; slice thickness=5mm (10% inter-slice gap); resolution=0.76×0.76mm^2; FOV=133×30mm^2; phase-oversampling=50%; 5/8 Partial-Fourier Imaging in phase-encoding direction; cardiac trigger delay=200ms; minimal time between triggers=1800ms. After acquisition, zero filling interpolation was used to double the in-plane resolution (0.38×0.38mm^2).

3.3.6 Image Processing

3.3.6.1 Lesion segmentation

Using the Jim 6.0 software (Xinapse systems, Aldwincle, UK), the lesion was segmented on the midsagittal T2-weighted images being visible as a high signal intensity area within the spinal cord as previously described (Huber *et al.* , 2017). Following parameters were quantified: 1) midsagittal anterior-posterior lesion width (=maximal anterior-posterior width of the lesion), 2) midsagittal rostrocaudal lesion length (=maximal caudocranial extent of the lesion), 3) total midsagittal lesion area, and 4) midsagittal thickness of midsagittal ventral and dorsal tissue bridges at the widest point of the lesion which was summed up to the total amount of midsagittal tissue bridges.

3.3.6.2 Processing of high-resolution macrostructural data above the level of injury

We used serial longitudinal registration (Ashburner and Ridgway, 2012) embedded within SPM 12 to average the five 3D MEDIC volumes, accounting for intra-subject motion. To further increase signal-to-noise ratio, the average volume was resampled at a double slice thickness. We then used the Jim 6.0 software to measure cross-sectional SCA of 3 slices. After marking the midpoint of the spinal cord manually in each slice, the SCA was calculated automatically using the semi-automatic 3D active-surface model (Horsfield *et al.* , 2010). GMA, DCA, and VHA (approximately lamina VI-IX) and DHA (approximately lamina I-V) were extracted manually (Grabher *et al.* , 2017). WMA was calculated by subtracting the GMA from the SCA. The mean inter- and intra-observer reliability for these measures was previously shown (Morelli *et al.* , 2010, Grabher *et al.* , 2016).

3.3.6.3 Pre-processing and estimation of DTI data

All processing of the DTI data was carried out using a modified version of the Matlab-based ACID toolbox optimized for the spinal cord. First, we reduced the in-plane FOV to 24×24mm^2 to exclude much of the non-spinal cord tissue in each participant. Then, DTI volumes were slice-wise linearly registered with 3 degrees of freedom (translation in the frequency- and phase-encoding direction, scaling in the phase-encoding direction) to correct for intra-subject motion and eddy-current artifacts (Mohammadi *et al.* , 2010). A diffusion tensor was fitted using a robust tensor fitting algorithm that accounts for outlier volumes due to motion and physiological artifacts (Mohammadi *et al.* , 2010). Following DTI index maps were extracted: fractional anisotropy (FA), and mean, axial and radial diffusivity (MD, AD, RD).

These DTI index maps were then spatially normalized to a self-constructed mean diffusivity template residing in the spinal MNI space (Fonov *et al.* , 2014). To further refine the accuracy of the registration, a manual slice-by-slice registration (in-plane translation and scaling) was performed. Finally, all DTI index maps were smoothed using a full-width at half maximum Gaussian kernel with 0.5×0.5×5mm^3.

3.3.7 Statistical Analysis

Statistical analysis of all macrostructural MRI data, neurophysiological and clinical data was performed using Stata13 (StataCorp LP, Texas, USA). The mean age was not statistically different between healthy controls and patients (Mann-Whitney U test: z=-1.61, p=0.10). All images were visually inspected for artifacts and the analysis was conducted on 3 slices from each modality at the same level.

First, we assessed the morphometric differences in SCA, GMA, WMA, DCA, VHA and DHA between patients and healthy controls by means of ANCOVA, adjusted for age. For microstructural differences between patients and healthy controls, we used SPM12 for voxel-based analysis of the different DTI indices (FA, MD, AD, RD) by means of ANCOVA, adjusted for age. All statistical parametric maps were initially thresholded with a cluster defining threshold of $p<0.01$ (uncorrected) and clusters surpassing a cluster threshold of $p<0.05$ (family-wise error corrected) are reported. Next, we used linear regression analysis to investigate the relationship between changes at the lesion site (midsagittal lesion area, length and width, and size of midsagittal tissue bridges) and remote cord macro- and microstructural changes. We then determined associations between macrostructural (SCA, GMA, WMA, DCA, VHA and DHA) and microstructural (DTI indexes within lateral corticospinal tract, dorsal column and spinal lemniscus) parameters, and tract-specific clinical measures (motor, pin-prick, and light-touch score, GRASSP, SCIM) using linear regression models, adjusted for age and lesion area. Finally, we investigated associations between macro- and microstructural MRI indices and neurophysiological outcome measures using linear regression models, adjusted for age and lesion

area. Note, that only patients with both recordable electrophysiological potentials and available MRI data entered this regression analysis, resulting in a total number of 8 patients. For all microstructural associations, we extracted mean values of DTI indexes within anatomical region of interests (lateral corticospinal tract, dorsal column and spinal lemniscus (containing spinothalamic and spinoreticular tracts)) as embedded in the Spinal Cord Toolbox (De Leener *et al.* , 2017). The level of significance was set to $p<0.05$.

3.4 Results

3.4.1 Radiologic, clinical and neurophysiological characteristics

Patients were scanned 6.7±7.8 years after injury. An area of hyper-intense signal was visible on the T2-weighted sagittal images in 16 patients [Fig. 5AB]; 13 patients showed hyper-intensities in their dorsal column, covering, on average, 41.4±21.0 % of the whole dorsal column and two patients showed hyper-intensities in the dorsolateral funiculus (e.g. corticospinal tract). The radiological level of injury (hyper-intense T2-weighted signal) covered the vertebral level C3-C5 in one patient, C3 in one patient, C4 in two patients, C4-C5 in one patient, C5 in two patients, C6 in two patients, C6-C7 in four patients and C7 in two patients. Two patients showed no signal alteration within the cord. The average lesion area was 45.4±66.6 mm^2 with a lesion length of 11.3±9.4 mm and a lesion width of 4.3±3.5 mm. In two patients, the lesion occupied the full cord area and no midsagittal tissue bridges could be identified. In the remaining 15 patients, the midsagittal tissue bridges had an average width of 2.9±1.9 mm. No MR abnormalities were identified in the control group.

Two patients were motor and sensory complete, two patients were motor complete and sensory incomplete, and the remaining 13 patients were motor and sensory incomplete. The motor score [max. 100] was 68.1±30.4, the light-touch score was (mean ± SD) 66.3±32.7 [max. 112], and the pin-prick score [max. 112] was 52.7±35.0. Manual dexterity was impaired as assessed by the GRASSP score, (149.8±66.3 [max. 232]) and functional independence was impaired as assessed by the SCIM score ([63.1±31.3 [max. 100]). Eight patients were able to walk independently [20/20 points in the WISCI score], two patients were dependent on walking aids [5/20 and 9/20 points in the WISCI score] and seven patients were not able to walk [0/20 points]. All data is summarized in Table 5.

All patients had neurophysiological impairment of the spinothalamic tract, and a majority had impaired function of the dorsal column below the level of lesion as assessed by CHEPs and SSEPs, respectively. The mean (± SD) perception/pain thresholds as well as amplitudes and latencies of the recorded signals are shown in Table 6.

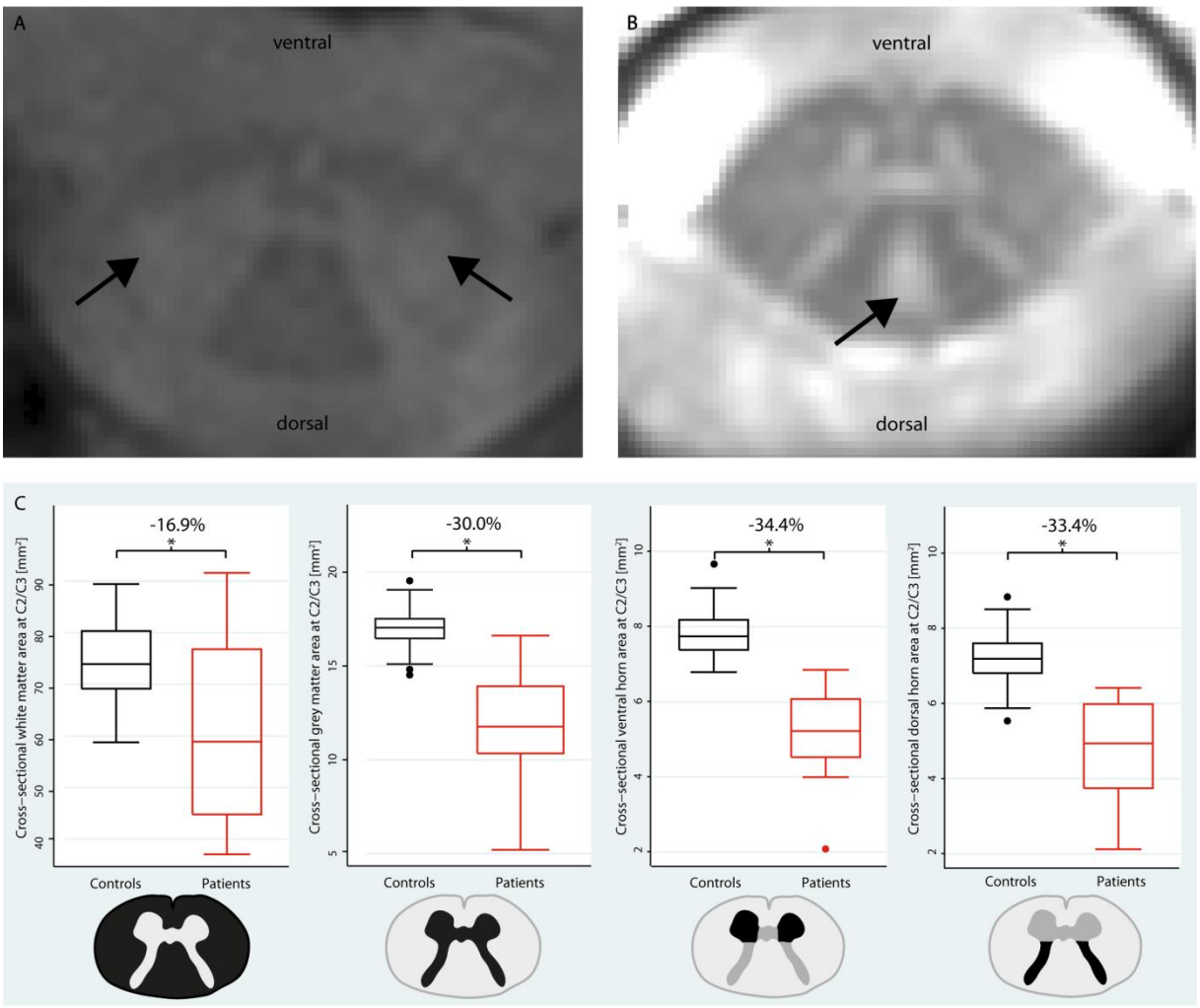

Figure 5: Macrostructural changes above the level of injury. Hyperintense regions most likely indicating A) retrograde degeneration in the corticospinal tract, and B) anterograde degeneration in the dorsal column. Arrows are indicating the corresponding locations. C) Differences between the cross-sectional white matter area, cross-sectional grey matter area, cross-sectional ventral horn area, and cross-sectional dorsal horn area in patients compared to healthy controls.

ID	Gender	Age [y]	Years since injury	Radiological level of injury	AIS grade	Neurological level of injury	Motor score	Light-touch score	Pin-prick score	SCIM score	GRASSP score	WISCI
1	male	29	1.0	C4-C5	A	C4	14	16	13	22	21	0
2	female	40	7.0	C3-C5	A	C4	7	71	12	19	43	0
3	female	39	25.0	C6-C7	B	C5	30	32	34	28	125	0
4	male	50	25.1	C6-C7	B	C7	46	62	26	63	188	5
5	male	70	0.7	C5	C	C2	46	48	34	19	71	0
6	female	32	1.2	C6-C7	C	C6	44	33	24	23	92	20
7	male	51	4.3	NS	D	C1	82	90	57	100	130	20
8	male	56	5.6	C4	D	C2	88	56	26	40	151	0
9	male	43	13.1	C7	D	C2	76	55	55	74	225	0
10	male	60	0.3	C3	D	C3	78	60	60	67	NA	9
11	male	50	7.6	C4	D	C3	84	10	10	97	136	20
12	male	48	1.8	NS	D	C4	100	112	107	100	232	20
13	female	63	0.3	C5	D	C6	85	109	99	70	172	20
14	male	69	0.2	C6	D	C6	99	109	99	87	206	20
15	male	67	12.6	C6-C7	D	C7	91	110	107	99	183	20
16	male	27	4.7	C6	D	C7	92	72	45	75	189	20
17	male	33	3.0	C7	D	C8	96	82	88	89	232	20

Table 5: Clinical and epidemiological data for all patients included in the study.

Abbreviations: AIS = American Spinal Injury Association Impairment Scale; GRASSP = Graded Redefined Assessment of Strength, Sensibility and Prehension; NA = not available; NS = no signal alteration within myelon; SCIM = Spinal Cord Independence Measure; WISCI = Walking Index for Spinal Cord Injury

	C4 Dermatome		C6 Dermatome		C8 Dermatome	
CHEPs	Left	Right	Left	Right	Left	Right
Heat perception threshold [°C]	43.97 ± 3.26 (15/15)	44.94 ± 4.20 (13/14)	45.18 ± 5.69 (11/15)	41.86 ± 4.36 (11/15)	47.08 ± 3.82 (10/14)	45.27 ± 4.28 (8/14)
Pain threshold [°C]	50.12 ± 2.58 (11/15)	49.21 ± 3.53 (10/14)	49.56 ± 3.78 (6/15)	51.33 ± 2.75 (10/15)	49.50 ± 3.60 (4/14)	51.51 ± 2.12 (7/14)
Detectable signal	8/15	8/14	4/15	7/15	0/14	5/14
Pathological signal	3/8	1/8	1/4	1/7	-	0/5
N2 latency [ms]	409.12 ± 108.68	349.56 ± 78.45	357.38 ± 114.40	400.33 ± 63.15	-	352.88 ± 102.19
P2 latency[ms]	506.63 ± 109.63	479.06 ± 90.75	461.38 ± 114.78	530.92 ± 45.90	-	466.13 ± 128.11
N2P2 amplitude [µV]	39.28 ± 34.59	40.57 ± 48.16	33.21 ± 29.96	25.72 ± 20.05	-	30.45 ± 26.18
SSEPs	Left	Right	Left	Right	Left	Right
Electrical perception threshold [mA]	4.26 ± 2.87 (11/12)	3.30 ± 1.94 (12/12)	6.49 ± 10.15 (13/14)	8.18 ± 13.35 (12/14)	7.28 ± 7.75 (12/14)	5.59 ± 4.52 (11/14)
Pain threshold [mA]	24.1 ± 12.02 (11/12)	26.24 ± 14.81 (12/12)	17.72 ± 6.56 (12/14)	17.63 ± 7.35 (11/14)	19.06 ± 12.60 (11/14)	15.7 ± 8.04 (10/14)
Detectable signal	10/12	11/12	11/14	9/14	9/14	9/14
Pathological signal	1/10	0/11	1/11	0/9	2/9	1/9
N1 latency [ms]	15.29 ± 3.07	15.78 ± 1.95	24.65 ± 2.23	23.92 ± 2.43	26.31 ± 3.20	26.08 ± 2.68
P1 latency [ms]	21.57 ± 4.95	23.40 ± 3.10	29.71 ± 3.18	29.60 ± 2.69	31.07 ± 3.58	31.30 ± 2.87
N1P1 amplitude [µV]	1.04 ± 1.49	1.22 ± 1.64	1.06 ± 0.62	1.33 ± 0.75	0.81 ± 0.47	1.08 ± 0.57

Table 6: Neurophysiological data acquired in patients. Mean ± SD are shown. Numbers in brackets refer to the amount of patients with detectable threshold/signals over the total amount of measured patients.

Abbreviations: CHEPs = contact heat evoked potentials; SSEPs = somatosensory evoked potentials

3.4.2 Pathophysiological changes in the cervical cord above the level of injury

Compared to healthy controls, patients showed a decreased SCA of 20.2% ($p<0.001$, healthy controls: 92.30±8.49mm^2, patients: 73.71±20.04mm^2). In patients, WMA was decreased by 16.9% ($p=0.001$, healthy controls: 75.34±8.06mm^2, patients: 62.64±18.22 mm^2), and GMA was decreased by 30.0% ($p<0.001$, healthy controls: 16.96±1.25mm^2, patients: 11.93±2.73mm^2). In the white matter, DCA was decreased by 21.4% ($p<0.001$, healthy controls: 23.73±2.99mm^2, patients: 18.65±4.76 mm^2). Within the grey matter, the bilateral VHA showed a 34.4% decrease in patients compared to healthy controls (left: $p<0.001$; healthy controls: 3.84±0.29mm^2, patients: 2.56±0.62mm^2; right: $p<0.001$, healthy controls: 3.95±0.40mm^2, patients: 2.61±0.58mm^2). In patients, the DHA was decreased bilaterally by 33.4% (left: $p<0.001$, healthy controls: 3.63±0.41 mm^2, patients: 2.42±0.66mm^2; right: $p<0.001$, healthy controls: 3.60±0.51mm^2, patients: 2.37±0.66mm^2) [Fig. 5C], and smaller DHA was associated with smaller DCA ($p<0.001$, $R^2=0.74$, 95%CI (2.21 4.28)).

Voxel-based analysis of the cervical cord revealed a 16.6% decrease in FA in the left dorsolateral funiculus (e.g. containing spinothalamic and lateral corticospinal tracts; $p=0.003$; localization (x, y, z): -4.2, -18.5, 26; z score=4.42; cluster extent=154), 14.9% decrease in the right dorsolateral funiculus ($p=0.025$; localization (x, y, z): 6, -18.5, 37; z score=4.34; cluster extent=85), and by 17.0% in the posterior funiculus (i.e. containing dorsal columns; $p=0.004$; localization (x, y, z): 0.7, -22.3, 37; z score=3.80; cluster extent=145) in patients compared to healthy controls. AD was also decreased in patients compared to healthy controls in the same regions, namely by 12.8% the left dorsolateral funiculus ($p=0.014$; localization (x, y, z): -3.1, -19.2, 26; z score=3.72; cluster extent=58), by 12.8% the right dorsolateral funiculus ($p=0.002$; localization (x, y, z): 4.1, -18.8, 26; z score: 4.70; cluster extent=94), and by 9.9% in the posterior funiculus ($p=0.020$; localization (x, y, z): 0.7, -19.2, 32; z score=3.69; cluster extent=52). RD increased by 31.8% in the dorsal column ($p=0.022$; localization (x, y, z): 0.3, -20.7, 37; z score=3.47; cluster extent=70) and by 34.0% in the left dorsolateral funiculus ($p=0.023$; localization (x, y, z): -5, -19.2, 32; z score=3.22; cluster extent=69) in patients compared to healthy controls. MD was not significantly different between patients and healthy controls [Fig. 6].

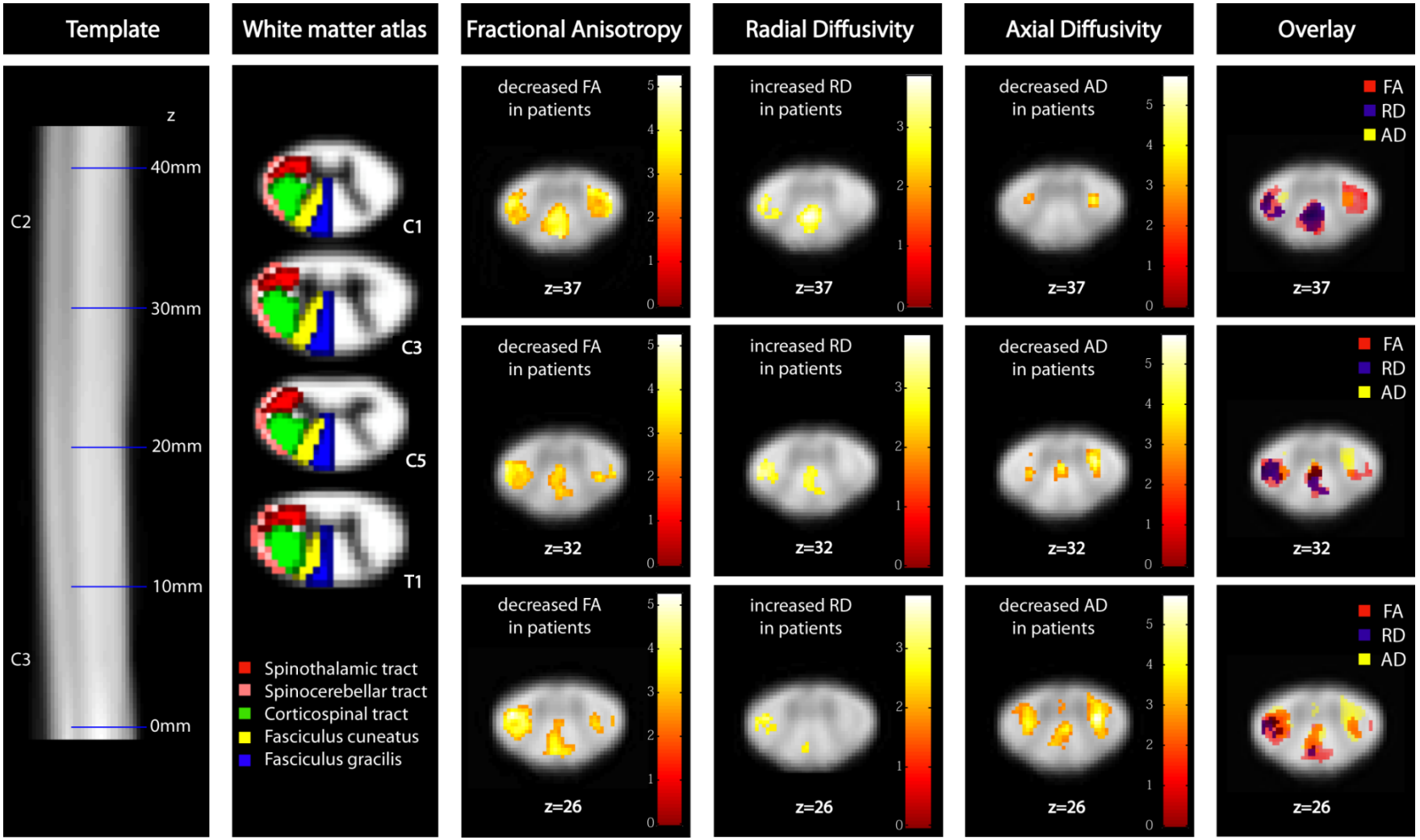

Figure 6: Microstructural changes above the level of injury. Voxel-wise analysis of microstructural changes above the level of injury in patients compared to healthy controls. The first row shows the spinal cord template and the second row shows the white matter atlas adapted from De Leener (2017). Note, the spatial overlap of the different DTI metrics showing that regions of decreased AD (e.g. axonal degeneration) but unaltered RD (e.g. no demyelination) lay mostly adjacent to the gray matter, where unmyelinated propriospinal neurons are located.

3.4.3 Relationship between lesion severity and remote tissue-specific neurodegeneration

Greater lesion area and length were associated with greater SCA decrease above the level of injury (lesion area: p=0.048, R^2=0.25, 95%CI: (-3.64, -0.23)1/mm^2; lesion length: p=0.006, R^2=0.42, 95%CI: (-0.55, -0.11)1/mm^2), independent of age. The width of total midsagittal tissue bridges was associated with less SCA decrease (p=0.007, R^2=0.39, 95%CI: (0.02, 0.11)1/mm^2). Greater lesion length was associated with smaller GMA (p=0.012, R^2=0.40, 95%CI: (-3.74, -0.57)1/mm^2), VHA (p=0.039, R^2=0.29, 95%CI: (-8.33, -0.25)1/mm^2), and DHA (p=0.004, R^2=0.49, 95%CI: (-8.36, -2.03)1/mm^2) while midsagittal tissue bridges were positively associated with GMA (p=0.035, R^2=0.28, 95%CI: (0.33, 0.78)1/mm^2) and DHA (p=0.011, R^2=0.38, 95%CI: (0.26, 1.74)1/mm^2) [Fig. 7A]. Greater lesion length and preserved midsagittal tissue bridges were associated with WMA (lesion length: p=0.014, R^2=0.38, 95%CI: (-0.61, -0.08)1/mm^2; tissue bridges: p=0.011, R^2=0.38, 95%CI: (0.02, 0.12)1/mm^2) above the level of injury [Fig. 7B].

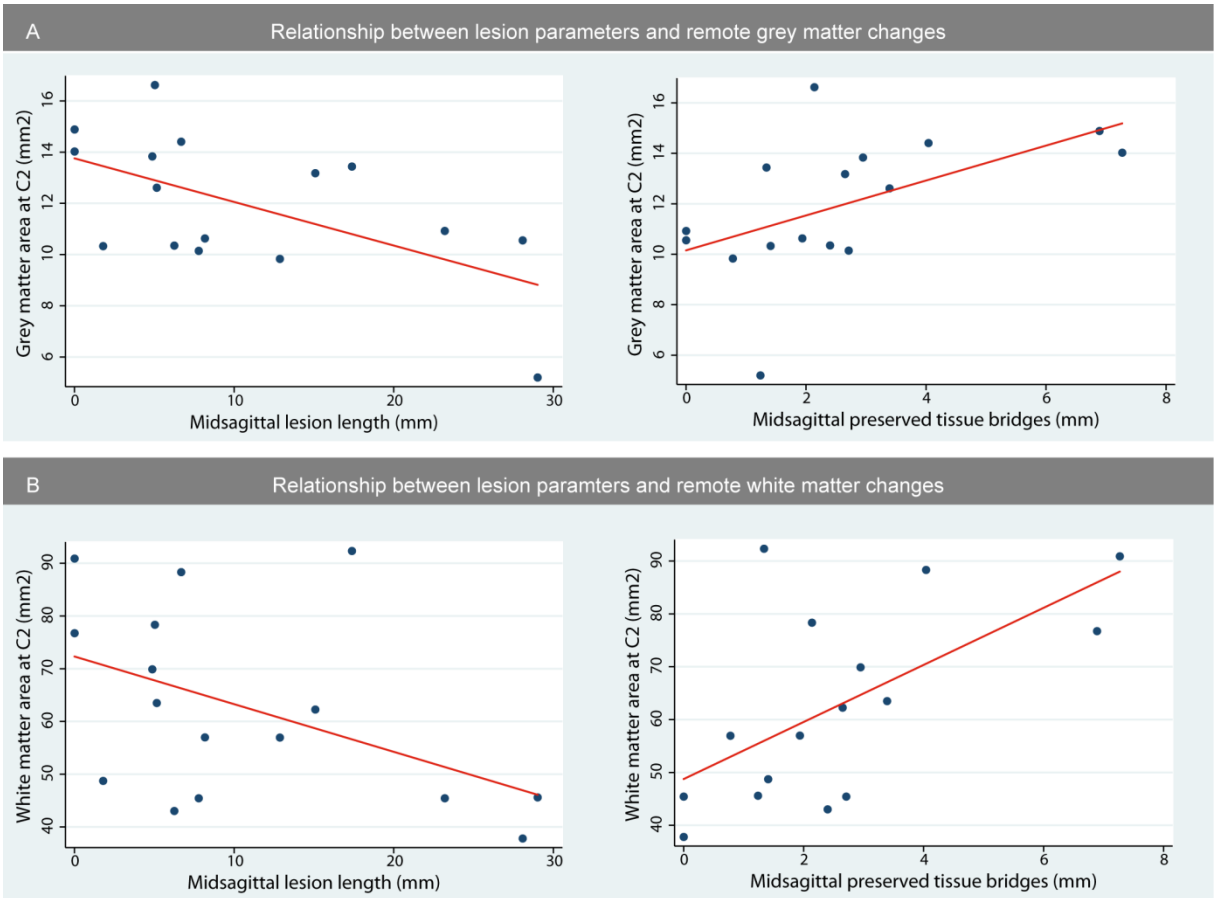

Figure 7: Relationship between lesion severity and neurodegeneration above the level of injury. The magnitude of tissue damage at the lesion site is associated with the amount of neurodegeneration above the level of injury. Lesion length and midsagittal tissue bridges are associated with remote grey matter (A) and white matter (B) atrophy.

The width of total midsagittal tissue bridges was associated with DCA above the level of lesion (p=0.019, R^2=0.29, 95%CI: (0.25, 2.39)1/mm^2). Neither lesion size nor midsagittal tissue bridges were associated with microstructural changes above the level of lesion.

3.4.4 Relationship between remote neurodegeneration and neurophysiological outcome

The size of the cross-sectional area of the dorsal columns identified those patients with bilateral recordable SSEPs of the dermatomes C6 and C8 [Fig. 8]. This relationship was not evident for the WMA and CHEPs. Higher AD values within the dorsal column were associated with shorter SSEP N1P1 latency at the C4 dermatome (p=0.0024, R^2=0.83, 95%CI: (-.00007, -.00001)10^{-3}*s^2/mm^2), corrected for age and lesion area. DTI metrics within the spinothalamic tracts were not associated with CHEPs recordings.

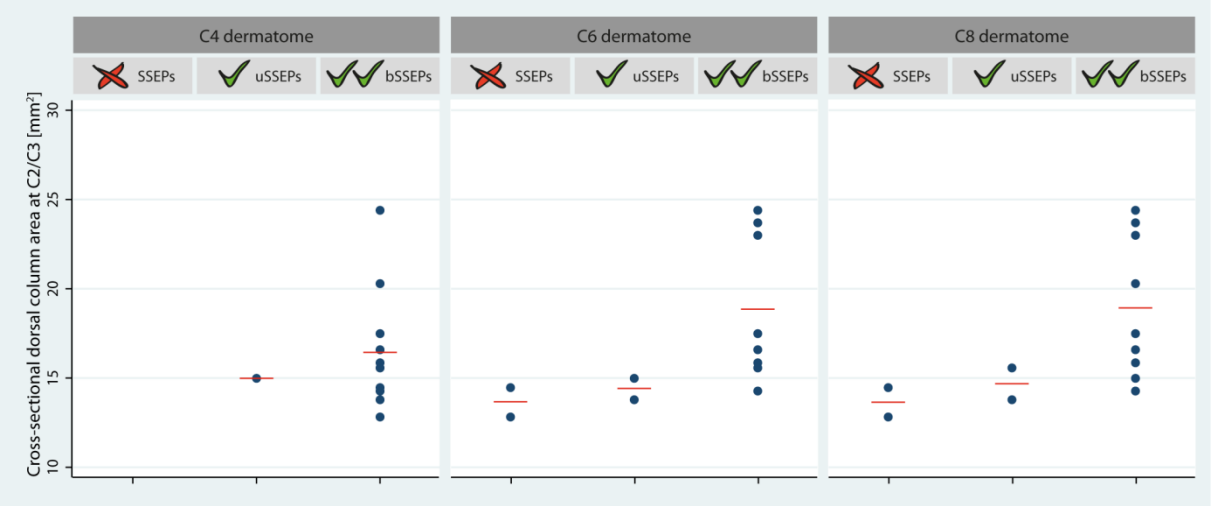

Figure 8: Relationship between neurodegeneration above the level of injury and electrophysiological outcome. Patients were grouped into 3 cohorts: without, with unilateral or with bilateral recordable dermatomal SSEPs at the level C4, C6 and C8. Patients with recordable dermatomal SSEPs showed a tendency towards larger dorsal column area above the level of injury. *Abbreviations: bSSEPs = bilateral somatosensory-evoked Potentials; uSSEPs = unilateral somatosensory-evoked potentials*

3.4.5 Relationship between remote neurodegeneration and clinical outcome

GMA was associated with motor score (p=0.007, R^2=0.72, 95%CI: (1.77, 9.26) and pin-prick score (p=0.003, R^2=0.58, 95%CI: (3.48, 13.90)), VHA area was associated with motor score (p=0.001, R^2=0.78, 95%CI: (6.74, 21.93)), and DHA was associated with pin-prick score (p=0.004, R^2=0.57, 95%CI: (7.43, 31.52)) when corrected for lesion area and age [Fig. 9A].

To quantify tract-specific associations with appropriate clinical outcome, we used the extracted mean values of DTI indexes within the regions of interest (i.e. corticospinal tract, dorsal column and spinothalamic tract). FA and RD within corticospinal tract and the dorsal columns were associated with SCIM score (corticospinal tract: FA: p=0.002, R^2=0.80, 95%CI: (105.82 361.55); RD: p=0.001, R^2=0.83, 95%CI: (-169829.70 -60547.48); dorsal columns: FA: p=0.002, R^2=0.80, 95%CI: (106.07 341.42); RD: p=0.003, R^2=0.79, 95%CI: (-216944.1 -60854.36)), independent of lesion extent and age [Fig. 9B]. AD within the dorsal columns was associated with GRASSP score, independent of lesion extent and age (p=0.30, R^2=0.60, 95%CI: (40298.4 646999.7)).

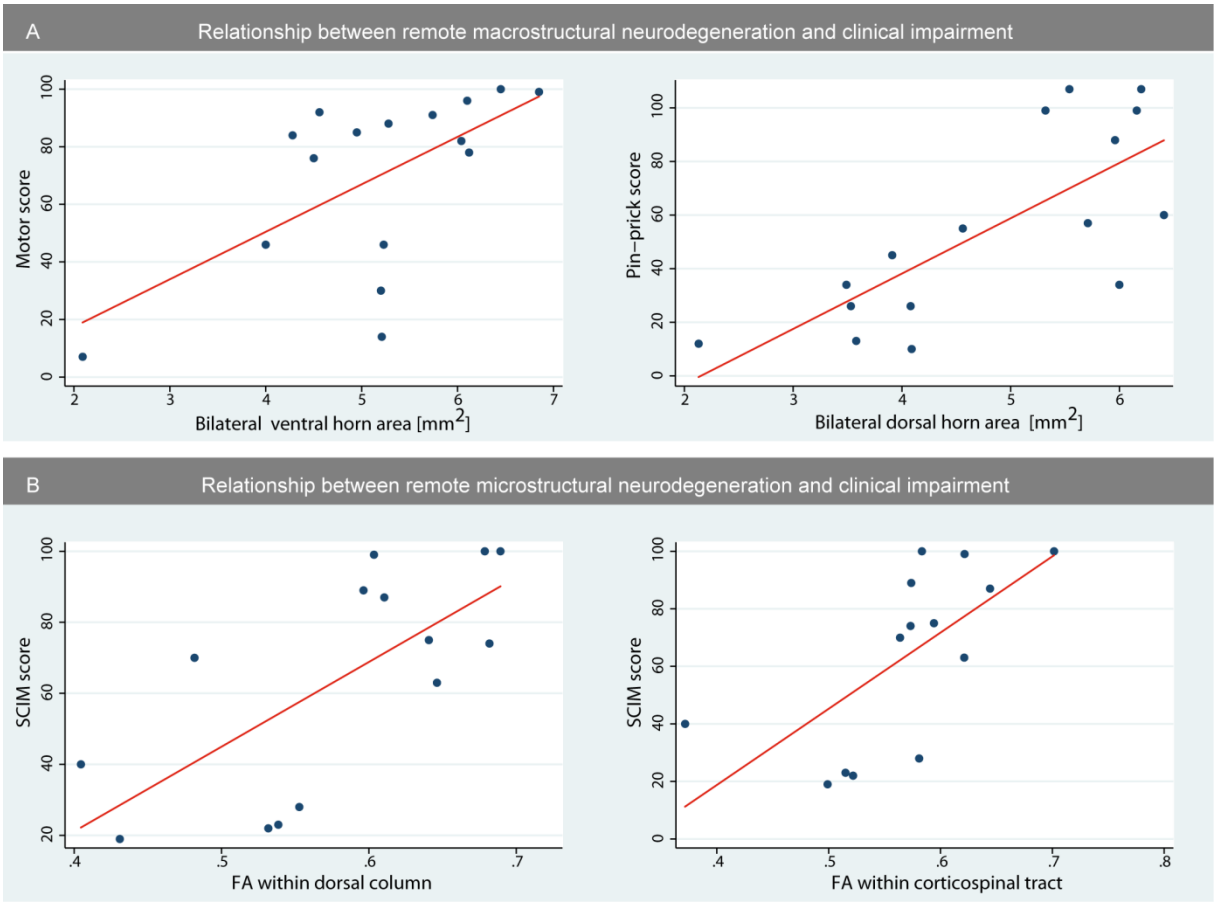

Figure 9: Relationship between neurodegeneration above the level of injury and clinical outcome. Associations between A) remote tract-specific macrostructural MRI parameters above the level of injury and clinical impairment, and B) remote tract-specific microstructural MRI indices above the level of injury and clinical impairment.

3.5 Discussion

This study shows the in-vivo structure function relationship between the extent of tissue-specific cord pathology and neurophysiological and clinical impairment following traumatic SCI. Crucially, we show that the magnitude of tissue damage at the lesion epicenter is associated with the extent of neurodegeneration above the level of lesion; which, in turn, is associated with clinically relevant impairment and neurophysiological abnormalities. These findings allow us to investigate the extent of tissue-specific neurodegeneration above the level of injury, its relationship to neuronal tissue loss at the site of the lesion, and its effect on neurophysiological and clinical outcome.

Tissue damage at the epicenter of a traumatic SCI results from both the direct effect of the traumatic insult, but also from damage to the vascular architecture and the ensuing ischemic effects on the neuronal and glial cell populations within the acute phase of injury (Schwab and Bartholdi, 1996). Remote from the epicenter of the lesion, secondary neurodegeneration within white (Crowe *et al.* , 1997, Ward *et al.* , 2014) and grey matter (Huang *et al.* , 2007) follows with a time lag and is driven by a multiphasic response to cellular inflammation (Beck *et al.* , 2010). While the extent of secondary remote atrophy has been quantified in vivo after injury (Freund *et al.* , 2011a, Lundell *et al.* , 2011, Freund *et al.* , 2012ab), we provide evidence that changes within both grey and white matter contribute to cord atrophy above the level of injury. This is in agreement with spinal grey matter degeneration distant to the initial site of damage in multiple sclerosis patients (Calabrese *et al.* , 2015) and experimental SCI (Pearse *et al.* , 2005). Although the relative decrease is larger within ventral and dorsal horns (i.e. grey matter), the absolute magnitude of change is larger within white matter, contributing more to the overall loss of SCA by 20.2%.

We uncovered an in-vivo relationship between neuronal tissue loss (i.e. lesion severity) and remote tissue-specific cord pathology above the level of injury. Moreover, we show an interdependence of remote white and grey matter atrophy (i.e. DHA and DCA). Neurodegenerative changes within grey matter above the level of injury are not likely to be specific for any single pathological process, but rather are likely to represent a combination of different pathological mechanisms taking place after SCI. Possible mechanisms involve transsynaptic/transneuronal degeneration affecting the propriospinal systems (Yu *et al.* , 2016, Grumbles and Thomas, 2017) and motor neurons located in the proximity of the spinal injury (Filli *et al.* , 2015). Next to direct effects of neurodegenerative processes, reduction in muscle activity of the upper extremity could lead to reduction of neuronal activity above the level of injury which translates into shrinkage of the neurons soma size.

Furthermore, demyelination of corticospinal projections to the dorsal horns (Lemon and Griffiths, 2005), the expression of neurotrophic factors from non-neuronal cells around neighboring degenerating axons (Lemon and Griffiths, 2005), growth-factor dysregulation (Bareyre and Schwab,

2003), as well as vascular remodeling (Cao *et al.* , 2017) could contribute to grey matter pathology. As white matter damage is known to induce microglial activation altering glutamate signaling, this process is thought to be responsible for the dying back of axons and their parternal neurons (Matute *et al.* , 2007), which might be a shared underlying disease mechanism. Thus, next to anterograde and retrograde degeneration of white matter tracts (Buss *et al.* , 2005, Kerschensteiner *et al.* , 2005, Freund *et al.* , 2012b), the neuronal circuits within the spinal cord far above the level of injury undergo a temporary structured neurodegeneration (Ward *et al.* , 2014).

Within the microstructure of the atrophied white matter, we found indications of both axonal degeneration and demyelination (Brennan *et al.* , 2013), represented by decreased FA and AD, and increased RD in the dorsolateral funiculus (e.g. containing the lateral corticospinal and spinothalamic tracts) and the posterior funiculus (e.g. containing the dorsal columns). Within the corticospinal tract and the dorsal column, leg function is represented most laterally, whereas arm function is located either medially (i.e. corticospinal tract) or centrally (i.e. dorsal column). Our observed changes cover the entire lateral corticospinal tract and the dorsal columns, indicating neurodegenerative processes affecting axons which convey information relating to leg and arm function. Spatially overlaying the different DTI metrics changes revealed that regions showing decreased AD (e.g. axonal degeneration), but unaltered RD (e.g. no demyelination), lay mostly adjacent to the gray matter border. This region contains the fasciculi proprii and contains mostly short, mainly unmyelinated propriospinal neurons (Flynn *et al.* , 2011). This underlies our hypothesis that SCI might lead to degeneration affecting interneurons within the spinal cord.

Our findings complement previous studies in SCI patients (Cohen-Adad *et al.* , 2011, Kamble *et al.* , 2011, Petersen *et al.* , 2012, Koskinen *et al.* , 2013) as it now locates these changes to grey and white matter rather than being non-specific in terms of location and tissue. Thus, our in vivo cord MRI measurements demonstrate a combination of structural and functional processes occurring over several segments above the level of injury affecting both grey and white matter and which is driven by lesion severity.

We show that tract-specific micro- and macrostructural changes are associated with prolonged conduction of appropriate electrophysiological recordings. This association suggests a structure-functional relationship, because the amount of neurodegeneration was directly associated with impairment of neurophysiological information flow. As the DTI signal is sensitive to altered diffusion properties occurring as a response to CNS damage (i.e. demyelination/ degeneration), and neuronal excitability is affected by morphometry of the axon and its myelin, it seems plausible that neurophysiological changes might be reflected in remote macro- and microstructural changes above the level of injury. Our findings complement previous findings showing that the topography and the

excitability of corticomotor projections were associated with cervical cord atrophy (Freund *et al.* , 2011ab).

Current assessments in SCI patients lack sensitivity to minimal changes in motor and sensory function (Ellaway *et al.* , 2011) as they cannot detect subtle changes due to remyelination and axonal regeneration. Neuroimaging biomarkers have the potential to track these subtle abnormalities as they are sensitive to microstructural changes (Huber *et al.* , 2015). In this study, the magnitude of both remote macro- and microstructural changes within grey and white matter was significantly associated with clinical impairment, independent of lesion extent. In particular, the extent of remote ventral horn atrophy was associated with motor impairment, whereas dorsal horn atrophy was associated with sensory disturbance. Microstructural tract-specific changes above the level of injury were related to measures of functional independence (i.e. SCIM) and strength, sensibility and prehension of the upper limbs (i.e. GRASSP). This suggests that high-resolution MRI sequences applied above the level of injury provide superior information on patient's clinical status compared to standard clinical sequences at the lesion site. In addition, the latter findings are striking as they suggest that remote neurodegeneration within grey matter above the level of injury contributes, in addition to white matter pathology, to motor and sensory impairment. This multi-level interaction supports the view that SCI leads to a cascade of activity-dependent neurodegenerative changes affecting the entire spinal cord and brain (Freund *et al.* , 2016). Characterizing these secondary neurodegenerative events has the potential to provide insights into new therapeutic interventions in addition to providing opportunities for monitoring treatment effects in trials conducted in acute and chronic SCI patients.

3.5.1 Limitations

This study had several limitations. Although our cohorts did not show a significant age difference; the mean age was on average higher in the patients group, which could potentially affect the analysis. We therefore adjusted for age as a potential confounder of no interest in all analyses. Further, unbiased voxel-based morphometry of DTI indices in the spinal cord have just started emerging[3] and the automated post-processing methods for spatial normalization of the spinal cord into common space are in their infancy. To increase the reliability of our analysis, we therefore manually corrected the spatial normalization to the template.

3.6 Conclusion

This study shows that the magnitude of dorsal and ventral horn and white matter structural changes above the level of injury are associated with appropriate clinical and neurophysiological impairment and are driven by the lesion severity. These findings suggest a combination of different pathological processes affecting both grey and white matter several segments above the level of injury, which are

clinically eloquent. Therefore, these neuroimaging biomarkers might serve as promising surrogate markers for future clinical trials supplementing (or complementing) clinical outcome measures.

4 Study III

Spectroscopic Insights into Neuroinflammation and Clinical Impairment in Chronic Spinal Cord Injury

Patrik O. Wyss*, Eveline Huber*, Armin Curt, Spyros Kollias, Patrick Freund* and Anke Henning*
Contributed equally as first and equal last author

This orginal article is currently under review in elife.

This study was designed by PW, EH, and AH. PW and EH performed all measurements and analyzed the data. Data were discussed and interpreted by PW, EH, PF, and AH. First draft of the paper was written by PW and EH. All authors reviewed the manuscript and approved the final version.

4.1 Abstract

Cervical neurodegenerative changes above the level of injury are evident following traumatic spinal cord injury (SCI), resulting in up to 30% atrophy of the cervical cord. This study investigates with Magnetic Resonance Spectroscopy (MRS) underlying metabolic changes in 18 SCI patients and 11 controls that may subtend the development of atrophy. The amount of N-acetylaspartate (tNAA, cell integrity marker), myo-Inositol (mI, neuroinflammatory marker), choline (tCho, cell membrane marker), creatine (Cr, energy metabolism marker) and glutamate/glutamine (Glx, representing neurotransmission) was measured in the atrophied cervical cord above the level of injury. Regression analysis revealed relationships between metabolic changes in the atrophied cord, lesion severity, and clinical outcome. We found lesion-level dependent metabolic alterations related to chronic neuroinflammation, neurodegeneration and demyelination. Lesion severity and greater clinical impairment was linked to the amount of neuroinflammation. These metabolic alterations might be promising surrogate markers in therapy monitoring and clinical trials for SCI patients.

4.2 Introduction

Spinal cord injury (SCI) results in most cases in permanent sensorimotor deficits, affecting permanently the quality of life. During the last years, many studies attempted to characterize and understand injury-induced remote neurodegeneration and reorganization along the neuraxis and their relationship to clinical outcomes (Freund *et al. ,* 2011a, Chandra *et al. ,* 2012, Grabher *et al. ,* 2015, Huber *et al. ,* 2017b). This is of high clinical relevance as in-vivo neuroimaging biomarkers are able to assess volumetric as well as microstructural changes of the central nervous system and therefore might help to improve prediction of outcome and stratification of patients for future interventional trials (Huber *et al. ,* 2015).

At the cervical cord level C2, previous studies showed cord atrophy of up to 30% (Freund *et al. ,* 2011a), affecting both grey and white matter equally (Huber *et al. ,* 2017a). Such changes are usually thought to represent neuronal degeneration and demyelination. However, as animal studies mainly focus on characterizing changes at the lesion site to identify possible repair strategies, little is known whether the environment and the function of preserved axons is also altered remote from the site of injury. Pre-clinical studies suggest that surviving cells might have reduced mitochondrial function (Cao *et al. ,* 2013), altered membrane turnover (Arima *et al. ,* 2014) and energy metabolism (Schwerdtfeger *et al. ,* 2012), and changes in spinal excitatory synaptic transmission (Kim *et al. ,* 2011). In addition, there might be widespread changes such as chronic neuroinflammation (Qian *et al. ,* 2010). It is still unknown, how these processes are altered in-vivo after human SCI above the level of injury, and whether these mechanisms might be underlying factors contributing to cervical spinal cord atrophy.

To extend the analysis of metabolic processes in SCI and to obtain biochemical information non-invasively and in-vivo, magnetic resonance spectroscopy (MRS) is the tool of choice. MRS allows for non-invasive assessment of morphological, microstructural and metabolic changes. However, the spinal cord is one of the most difficult areas within the central nervous system to acquire MRS data in terms of signal-to-noise ratio and magnetic field homogeneity due to its deep location and the heterogeneity of the surrounding tissue (Solanky and De Vita, 2014, Hock *et al. ,* 2013b). The acquisition quality of spinal cord MRS recently improved (Hock *et al. ,* 2013a, Hock *et al. ,* 2013c) and allows detecting metabolites such as N-acetylaspartate (cell integrity marker), myo-Inositol (sensitive to neuroinflammatory changes), choline (marker of cell membrane turnover), creatine (indicator of energy metabolism), and glutamate/glutamine (representing neurotransmission). These metabolites have been investigated in the spinal cord of patients in different neurological diseases such as Multiple Sclerosis (Kendi *et al. ,* 2004, Blamire *et al. ,* 2007, Ciccarelli *et al. ,* 2010, Ciccarelli *et al. ,* 2007, Marliani *et al. ,* 2010, Bellenberg *et al. ,* 2013, Abdel-Aziz *et al. ,* 2015), amyotrophic lateral

sclerosis (Carew *et al. ,* 2011), cervical spondylotic myelopathy (Holly *et al. ,* 2009), and Friedreich's ataxia (Henry *et al. ,* 2014, Lenglet *et al. ,* 2016). However, to best of our knowledge, MRS has not been applied in SCI patients yet, a disorder where immediately traumatic and secondary inflammatory processes are considered to impact the clinical outcome.

In this study, we investigated metabolic alterations above the level of injury at the vertebral level C2, and assessed their relationship to spinal cord atrophy, lesion severity, and clinical impairment by using MRS. We hypothesize that 1) metabolic alterations relating to neuroinflammation and neurodegeneration, and changes in spinal excitatory synaptic transmission above the level of injury are evident in the severely atrophied cervical cord in chronic SCI patients; and 2) the amount of metabolic alterations is driven by lesion severity, and relates to the level of lesion, completeness of injury and clinical impairment.

4.3 Materials and Methods

4.3.1 Participants

Inclusion criteria for SCI patients were 1) chronic traumatic injury (>1 year post injury), 2) no other neurological or mental disorders, 3) MRI compatible.

The local Ethics Committee of Zurich approved the present study (KEK-ZH-No. 2014-610, PB_2016-00126) which was in accordance with the Declaration of Helsinki. We recruited all participants for this study between March 2016 and January 2017. All participants were informed about the aim and procedure of the study prior to measurement and gave written informed consent.

4.3.2 Experimental Design

4.3.2.1 Clinical Assessments

SCI patients underwent a comprehensive clinical protocol including a) the International Standards for Neurological Classification of Spinal Cord Injury (ISNCSCI) protocol for motor, light-touch and pin-prick score (Kirshblum et al. , 2011) and b) the Spinal Cord Independence Measure (SCIM) to measure daily life independence (Itzkovich et al. , 2007). The ISNCSCI also provides the basis for the neurological classification of SCI, the American Spinal Injury Association (ASIA) Impairment Scale (AIS) classifying the functional completeness of the injury. In this classification, AIS A is referred to as a complete injury (i.e. no sensory or motor functions preserved in sacral segments), whereas AIS B, C or D is referred to as an incomplete injury. The neurological level of lesion is defined as the uppermost neurological intact segment. In addition, upper limb function of the tetraplegic patients was assessed using the Graded Redefined Assessment of Strength, Sensibility and Prehension (GRASSP) (Kalsi-Ryan et al. , 2012ab). All patients completed the full protocol.

4.3.2.2 MRI Protocol

The study was performed on a 3T Philips scanner (Achieva, Release: 3.2.3, Philips Healthcare, Best, The Netherlands) using the 16 channel SENSE neurovascular coil (Philips Healthcare, Best, The Netherlands) to acquire spectra from the cervical cord above the level of injury (Fig. 10). The participants laid in the scanner in a head first supine position and the total scan duration was approximately 45 minutes. MR measurement sequences included a survey scan, anatomical T_1 and T_2 weighted scans and spectroscopic measurements.

At the C2 level, we used a T_2 weighted image (TR: 3000ms, TE: 120ms, flip angle: 90°, in-plane resolution: 0.5mm x 0.5mm, slice thickness: 3.2mm) to place the spectroscopic volume of interest (VOI, dimensions: 6mm x 9 mm x 35mm, 1.9ml). We applied the metabolite cycling (MC) technique (Hock *et al. ,* 2013c) in combination with inner volume saturation (IVS) (Edden *et al. ,* 2006) and outer volume suppression (OVS) (Wilm *et al. ,* 2007, Schulte *et al. ,* 2007, Hock *et al. ,* 2013b), and used a second-order projection-based shimming routine (Gruetter, 1993, Hock *et al. ,* 2013a). We split the spectroscopic acquisition in measurement acquisition blocks of 128 or 256 signal averages and re-adjusted the VOI based on an updated T_2 image to minimize patient motion (TR: 2000-2500ms (heart beat triggered), TE: 30ms, number of signal averages (NSA): 512, spectral bandwidth: 2000Hz, readout duration: 512ms).

At the lesion site, we used a standardized clinical protocol for all tetraplegic patients, which was previously acquired at a 1.5T (for two patients) or 3T (for seven patients) Siemens scanner (Siemens Healthcare, Erlangen, Germany). At the lesion epicenter, a sagittal T_2-weighted image (for 1.5T: TR: 4125ms, TE: 106ms, flip angle: 150°; for 3T: TR: 3500ms, TE: 84ms, flip angle: 160°) was acquired to assess lesion severity.

4.3.3 MRI Post-Processing

4.3.3.1 Post-Processing and quantification of spectroscopic data

We reconstructed the spinal cord spectroscopic data from the scanner raw data using the MRecon framework (GyroTools LLC, Zurich, Switzerland) carried out in MATLAB 2014b (MathWorks, Inc., Natick, MA, USA). We used a custom-build script to apply eddy current correction and frequency alignment, and to reconstruct the data from the non-water suppressed measurements series and to eventually merge all acquisition blocks for every participant as previously reported (Hock *et al. ,* 2013c). In addition, we applied truncation and zero filling in the time domain after 200ms before quantification. Metabolic concentration values were scaled to the internal creatine value, since absolute quantification by internal water referencing in the spinal cord is not reliable due to the pulsating surrounding CSF. We applied LCModel (Provencher, 1993) to the spectroscopic data of the spinal cord to quantify the metabolic ratios. A basis set for TE=30ms was used including simulated

basis set model data of N-Acetylaspartate (NAA), N-Acetyl-Aspartyl-Glutamate (NAAG), Glutamate (Glu), Glutamine (Gln), Glycerophosphocholine (GPC), Phosphocholine (PCh), Creatine(Cr), scyllo-Inositol (sI) and myo-Inositol (mI). Due to strongly overlapping resonances lines, we combined the spectra of the following metabolites: NAA + NAAG = tNAA, GPC + PCh = tCho and Glu + Gln = Glx. The spectral range used covered in the fitting settings was 0.4 to 4.0 ppm. We aimed at preventing artificial cut-off effect introduced by a cut-off value of 20% (Kreis, 2016). Therefore, following the debate and the recommendation of the consensus discussion at the MRS workshop (Lake Constance, August 2016), metabolic ratios of metabolites were included in case the Cramer-Rao lower bounds (CRLB) were smaller than 100%.

4.3.3.2 Post-Processing of MRI data above the level of injury

The cross-sectional spinal cord area (SCA) above the level of injury was assessed in the T_2 images using Jim 6.0 (Xinapse systems, Aldwincle, UK) in all participants. We determined the bottom of the C2 vertebra and determined the SCA in three consecutive slices at the C2 level. We first placed a region of interest in the middle of the cord. The SCA was then calculated automatically using an active-surface model (Horsfield *et al. ,* 2010). In three participants, manual correction of the surface outline was necessary.

4.3.3.3 Lesion segmentation

In tetraplegic patients, the lesion severity was assessed on the midsagittal slice of the T2-weighted images using Jim 6.0 (Xinapse systems, Aldwincle, UK) as previously described (Huber *et al. ,* 2017b). We quantified the midsagittal anterior-posterior lesion width (=maximal anterior-posterior width of the lesion), the midsagittal rostro-caudal lesion length (=maximal caudocranial extent of the lesion), total midsagittal lesion area, and the thickness of midsagittal ventral and dorsal tissue bridges at the widest point of the lesion which was summed up to the total amount of tissue bridges. An illustration of the tissue bridges is shown in Fig 1B by Huber *et al.* (Huber *et al. ,* 2017b).

4.3.4 Statistical analysis

For statistical analysis we used the R software package (R Core Team, 2016) version 3.3.1 including the package ggplot2 (Wickham, 2009) for visualization. Data in the graphics show boxplot including the median and the quartiles.

First, we assessed group differences for all metabolite concentration ratios at the spinal cord between SCI patients and healthy controls using a Kruskal–Wallis test followed by pairwise Mann–Whitney U tests. We also investigated differences between para- and tetraplegic patients and further examined metabolite ratios that showed significant group differences between HC and all SCI patients. To investigate how the amount of cervical atrophy of all SCI patients is related to cervical chemical concentration changes, we performed Spearman's rank correlation tests. Second, within

tetraplegic SCI patients, we assessed the relationship between the level of injury, lesion severity (lesion area, length and width, and tissue bridges) and cervical chemical concentration ratios using Spearman's rank correlation tests. Last, we examined the relationship between metabolites concentration ratios and clinical outcome using Spearman's rank correlation tests.

The confidence interval is set to 95%. Age was included in the statistical model as a covariate of no interest to control for age dependency.

4.4 Results

4.4.1 Demographics

We included nine patients with a paraplegic injury (injury below neurological level T1 of the spinal cord; mean age: 47.6±5.4 years), nine patients with a tetraplegic injury (above level T2; mean age: 52.6±14.0 years), and 11 healthy controls (HC, mean age: 44.5±11.7 years) in the study without significant difference in age. All participants were male and the demographic data is summarized in Table 7.

All patients completed the MRI examination and clinical assessment. The mean age at injury and the years since injury was 31.7± 12.8 and 15.9±10.0 for the paraplegic patients, and 40.7±13.0 and 11.9± 10.0 for the tetraplegic patients, respectively. Para- and tetraplegic patients did neither significantly differ in age at injury (P=0.34) nor in years since injury (P=0.42) Eight patients were classified as functionally complete (American Spinal Injury Association Impairment Scale [AIS] A) and 10 as incomplete (AIS B-D; Table 7).

			ISNCSCI		Outcome Measures			
ID	Age at Injury	Years since Injury	AIS	Level of Injury	Motor Score	Light-Touch	Pin-Prick	SCIM
1	30	13	D	C2	75	55	55	74
2	51	6	D	C2	86	56	26	48
3	28	2	A	C4	11	23	23	18
4	31	2	A	C4	22	31	20	28
5	46	12	C	C4	97	112	97	100
6	60	4	D	C4	89	79	64	100
7	41	24	A	C5	38	22	20	63
8	24	31	B	C5	31	68	68	64
9	50	13	D	C7	91	110	107	100
10	44	10	A	T2	50	39	41	58
11	19	27	A	T4	50	71	72	73
12	33	19	A	T4	50	51	48	75
13	14	25	B	T4	50	78	78	66
14	19	29	B	T4	50	50	50	73
15	26	20	A	T5	50	48	48	68
16	46	7	A	T11	67	87	82	69
17	48	2	D	T12	100	94	82	98
18	36	4	D	L1	92	106	104	98

Table 7: Clinical and Epidemiological Data for All Patients Included in the Study
AIS=American Spinal Injury Association Impairment Scale, ISNCSCI= International Standards for Neurological Classification of Spinal Cord Injury, SCIM=Spinal Cord Independence Measure

4.4.2 Quality of MRS measurements

Representative spectra acquired in the spinal cord at level C2 are shown in Fig. 10. The spectroscopic voxel of interest placement is shown in A). Measured spectra and fitting results with separate metabolite components are shown in B) for a healthy control subject, a paraplegic and a tetraplegic patient. In every participant, 512 signal echo averages were included and no measurement block had to be excluded due to motion. Valid concentration values could be determined for all metabolites in all participants with the exception of Glx. It could not be determined and zero was assumed in one healthy control and one paraplegic patient. No significant differences in the metabolite line width (full-width at half-maximum (FWHM) of the NAA peak) between healthy controls and SCI patients has been found (P=0.51). This indicates a homogenous magnetic field in the region of interest also in the case of patient with implants and therefore a methodological bias in the metabolic level is minimal.

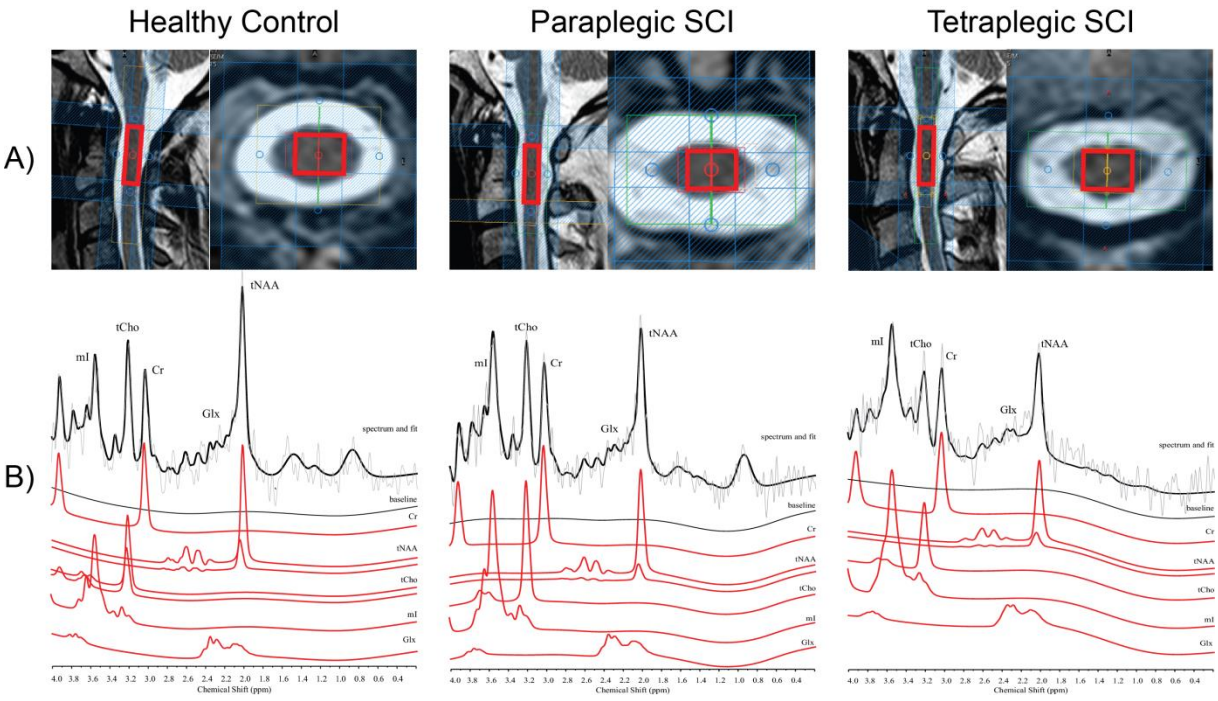

Figure 10: Spectroscopic Voxel Localization and Representative Spectra. The placement of the spectroscopic voxel of interest is shown in A). A representative spectrum of a healthy volunteer, a paraplegic patient and a tetraplegic patients (underlying in grey) and the resulting fit (black) is shown in B). The metabolic components identified in the fit are shown below in red for Creatine (Cr), total NAA (tNAA), choline containing compounds (tCho), myo-Inositol (mI) and the combined Glutamate and Glutamine signal (Glx).

4.4.3 Metabolic changes in the severely atrophied cervical cord

In SCI patients, cross-sectional SCA at C2 was reduced by 17% when compared to controls (P<0.001), with more pronounced changes in tetraplegic patients (-25%, P<0.001) than in paraplegic patients (-10%, P=0.005).

In terms of metabolic changes within this atrophied cord area, we found significantly lower tNAA/mI and tCho/mI ratios in SCI patients compared to controls (tNAA/mI: P=0.003; tCho/mI: P=0.043) [Fig. 11AC]. This group difference was mainly driven by the tetraplegic patient group who significantly differed from the healthy control group (tNAA/mI: P=0.002; tCho/mI: P=0.033), whereas paraplegic patients only showed a trend towards lower ratios (tNAA/mI: P=0.056; tCho/mI: P=0.224) [Fig. 11BD]. Within patients, tetraplegic patients had lower tNAA/mI ratios compared to paraplegic patients (P=0.042), but no difference between patient subgroups was detected for tCho/mI (P=0.25). Patients with greater cord atrophy had lower levels of tNAA/mI (P=0.003) and showed the same trend for tCho/mI (P=0.094) [Fig. 12].

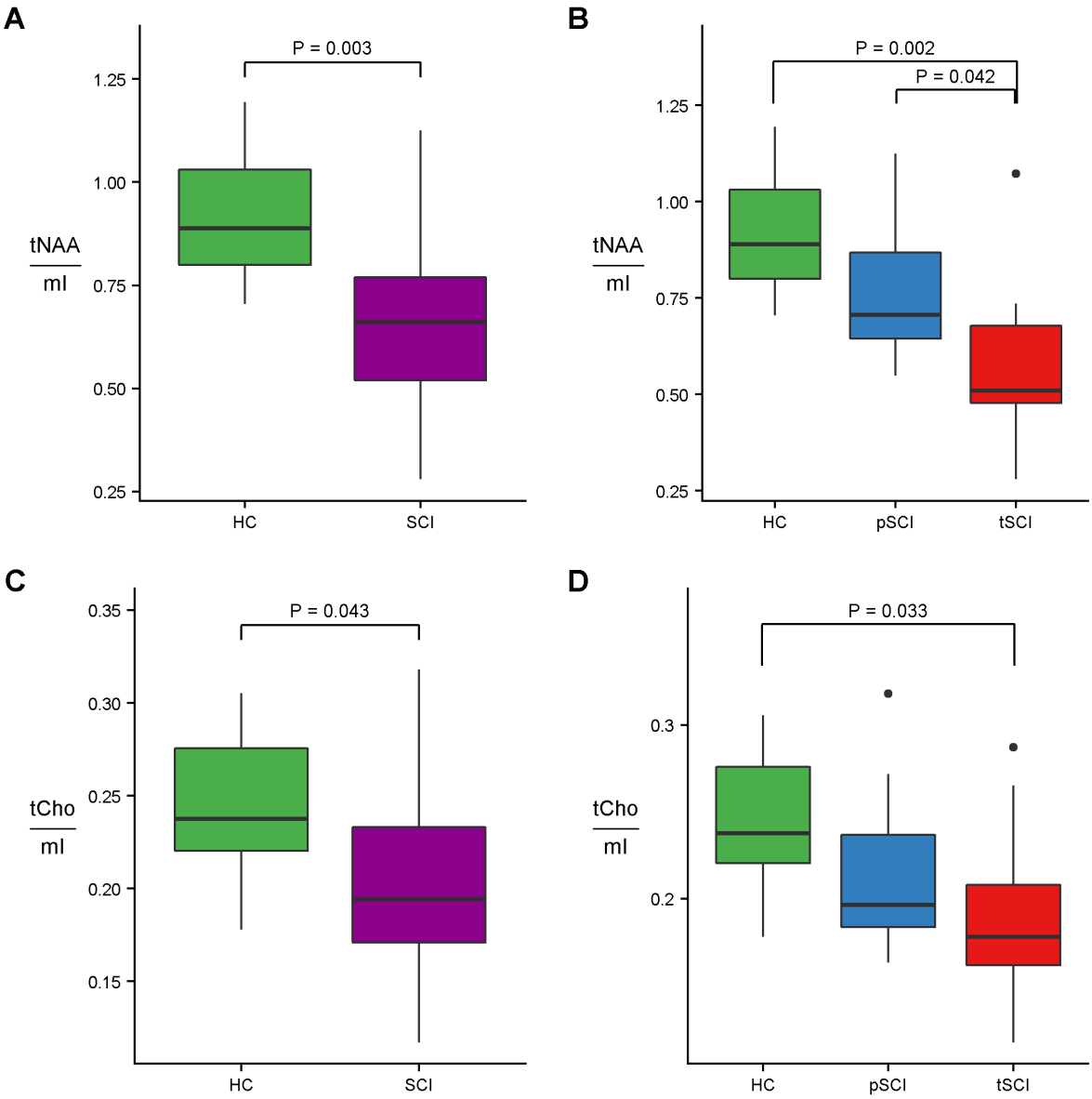

Figure 11: Metabolic Ratios Group Differences. The group differences of tNAA/mI (A,B) and tCho/mI (C,D) are shown for healthy controls (HC) and spinal cord injury patients (SCI) (A,C) and for healthy controls (HC), paraplegic SCI (pSCI) and tetraplegic SCI (tSCI) (B,D). Significant differences are labelled and un-corrected P values are denoted.

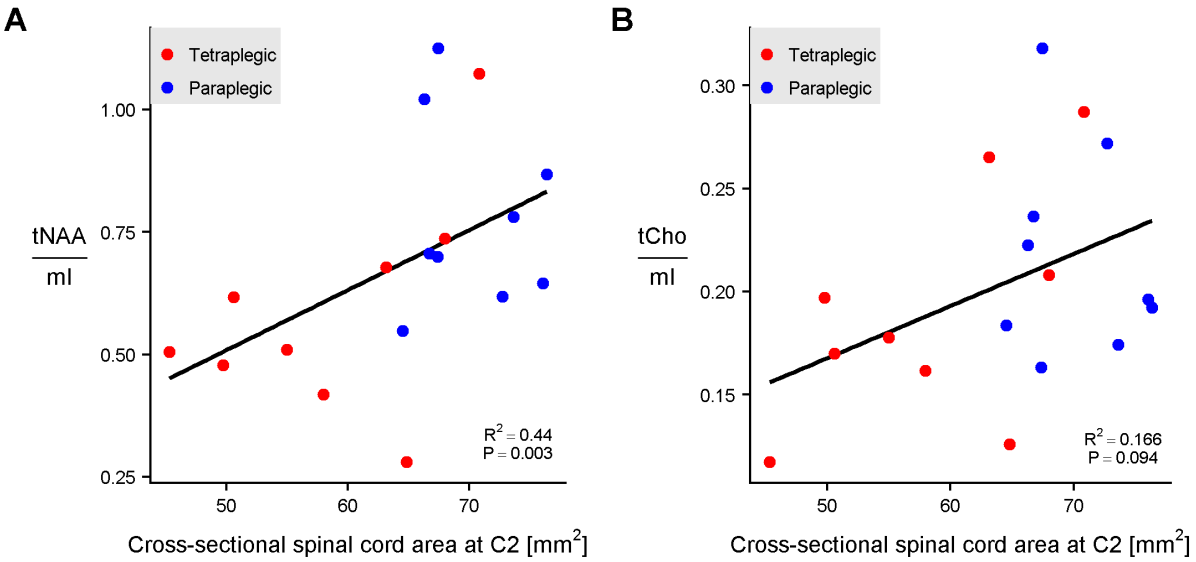

Figure 12:Spinal Cord Atrophy and Metabolic Ratios. The cross-sectional spinal cord area at C2 is shown in Spinal Cord Injury (SCI) patients as relation to tNAA/mI (A) and tCho/mI (B).

4.4.4 Relationship between lesion characteristics, metabolic changes at C2 level and clinical outcome

Lesion level was positively associated with tNAA/mI (P=0.005) and showed the same trend for tCho/mI (P=0.062) [Fig. 13AC]. When only looking at complete patients (i.e. AIS A), significant associations between lesion level and both tNAA/mI (P=0.022) and tCho/mI (P=0.009) were found [Fig. 13BD]. Further, an increased tNAA/tCho ratio was associated with time since injury (P=0.009) [Fig. 14A], but did not differ between complete and incomplete patients (P=0.69) [Fig. 14B]. In tetraplegic patients, the size of midsagittal tissue bridges at the lesion site was positively correlated with tNAA/mI (P=0.006) as well as tCho/mI ratios (P=0.032) above the level of injury [Fig. 14CD].

The tNAA/mI ratio as well as Cho/mI ratio were positively associated to SCIM (tNAA/mI: P<0.001, R^2=0.560; tCho/mI: P=0.002, R^2=0.458) and pinprick score (tNAA/mI: P=0.009, R^2=0.353; tCho/mI: P=0.004, R^2=0.415) [Fig. 15ABCD]. In addition, lower levels of tCho/mI ratio was associated with lower light-touch (P=0.001, R^2=0.529) and motor score (P=0.001, R^2=0.531) [Fig. 15EF].

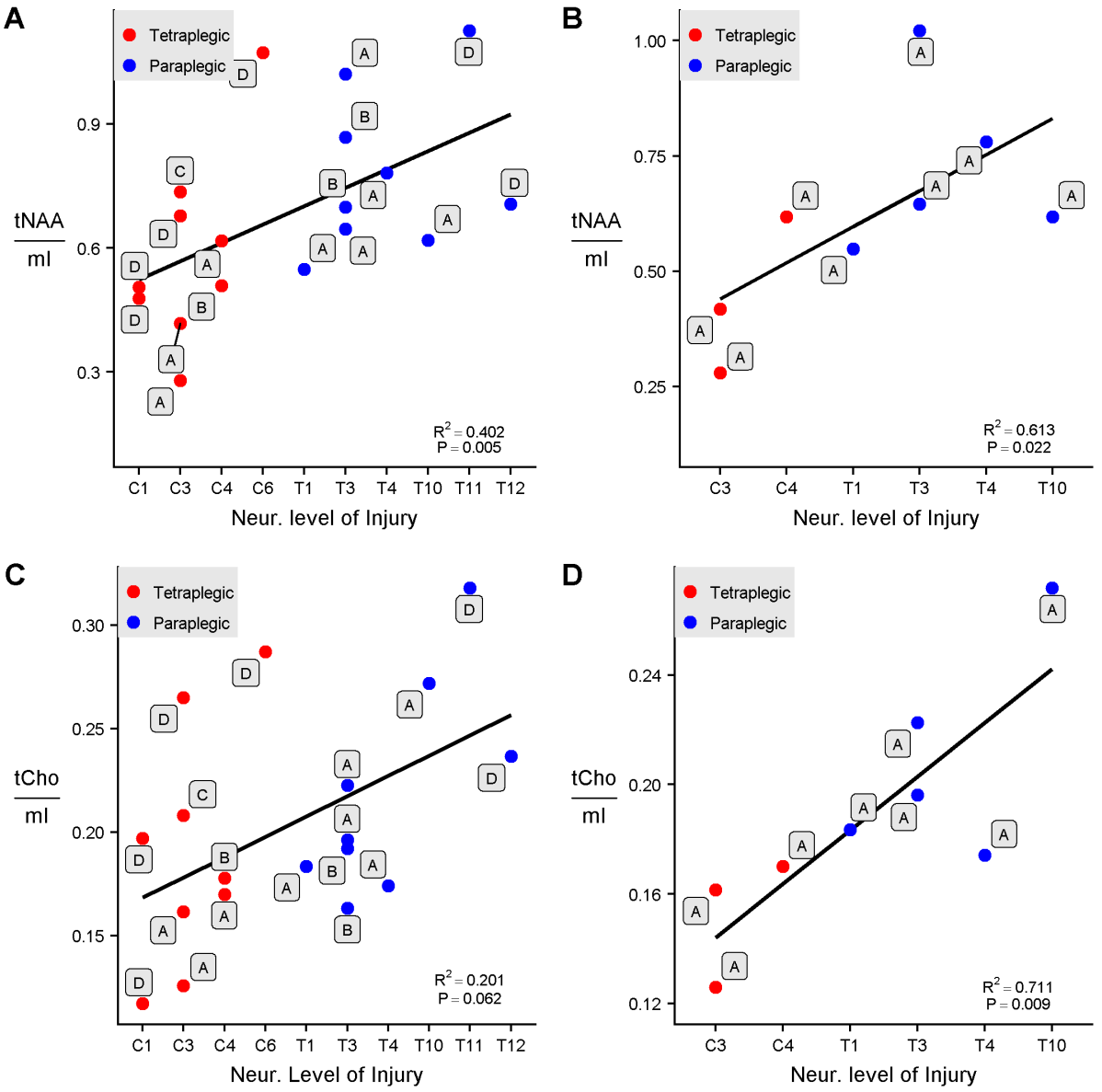

Figure 13: Lesion proximity and Metabolic Ratios. The correlation of the neurological level of injury (C1 to T12) and the ratios of tNAA/ml (A,B) and tCho/ml (C,D) are shown. The patients are labelled according to their American Spinal Injury Association Impairment Scale (AIS) from A to D. All spinal cord injury patients are included in (A,C), whereas only patients diagnosed with complete injury (AIS A) are shown in (B,D).

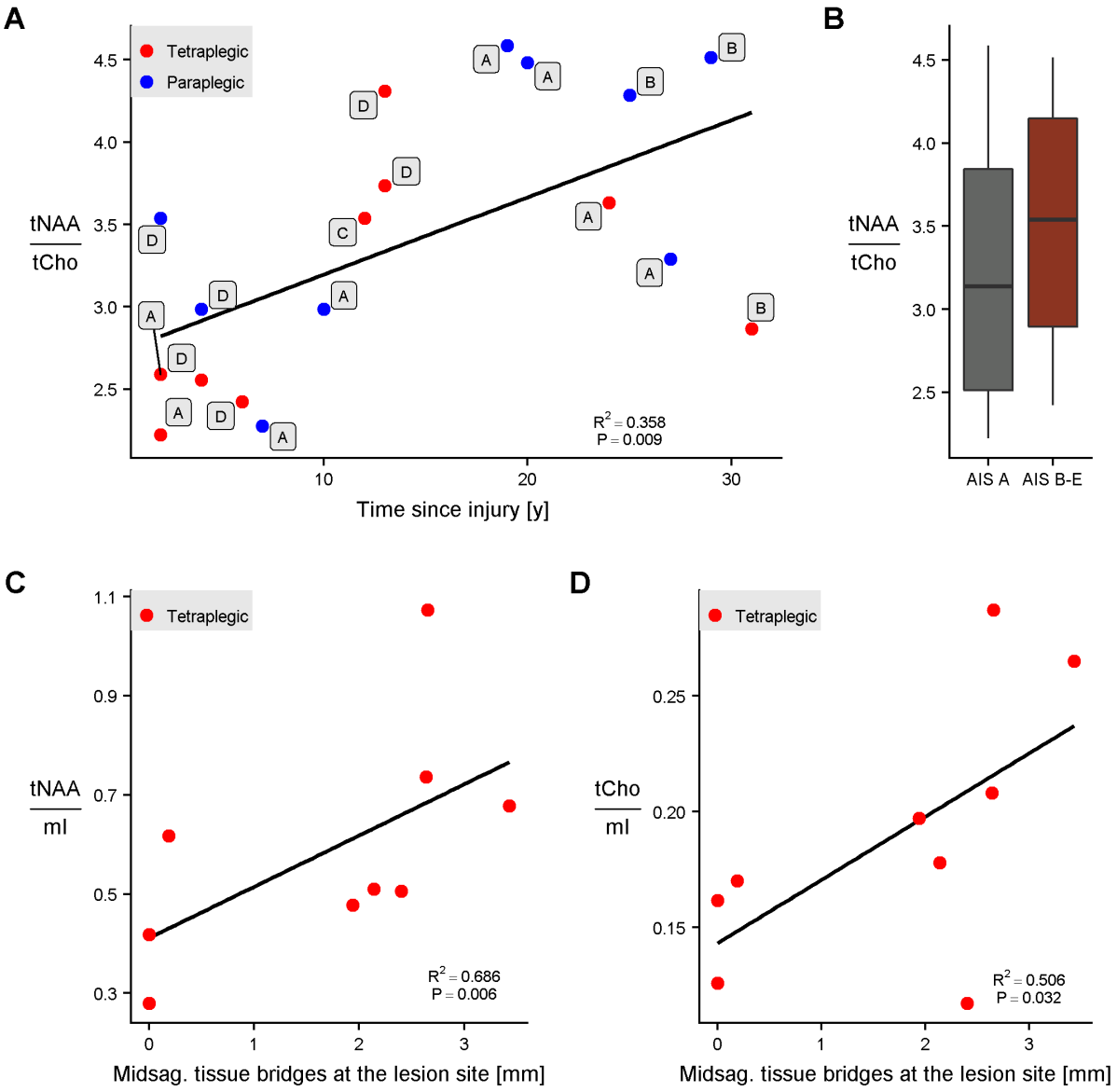

Figure 14: Lesion Characteristics and Metabolic Ratios. The correlation between the time since injury and the tNAA/tCho ratio is shown in A. In B, the ratio tNAA/tCho is shown for complete (AIS A) vs. non-complete (AIS B, AIS C, AIS D and AIS E) spinal cord injury patients. The relation between the midsagittal tissue bridges size and the metabolic ratios of tNAA/mI (C) and tCho/mI (D) are shown for tetraplegic spinal cord injury patients (tSCI).

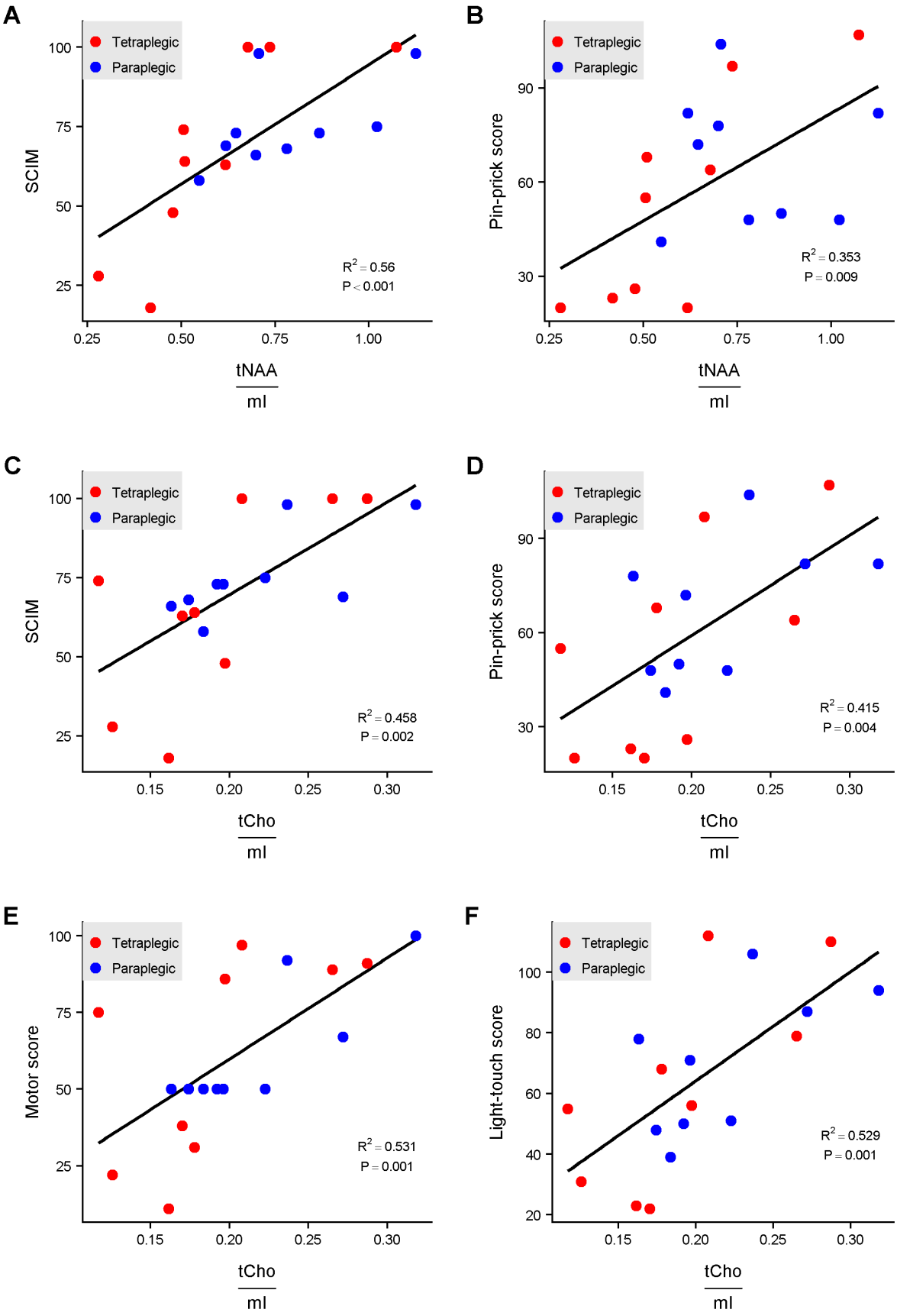

Figure 15: Metabolic Ratios and Outcome Measures. This figure shows the correlations of the metabolic ratios tNAA/mI (A,B) and tCho/mI (C,D,E,F) in spinal cord injury patients (SCI) to outcome measures including Spinal Cord Independence Measure (SCIM) (A,C), Pin-Prick (B,D), Motor (E) and Light-touch scores (F).

4.5 Discussion

This study is the first to investigate underlying metabolic alterations in areas of spinal cord atrophy above the level of injury after SCI. Above the level of injury, we found altered metabolic ratios that positively correlated with the extent of atrophy and the sensorimotor outcome and were driven by lesion severity (i.e. level of lesion and extent of lesion). These findings may point to cellular and molecular factors underlying consecutive cervical cord atrophy after SCI, i.e. indication of neuroinflammation and deterioration of axonal metabolism, and how altered metabolism influences patient outcome.

4.5.1 Metabolic changes in the severely atrophied cervical cord

We show that tNAA/mI and tCho/mI are decreased in the atrophied cervical cord in SCI patients, with more pronounced changes in tetraplegic patients compared to paraplegic patients. Importantly, the more caudal the lesion level, the higher the ratios of tNAA/mI and tCho/mI, which reflects values being closer to healthy controls.

Specifically, reductions of tNAA/mI and tCho/mI ratios can be either attributed to a decrease in N-acetylaspartate and choline, or an increase in myo-Inositol, or both. N-acetylaspartate is synthesized in the mitochondria of neurons from aspartic acid and acetyl-coenzyme A (Truckenmiller *et al. ,* 1985, Ariyannur *et al. ,* 2010), and is predominantly present in neuronal cell bodies and axons, while synaptic elements and astrocytes are low in N-acetylaspartate (Nordengen *et al. ,* 2015). In accordance, Manganas and colleagues (Manganas *et al. ,* 2007) showed that the N-acetylaspartate amplitude measured with MRS primarily arises from N-acetylaspartate within neurons, whereas oligodendrocytes and astrocytes only contribute 5%, respectively 10%, to this signal. This suggests that decreased N-acetylaspartate reflects a combination of axonal/neuronal loss (Bjartmar *et al. ,* 2000) and reduced mitochondrial metabolism (Bates *et al. ,* 1996). In addition, it was shown that N-acetylaspartate could be released into the extracellular space and be taken up by oligodendrocytes, where N-acetylaspartate is degraded back to aspartate and acetate by aspartoacylase (Chakraborty *et al. ,* 2001, Wang *et al. ,* 2007, Moffett *et al. ,* 2011). It was further suggested that acetate generated by this reaction is used to build lipids for maintaining myelination (Chakraborty *et al. ,* 2001). Therefore a reduction in N-acetylaspartate might also relate to demyelination, a mechanism also known in Canavan's disease (Kaul *et al. ,* 1993). In line, various MRS studies in neurodegenerative diseases like Multiple Sclerosis (Abdel-Aziz *et al. ,* 2015, Ciccarelli *et al. ,* 2010), amyotrophic lateral sclerosis (Carew *et al. ,* 2011), and Friedreich's ataxia (Lenglet *et al. ,* 2016) showed reduced levels of N-acetylaspartate.

On the other hand, myo-Inositol is also considered as a glial marker as it is primarily located within astrocytes and presumed to act as an osmolyte, maintaining glial cell volume (Strange *et al. ,* 1994,

Isaacks *et al. ,* 1994). Activated glial cells present large cell volumes and are therefore accompanied by increases in myo-Inositol. Supporting this, preclinical findings showed upregulation of astrocytes after SCI (Gwak *et al. ,* 2017, Rust and Kaiser, 2017), indicating chronic neuroinflammation. Consistently, in patients with Multiple Sclerosis, where neuroinflammation plays a major role, myo-Inositol levels (and their ratios) are elevated (Kirov *et al. ,* 2013), also in patients with remitting relapsing Multiple Sclerosis without recent relapses (Bagory *et al. ,* 2012). However, myo-Inositol is also a precursor of phosphatidylinositol, a minor component of the cell membrane (Holub, 1982). Inter alia, the phosphatidylinositol signaling pathway is capable of activating other proteins and thereby is capable of changing their catalytic activities (Cockcroft, 2012). Specifically, in spinal oligodendrocytes, glucosamine and mannose can be glycosidically bound to phosphatidylinositol. Such glycosyl-phosphatidylinositol is expressed at the node of ranvier and inhibits neurite outgrowth (Huang *et al. ,* 2005). Therefore, it seems likely that increases in myo-Inositol levels primarily indicate upregulation of astrocytes, indicating neuroinflammation, but might also hint to altered cell membrane properties inhibiting regeneration.

Finally, total choline receives contribution from free choline, glycerophosphocholine and phosphocholine, which are precursors of phosphatidylcholine (Wang *et al. ,* 2008, Lindner *et al. ,* 2017), used for cell membrane synthesis, as well as for the synthesis of the neurotransmitter acetylcholine (Wang *et al. ,* 2008). Total choline is typically increased when there is an increased membrane turnover or when there is inflammation (Howe and Opstad, 2003). In Multiple Sclerosis for example, choline is typically increased in acute phases of demyelination as the degradation of myelin leads to the release of phosphatidylcholine (Richards, 1991). Chronic neuroinflammation and demyelination in SCI is expected to lead to increased myo-Inositol levels along with increased choline levels as choline is two to threefold higher in glial cells than in neurons (Brand *et al. ,* 1993). However, in our cohort, choline behaves oppositely leading to the conclusion that two biological scenarios might account for the observed ratio changes: 1) tNAA levels are decreased and myo-Inositol is increased indicating neurodegeneration, demyelination and chronic neuroinflammation, or 2) tNAA and choline levels are decreased suggesting neurodegeneration and altered membrane metabolism. Animal studies investigating the choline concentration after SCI (Qian *et al. ,* 2010) reported highly elevated levels of choline early after injury, and even tough choline levels declined over time, they were still elevated 56 days after injury. This suggests that following SCI, there is an initial high membrane turnover indicating cell membrane breakdown and/or demyelination, which levels off over time. Nevertheless, it seems plausible that once degeneration has terminated, the total amount of choline is reduced, as there are less viable neurons capable of undergoing membrane turnover. At which time after injury degenerative processes are actually reaching their plateau still remains a matter of debate (Huber *et al. ,* 2015); however our study included chronic

patients, on average 13.9 years after injury. In addition, we need to consider that choline is not only part of the membrane metabolism, but also acts as a precursor of acetylcholine. Acetylcholine is an important neurotransmitter whose inhibition/ breakdown leads to paralysis (Plaud *et al. ,* 2010), and conversely, after SCI choline receptors are decreased leading to a disturbed cholinergic metabolism (Chinthu *et al. ,* 2017). Therefore reductions in choline levels indicate neurodegeneration with potentially both altered membrane and neurotransmitter metabolism.

We therefore conclude that the observed lower ratios of tNAA/mI and tCho/mI in patients are driven by reduction in tNAA and choline and increases in myo-Inositol, primarily indicating neurodegeneration, demyelination and chronic neuroinflammation [Fig. 16].

In addition to the observed metabolic changes within areas of cord atrophy, the tNAA/mI ratio was positively associated with the amount of cord atrophy. This indicates that patients with a smaller SCA do not only have more pronounced neurodegeneration, but also the structure within the cord is altered; namely patients with smaller cord areas have less densely packed neurons and/or more ongoing neuroinflammation. Postmortem studies of humans with SCI suggest that damaged spinal neurons may be partly replaced by fibrous connective tissue and collagen (Norenberg *et al. ,* 2004), which might account for this finding. As there is no functional benefit in this replacement, this reorganization represents an impediment to axonal re-growth (Berry, 1982).

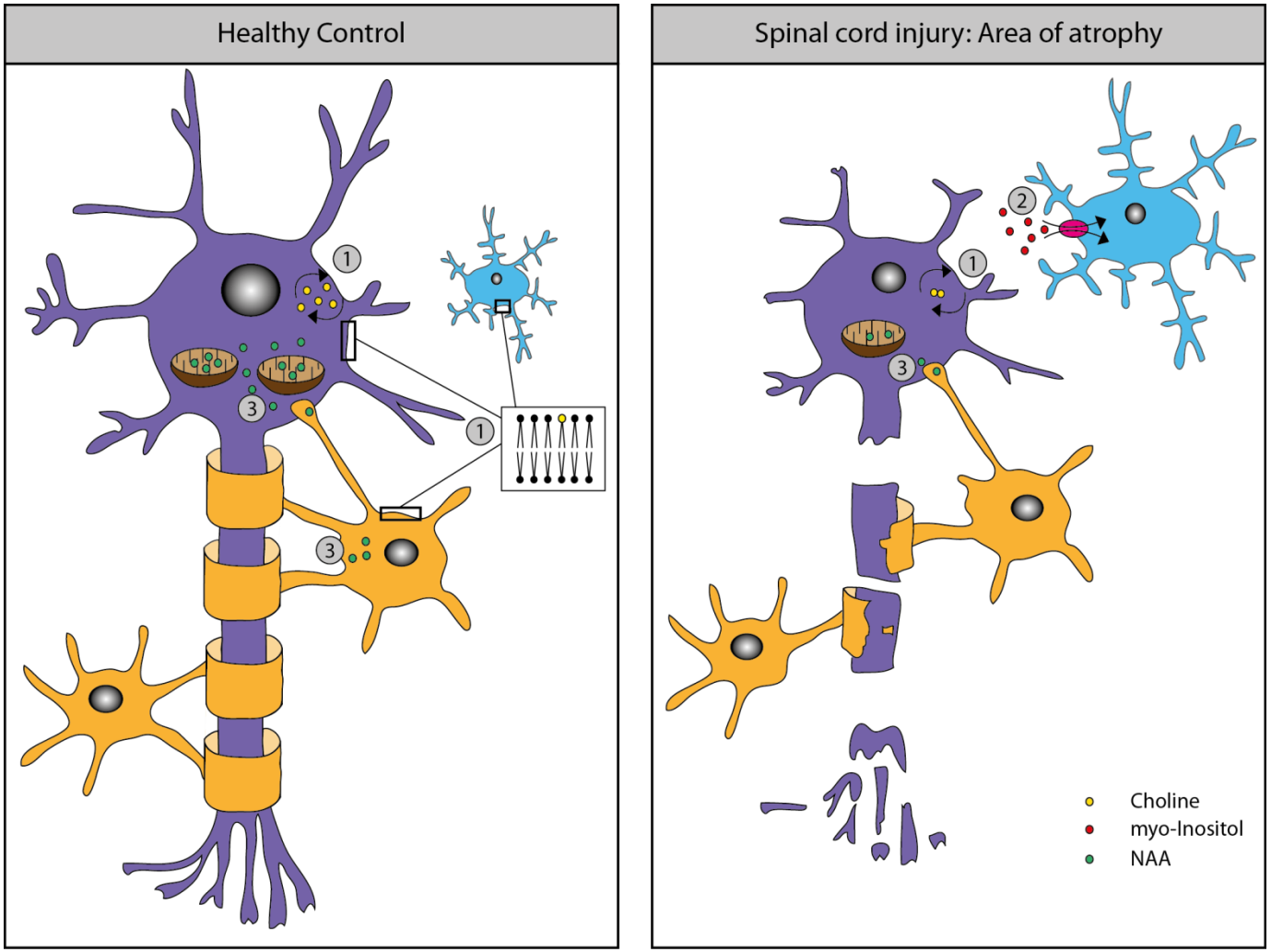

Figure 16: Schematic representation of possible mechanisms involved in metabolic alterations in chronic SCI taking place above the level of injury.

1. In healthy controls, choline is used for the synthesis of phosphatidylcholine, which is a part of the cell membrane of neurons, astrocytes and oligodendrocytes. In chronic SCI, there are less cells capable of undergoing membrane synthesis as neurons degenerate, which may lead to a reduction in free choline.
2. In healthy controls, resident astrocytes are present in the central nervous system. Injury to the CNS might lead to attenuation of reactive gliosis, which is characterized by cell body swelling of astrocytes mediated by the osmolyte myo-Inositol. Reactive astrocytes are one feature of neuroinflammation.
3. NAA is synthetized in the mitochondria of neurons and therefore reflects mitochondrial metabolism. In healthy controls, oligodendrocytes possess the ability to take up NAA and degrade it into aspartate and acetyl; the latter being used for the synthesis of the myelin sheet. After an SCI, there might be impaired mitochondrial metabolism and less neurons capable of synthesizing NAA (i.e. neurodegeneration), which may influence myelination as well.

4.5.2 Relationship between lesion characteristics, cervical metabolic changes and clinical outcome

We show that the size of tissue bridges at the lesion site is positively associated with tNAA/mI as well as tCho/mI ratio. This suggests that smaller tissue bridges, indicating less spared tissue (Huber *et al.* , 2017b), leads to a stronger decrease of N-acetylaspartate and larger increase in myo-Inositol above the level of injury. Thus, the larger the initial damage at the lesion site, the more axons above the level of injury undergo retro- and anterograde degeneration, and the more neuroinflammation is present. Interestingly, tNAA/tCho ratio increased significantly with time since injury. As atrophy is the end result of neurodegeneration, one would expect a decrease of both choline and N-acetylaspartate over time. It seems therefore likely that choline shows a relatively larger decrease compared to N-acetylaspartate. This progressive degeneration and change in molecular content is of particular importance when new treatments are investigated, as treatments in SCI patients should ideally start as early as possible to prevent further structural damage.

The tNAA/mI ratio as well as tCho/mI ratios were positively associated with sensory and motor scores, indicating that patients with lower N-acetylaspartate (and/or choline), and higher myo-Inositol levels have worse outcomes. Previous studies showed that neurodegeneration above the level of injury, reflected in a decreased total SCA, involves both grey and white matter and is associated with worse clinical outcome (Freund *et al.* , 2011a, Freund *et al.* , 2012b, Huber *et al.* , 2017b). In addition, higher myo-Inositol levels indicate the presence of reactive astrocytes, which produce chondroitin sulfate proteoglycans as well as keratins, which inhibit axonal regeneration (Silver and Miller, 2004).

4.5.3 Limitations

All the metabolic values are presented as ratios to other metabolites and not as absolute values with respect to the internal water (Gasparovic *et al.* , 2006). Although absolute quantification is possible in the brain and the brainstem referencing to the internal water signal (Zoelch *et al.* , 2017), this is not yet possible in the spinal cord, since the water reference scan in the spinal cord is affected by the surrounding cerebrospinal fluid due to partial volume effect and thus does not serve as a reliable and valid reference. Therefore, future studies should aim to quantify absolute metabolite concentrations. Our applied proton MRS is specific for metabolite changes mainly associated with the integrity and viability of neurons. Additional techniques, like Sodium or Phosphorus-31 MRS would be helpful for future studies to better understand ongoing mechanisms in neurodegeneration (e.g. access failure of action potentials) (Paling *et al.* , 2013, Solanky *et al.* , 2013) or to monitor changes in myelin phospholipids to follow changes in myelin structure (Husted *et al.* , 1994).

Despite the fact that the technique applied to acquire spectra in the spinal cord is the first to correct for phase and frequency shift, it lacks the possibility of patient motion correction. We minimized the

effect by using tight fitting cushions to restrict the possible range of motion of the patient's head and cord and we split the total number of signal echoes acquired in the spinal cord into measurement acquisition blocks of 128 or 256 averages and re-adjusted the VOI based on an updated T_2 image. Spinal cord MRS is a mixed readout of both grey and white matter tissue. In vivo MRS does not yet allow for differentiation of intracellular and extracellular metabolite levels.

4.6 Conclusion

Our study describes for the first time metabolic alterations of the atrophied cervical spinal cord in chronic SCI patients using non-invasive magnetic resonance spectroscopy. We show that the metabolic environment within the cervical cord is altered after SCI indicating a combination of chronic neuroinflammation, demyelination and neurodegeneration. Patients with larger cord atrophy showed more pronounced metabolic alterations. Further, the amount of metabolic changes is driven by lesion severity and relates to clinical impairment. Such sensitive and valid biomarkers hold the potential to improve outcome prediction and patient stratification for future clinical trials and interventions.

5 Study IV

Somatotopic reorganization of the basal ganglia and their relationship to outcome after spinal cord injury: A longitudinal study

Eveline Huber, Raihaan Patel, Mallar Chakravarty, Patrick Freund

This manuscript is in preparation and will be submitted to Brain.

EH, MC and PF were involved in the concept and design of the study. Analysis of data was conducted by EH and RP. Data were discussed and interpreted by EH, RP, MC and PF. EH and PF wrote the manuscript. All authors reviewed the manuscript and approved the final version.

5.1 Abstract

Objective: Spinal cord injury (SCI) leads to wide-spread structural changes of the pyramidal, sensory and limbic system. Animal models suggest that the extrapyramidal system, like the basal ganglia, plays a crucial role in recovering sensorimotor function after spinal trauma. We therefore investigated the spatial and temporal evolution of structural and microstructural changes and their association to outcome after acute SCI.

Methods: Surface morphology, myelin and iron changes of the basal ganglia (including thalamus, striatum and globus pallidus) were defined from 182 MRI datasets acquired in 17 SCI patients and 21 healthy controls. T1-weighted volumes, myelin-sensitive magnetization transfer saturation (MT) and longitudinal relaxation rate (R1), and iron-sensitive effective transverse relaxation rate (R2*=1/T2*) provided information on morphometry and microstructure. All participants were scanned at baseline, after 3, 6, 12, and 24 months; SCI patients were assessed with a comprehensive clinical protocol at the same time points. Using linear regression models, we investigated group difference in linear and non-linear trajectories of vertex-wise surface area, and underlying microstructural changes (i.e. myelin, iron). Basal ganglia changes at baseline were used to predict 24-month clinical outcome, adjusted for baseline clinical status.

Results: Surface-based analysis revealed contractions of surface area over time in the motor thalamus within regions representing lower extremities, within the pulvinar nucleus and within the striatum in patients compared to controls. Expansions of surface area were observed in the sensorimotor thalamus representing upper extremities, and in the striatum. As morphometric changes progressed, myelin-sensitive parameters decreased in the motor thalamus, in the striatum and in the globus pallidus. In addition, patients showed decreases in iron levels within the left post-commisural caudate over time. Increased surface area expansions at baseline within the motor caudate predicted 24-month lower extremity motor score.

Conclusion: This study provides evidence for progressive extrapyramidal macro- and microstructural changes after SCI, indicating large scale, transneuronal remodeling of primarily unaffected brain regions. We found a striking somatotopic reorganization pattern with foot representative regions, whereas hand representative areas exhibited compensatory local surface area increases. This study provides unbiased, quantitative readouts of extrapyramidal changes relating to clinical readouts, which might serve as future biomarkers.

5.2 Introduction

Spinal cord injury (SCI) is a devastating event, which in most cases, leads to permanent paralysis below the level of injury. Targeted neurorehabilitation can foster recovery of limb function but often only partial improvements in motor function can be achieved. Neuroimaging studies have recently revealed that a cascade of neurodegenerative changes after injury is early initiated affecting the pyramidal, sensory and limbic system (Freund *et al.* , 2012a, Freund *et al.* , 2013ab, Grabher *et al.* , 2015). Importantly, less neurodegenerative changes early after injury accounted for functional recovery; however, details of reorganization by the surviving networks are not fully understood. Moreover, next to the motor system, animal models suggest that the extrapyramidal system plays a role in recovering motor function after corticospinal tract injury (Lawrence and Kuypers, 1968, Belhaj-Saif and Cheney, 2000, Zaaimi *et al.* , 2012). However, in humans, there is sparse evidence for anatomical and functional significance of the extrapyramidal system (Lemon, 2008), or for its role in sensorimotor recovery after SCI. The extrapyramidal system contains the basal ganglia which consists of the caudate nucleus, the putamen (together refered as striatum), and the globus pallidus and is of high importance for sensorimotor tuning (Huston *et al.* , 1990). Studies indicate that SCI leads to a misbalance in the information flow between the basal ganglia, the thalamus (Cramer *et al.* , 2005) and the motor cortex (Min *et al.* , 2015), which could explain abnormal activation patterns in in pallido-thalamocortical loop and increased functional connectivity, respectively. Furthermore, an increased functional activation of the basal ganglia during passive toe movement early after injury was associated with increased neurological outcome (Jung *et al.* , 2011), suggesting that the basal ganglia might play a crucial role in sensorimotor recovery.

To better understand the role of the basal ganglia in sensorimotor recovery from a SCI, we acquired longitudinal data including T1-weighted volumes, myelin-sensitive magnetization transfer saturation (MT) and longitudinal relaxation rate (R1), and iron-sensitive effective transverse relaxation rate (R2*=1/T2*) in SCI patients and controls, providing information on morphometry and microstructure.

This study aims to (1) track the temporal and spatial (in terms of shape) pattern of structural basal ganglia changes within the first 24 months after SCI with distinct trajectories using T1-weighted volumes, (2) characterize associated microstructural changes like alterations in myelin and iron using MT, R1, and R2*, and (3) relate observed basal ganglia changes at 1-month post injury to appropriate 24-month clinical outcome. For analysis of the sensorimotor system, usually volume or tensor-based approaches are used (Ashburner and Friston, 2000, Ashburner and Ridgway, 2012), alongside with standard imaging segmentation methods with whose the basal ganglia cannot be accurately assessed. We therefore applied a recently developed shape analysis technique (Chakravarty *et al.* , 2013, Pipitone *et al.* , 2014) whose atlas is based on manually segmented serial histological data

(Chakravarty *et al.* , 2006); capable of segmenting thalamus, striatum, and globus pallidus fully automatically and unbiased. Such analyses hold the potential not only to complement traditional volumetric analysis, but might be even more sensitive in the detection of trauma-induced subcortical structural changes. To characterize structural trajectories of surface area and microstructural parameters, we modelled the MRI measures in terms of linear rate of change (reflecting degeneration/ plasticity) and non-linear changes in the rate (reflecting acceleration/ deceleration). Linear regression models were used for prediction of outcome.

5.3 Materials and Methods

5.3.1 Subjects

17 patients with SCI and 21 healthy controls were recruited at the Balgrist University Hospital and from neighborhood between July 2010 and July 2016. All patients suffered from a subacute SCI (<3 months) without brain injury, and all participants had no pre-existing neurological, mental or medical disorders affecting functional outcome, were older than 18 years, and had no contraindications to MRI.

All participants underwent a comprehensive MRI protocol. In total, 182 appointments were conducted from 38 participants (21 healthy controls, 17 SCI patients) at baseline and at 3, 6, 12 and 24 months. Follow-ups were performed successfully in 82.4%, 100%, 100% and 76.5% of the patients, respectively in 100%m 100%, 95.2% and 100% of the controls. At the same time points, patients were also clinical assessed including 1) International Standards for Neurological Classification of Spinal Cord Injury (ISNCSCI) protocol for motor, light-touch and pin-prick score (Kirshblum *et al.* , 2011), and 2) the Spinal Cord Independence Measure (SCIM) to measure daily life independence (Itzkovich *et al.* , 2007).

The study protocol was in accordance with the Declaration of Helsinki and was approved by the local ethics committee of Zurich (EK-2010-0271). All participants provided written informed consent before participation.

5.3.2 Image acquisition

Participants were scanned with a 3T Magnetom Verio or Skyra Fit MRI scanner (Siemens Healthcare, Erlangen, Germany) operated with a 16-channel radiofrequency receive head and neck coil and radiofrequency body transmit coil. To obtain high reproducibility and minimize motion artefacts, participants were carefully positioned in supine position and were asked to wear a stiff neck (Laerdal Medicals, Stavanger, Norway).

At each time point, the MRI measurement consisted of two protocols: (1) an optimized 3 dimensional high-resolution T1-weighted Magnetization Prepared Rapid Acquisition Gradient-Echo (MPRAGE)

sequence (Tardif *et al.* , 2009) used to segment the basal ganglia structures, and (2) a multi-parameter mapping (MPM) protocol based on multiecho 3D fast low angle shot (FLASH) sequence (Helms and Dechent, 2009, Draganski *et al.* , 2011) to extract underlying microstructural parameters.

For the T1-weighted MPRAGE sequence, 176 sagittal partitions were acquired with a resolution of 1mm isotropic within a nominal scan time of 9.04min (field of view (FOV) = 224x256mm^2, repetition time (TR) = 2420ms, echo time (TE) = 4.18ms , inversion time = 960ms, flip angle (FA)= 9°, readout bandwidth = 150 Hz/pixel.

The MPM protocol consisted of 3 volumes with different contrast-weights with 176 sagittal partitions and 1mm isotropic resolution scanned within a nominal time of 23min (FOV = 240 x 256mm^2, readout bandwidth = 480Hz/pixel). The 3 different contrast-weighted volumes included a T1-weighted image (TR = 25ms, FA = 23°), a proton density (PD)-weighted image (TR = 25ms, FA = 4°), and a magnetization transfer (MT)-weighted image (TR = 37ms, FA = 9°). For all MPM images, alternating gradient echoes were acquired at seven equidistant echo time points between 2.46ms and 17.22ms, whereas for T1-weighted and PD-weighted images one additional echo at 19.68ms was acquired. MT weighting was achieved by applying an off-resonance RF pulse prior to nonselective excitation. Parallel imaging with a speed-up factor of 2 was used in the phase-encoding (anterior–posterior) direction using a generalized auto-calibration partially parallel acquisition algorithm (GRAPPA) to reduce the overall acquisition time.

5.3.3 Image analysis

5.3.3.1 Segmentation of basal ganglia based on T1-weighted MPRAGE images

Thalamus, striatum, and globus pallidus were automatically identified using a newly developed segmentation algorithm known as the MAGeT brain algorithm (Chakravarty *et al.* , 2013, Pipitone *et al.* , 2014), which is based on serial histological data (Chakravarty *et al.* , 2006). In contrast to automated model-based segmentation approaches, where usually a single rater identifies an anatomical structure on a template which then serves as a label being co-registered to a specific subject's unique neuroanatomy (Chakravarty *et al.* , 2009a, Chakravarty *et al.* , 2009b), MAGeT brain uses a multi-atlas-based strategy while still relying on a single well-defined template. This strategy overcomes the limitations of model-based segmentation, namely reduced accuracy induced by errors in the transformation estimation, incompatible neuroanatomical differences between the neuroanatomy of the template and the subject, and resampling errors after the application of the transformation to the labels. MAGeT brain algorithm uses a single atlas containing the thalamus, striatum, and globus pallidus based on the average of 27 MRIs of the same individual (Holmes *et al.* , 1998). This atlas is first registered to a representative subset of the dataset (21 subjects) using nonlinear transformations (Chakravarty *et al.* , 2008, 2009ab). This set of subjects now serves as a set

of templates and all other subjects are now warped to these templates using non-linear registration, resulting in 21 candidate segmentations for each subject. Using a voxel-wise majority vote (Collins and Pruessner, 2010), the 21 candidate labels are fused to output the final segmentation. All segmented images were manually checked by two authors (RP, EH) to ensure high segmentation quality. After quality checking the segmentation, one baseline scan of one healthy control was excluded. This results in a total number of MPRAGE scans analyzed of 20/17 (controls/ patients) at baseline, 21/14 at 3-month, 21/17 at 6-month, 20/17 at 12-month and 21/13 at 24-month.

5.3.3.2 Surface area calculation

A surface-based methodology originally proposed by Lerch et al. (2008) was modified to benefit from the multiple nonlinear deformation fields, created during the image segmentation process, that map each subject to the original atlas. First, the shape of each structure was estimated by applying the marching cube algorithm (Lorensen and Cline, 1987) to the input atlas of each subject, which was then morphologically smoothed using the AMIRA software package (Visage Imaging; San Diego, CA, USA). The resulting surfaces consist of about 3000 per thalamus, 6300 vertices per striatum, and 1200 per globus pallidus. Second, transformations from the 21 candidate segmentations were averaged within each subject and then across the template library to reduce noise (Frey *et al.* , 2011).

This procedure also results in 21 possible surface segmentations, which are subsequently merged for each subject and time point, resulting in a new surface representation for each basal ganglia structure for each subject and time point. Surfaces are merged by identifying the median location of each vertex in all 21 possible surfaces. Then, for each vertex, a third of the surface of each connecting triangle is assigned to the vertex surface area. A surface-base diffusion-smoothing kernel was then applied (5 mm and 3 mm for the thalamus/ striatum and globus pallidus, respectively). This provides surface-area values (Raznahan *et al.* , 2014) parallel to the normal, offering measures of surface contraction and expansion.

5.3.3.3 Microstructural analysis

MT-weighted, PD-weighted, and T1-weighted FLASH volumes were used to calculated quantitative MT, R1, and R2* maps as described previously (Helms and Dechent, 2009, Draganski *et al.* , 2011, Weiskopf *et al.* , 2011). R1 maps were corrected for radiofrequency transmit field in homogeneities with UNICORT (Weiskopf *et al.* , 2011). For each subject and time point, MT, R1, and R2* maps were coregistered to their respective T1-weighted image using a 6 parameter registration with a normalized mutual information cost function (https://github.com/CobraLab/minc-toolkit-extras/blob/master/bestlinreg_g). After coregistration, segmentations of the thalamus, striatum, and globus pallidus (including the subnuclei) obtained from MAGeT Brain were used as a binary mask to extract mean values of MT, R1, and R2* for each subject and timepoint. The first subjects and

patients included in this study did not receive the MPM protocol. After quality checking, data was excluded from 1 healthy control at 3-month, and of 2 patients at baseline, and of 1 patient at 12-month resulting in a total number of scans analyzed of 17/12 (patients/controls) at baseline, 17/11 at 3-month, 18/16 at 6-month, 17/17 at 12-month, and 18/13 at 24-month.

5.3.4 Statistics

R software package (R Core Team, 2016) was used for all statistical analysis. Clinical measures and vertex-wise shape measures were analyzed using mixed-model regression as it permits the inclusion of multiple measurements per person at different time points and at irregular intervals between measurements (Pinheiro and Bates, 2000). We first compared rates of change of these measures between patients and healthy controls by including a group × time (reflecting degeneration /plasticity) and a group x squared time (reflecting acceleration/ deceleration) interaction in the regression model. For clinical measures, time was modelled on a log scale to account for non-linear recovery patterns. Age and sex terms were included to accommodate potential confounding effects. To identify in which specific nuclei group differences are observed, we superimposed a cytoarchtiectonic atlas for the thalamus (Chakravarty *et al.* , 2006, Chakravarty *et al.* , 2008) on our thalamic template. Second, in those structures that showed group differences in surface area over time, we explored for underlying differences in microstructure (MT, R1, R2*) using the same models. Last, associations between early shape structure at 1-month and clinical outcome at 24-month were investigated using linear regression models adjusted for age and gender. As baseline clinical scores are known to have an important influence on the primary outcome, we further adjusted significant models for appropriate clinical baseline scores. All vertex-wise analyses were corrected for multiple comparisons using the false discovery rate (FDR) at 10% (Genovese *et al.* , 2002).

5.4 Results

5.4.1 Demographics

We included a total of 17 SCI patients (43.8±19.9 years, 14 male) and 21 healthy controls (33.8±9.8 years; 13 male); they did not significantly differ in age compared to the controls ($p<0.05$). The baseline scan was acquired 1.4±0.5 months after injury, respectively at 3.5±1.5, 7.1 ± 1.9, 13.3±3.1 and 28.7±5.1 months after injury for the 3-, 6-, 12- and 24-month scan. Eight patients were tetraplegic and 9 patients were paraplegic. All clinical data of patients is summarized in Table 8.

Over the 2 years, patients recovered by 2.76 points per log month on their lower extremity motor score ($p=0.001$, 95%CI: (1.07 4.45)), by 0.91 point per log month on their upper extremity motor score ($p=0.046$, 95%CI: (0.02 1.80)), and by 7.89 points per log month on their SCIM score ($p<0.001$, 95CI: (5.03 10.75)). Light-touch and pin-prick score remained unchanged over time ($p=0.152$, $p=0.790$).

ID	Age at injury	Injury type	Initial Site of Impairment (motor/sensory)	INSCSCI upper extremity motor score (Baseline/ 24-months)	INSCSCI lower extremity motor score (Baseline/ 24-months)	INSCSCI light-touch score (Baseline/ 24-months)	INSCSCI pin-prick score (Baseline/ 24-months)	SCIM score (Baseline/ 24-months)
1	18	Fall	C5/ C4	19/ 22	0/ 0	24/ 30	27/ 32	4/ 22
2	23	Fall	C7/ C6	42/ 48	0/ 23	69/ 70	38/ 33	23/ 70
3	68	Fall	T10/ T10	50/ 50	2/ 31	78/ 74	75/ 65	41/ 46
4	44	Fall	T12/ T12	50/ 50	39/ 45	107/ 106	109/ 98	84/ 100
5	42	Fall	T11/ T11	23/ 26	0/ 0	27/ 21	20/ 17	18/ 41
6	71	Fall	C7/ C8	36/ 48	16/ 42	85/ 66	36/ 25	17/ 43
7	20	MVA	C5/ C5	21/ 21	0/ 0	21/ 45	19/ 18	4/ 39
8	30	MVA	C7/ C8	47/ 47	0/ 0	64/ 72	35/ 30	38/ 40
9	52	Fall	T9 / T9	50/ 50	48/ 49	95/ 94	89/ 90	84/ 100
10	42	MVA	C5/ C4	41/36	46/ 48	104/ 99	104/ 96	99/ 100
11	29	Fall	T11/ T11	50/ 50	10/ 12	86/ 76	88/ 69	52/ 68
12	71	ischemia	T1/ T10	50/ 50	43/ 50	88/93	72/ 67	47/ 69
13	71	CSM	T1/ T4	50/ 50	43/ 50	83/ 112	81/ 112	56/ 97
14	73	ischemia	T1/ T11	50/ 50	0/ 0	75/ 71	77/ 72	28/ 36
15	31	SA	C4/ C5	20/ 26	0/ 0	22/ 31	19/ 20	13/ 25
16	28	SA	C4/ C3	15/ 10	0/ 0	14/ 23	14/ 23	16/ 20
17	32	SA	T1/ T4	50/ 50	9/ 50	79/ 112	58/ 77	40/ 96

Table 8: Clinical and epidemiological data for all patients included in the study.

Abbreviations: AIS = American Spinal Injury Association Impairment Scale; GRASSP = Graded Redefined Assessment of Strength, Sensibility and Prehension; NA = not available; NS = no signal alteration within myelon; SA = Swimming Accident; SCIM = Spinal Cord Independence Measure; WISCI = Walking Index for Spinal Cord Injury

5.4.2 Time course of vertex-level surface area changes

The surface area analysis demonstrated linear changes over time in patients compared to controls in the thalamus and striatum, but not in the globus pallidus.

Specifically, both thalami showed surface expansion in patients compared to controls over time within the superior parts of the ventral anterior nuclei (VAN), and surface contractions within its inferior parts (Fig. 17). In the left thalamus, these changes were levelling-off over time (i.e. negative/ positive quadratic term) (Fig. 18). In the superior parts of the ventral lateral nuclei (VLN), both thalami showed linear surface expansions in patients compared to controls over time. In addition, the left thalamus showed surface contraction in patients compared to controls within the inferior parts of the VLN. Both thalami showed surface expansions within the posterior part of the ventral posterior nuclei (VPN). The right thalamus also showed contractions within the anterior part of the VPN. Both changes within the right VPN were levelling-off over time. Left and right pulvinar nuclei showed linear surface contractions in patients compared to controls, in particular within lateral and the medial pulvinar.

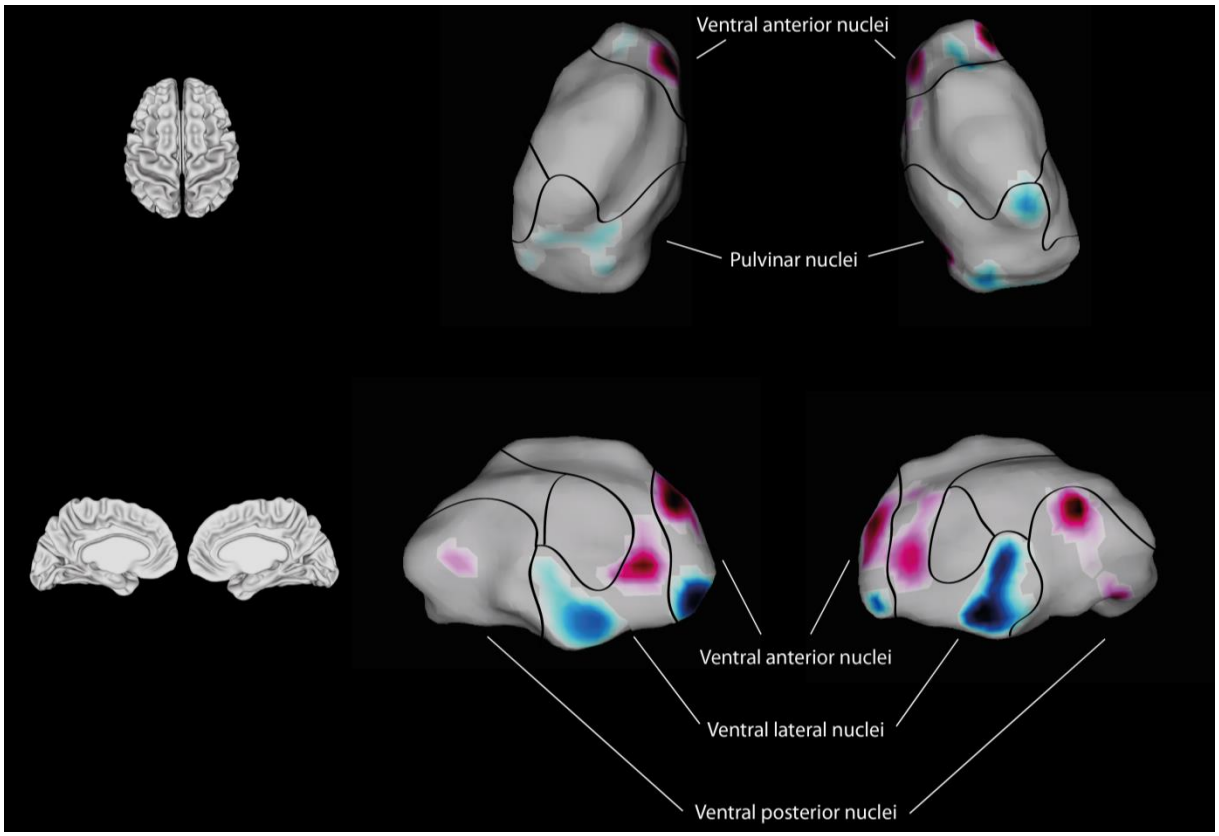

Figure 17: Linear shape differences within the thalamus estimated as significant surface area contractions and expansions. All surface area contractions (representing degeneration) are represented in blue color, and all surface area expansions (reflecting compensatory plasticity) are shown in red color. Compared to controls, patients showed contractions of surface area within the inferior part of the ventral anterior and ventral lateral nuclei (motor nuclei) and within the pulvinar nuclei over the first 24 month after SCI. Surface area expansions were evident in the superior parts of the ventral anterior and ventral lateral nuclei (motor nuclei), as well as within the ventral posterior nuclei (sensory nuclei).

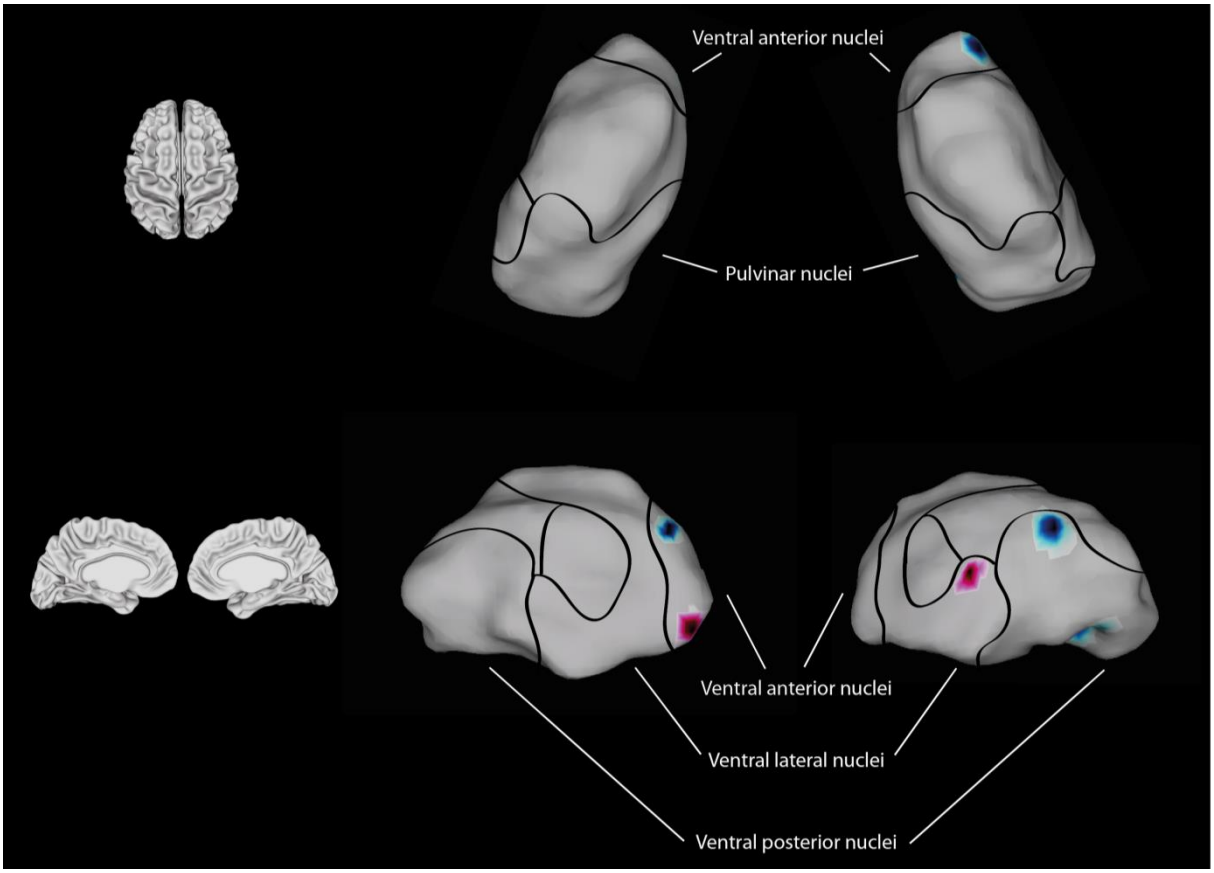

Figure 18: Quadratic shape differences within the thalamus estimated as significant surface area contractions and expansions. All surface area contractions are represented in blue color, and all surface area expansions are shown in red color (both reflecting levelling-off of linear changes). Compared to controls, patients showed levelling-off of surface area contractions within the left ventral anterior nucleus and within the right ventral lateral nucleus. Surface area expansions levelled-off bilaterally within the ventral anterior nuclei and within the left ventral posterior nucleus.

In the striatum, patients showed bilateral surface area contractions and expansions over time in the caudate and the putamen compared to controls. Specifically, bilateral contractions were evident medially within the central to posterior part of the caudate (Fig. 19A), which levelled-off over time in patients compared to controls (Fig. 20). Bilateral expansions of surface area were observed in the inferior part of the anterior caudate (Fig. 19B), also bilaterally levelling-off over time, and in the inferior parts of the ventral caudate (i.e. nucleus accumbens; Fig. 19C), which showed a levelling-off over time at the left side only. Unilateral contraction of surface area was evident in the left lateral part of the anterior caudate (Fig. 19D). Within the putamen, bilateral contractions of surface area were observed in the medial central (Fig. 19E) as well as the lateral anterior putamen (Fig. 19F). The surface area of the right lateral anterior putamen showed a levelling-off over time in patients compared to controls. In addition, surface area contractions were observed in the left medial posterior (Fig. 19G), left medial anterior (Fig. 19H) and left lateral superior posterior putamen (Fig 19I). Expansions in surface area were detected within the left medial anterior (Fig. 19J) and lateral anterior putamen (Fig 19K). Expansions within the left anterior putamen levelled-off over time in patients compared to controls.

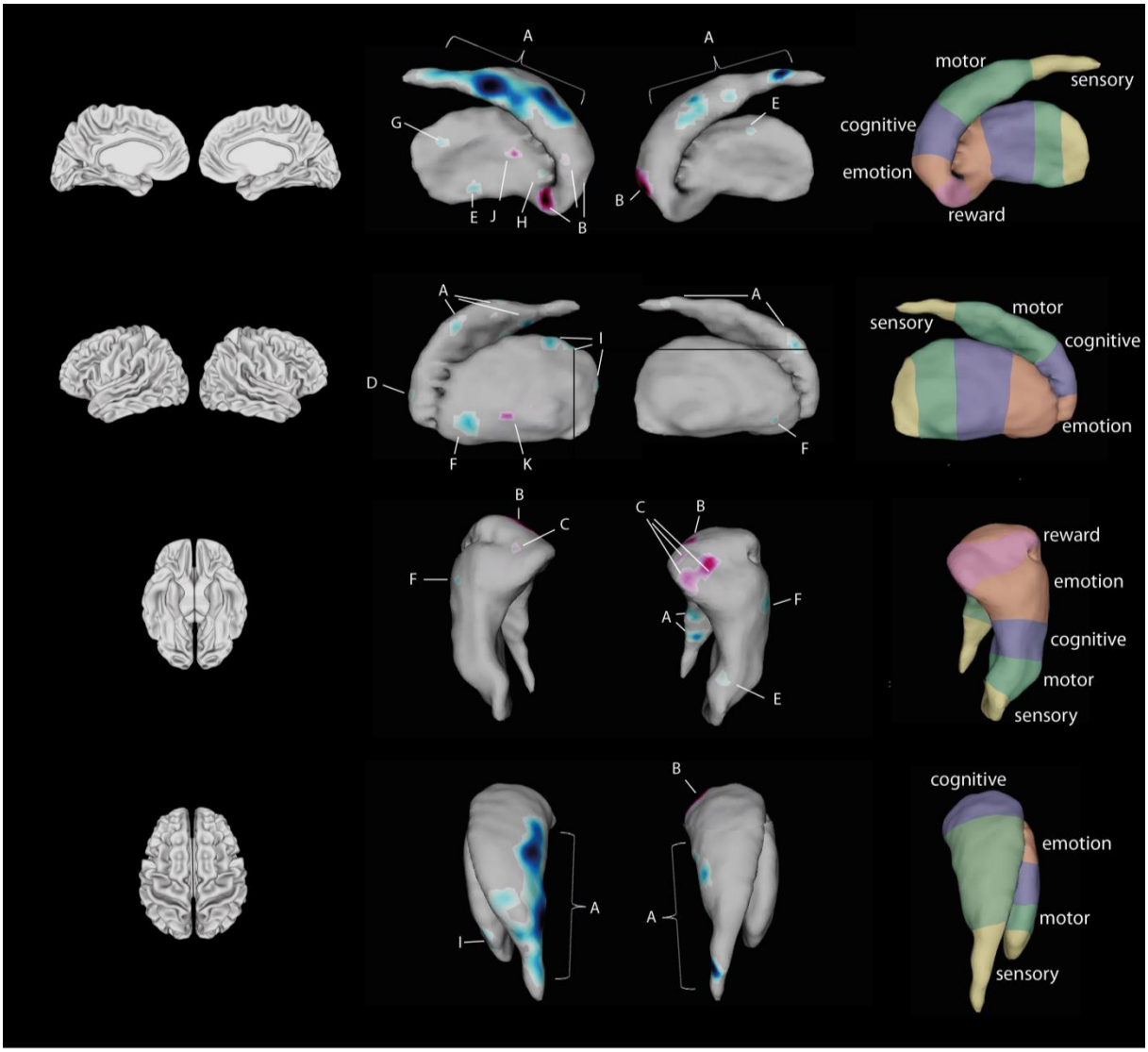

Figure 19: Linear shape differences within the striatum estimated as significant surface area contractions and expansions. All surface area contractions (representing degeneration) are represented in blue color, and all surface area expansions (reflecting compensatory plasticity) are shown in red color. Compared to controls, patients showed contractions of surface area within the putamen, and the caudate, in particular in regions involved in sensorimotor and emotion processing, and in cognitive function over the first 24 month after SCI. Surface area expansions were evident in regions involved in cognition, emotion and reward processing. Please note that the atlas on the right shows the somatotopy of the striatum, based on a review of functional MRI studies (Arsalidou, 2013). Labels therefore represent approximate regions of corresponding functions.

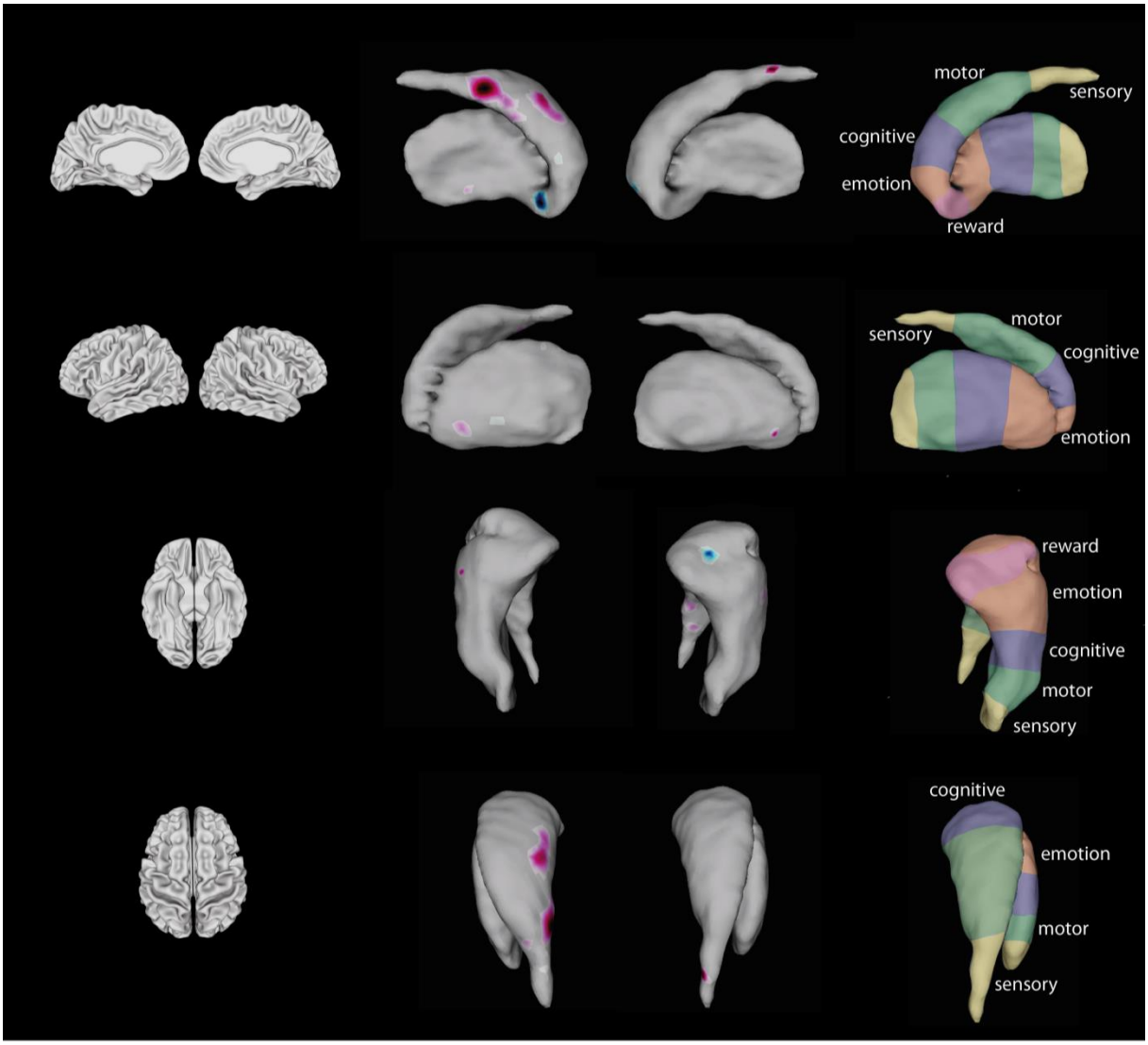

Figure 20: Quadratic shape differences within the striatum estimated as significant surface area contractions and expansions. All surface area contractions are represented in blue color, and all surface area expansions are shown in red color (both reflecting levelling-off of linear changes). Compared to controls, patients showed levelling-off of surface area contractions within regions involved in sensorimotor and emotion processing over the first 24 month after SCI. Surface area expansions levelled-off in regions involved in cognition, emotion and reward. Please note that the atlas on the right shows the somatotopy of the striatum, based on a review of functional MRI studies (Arsalidou, 2013). Labels therefore represent approximate regions of corresponding functions.

5.4.3 Time course of microstructural changes

Within the thalamus, the left VAN (patients decrease by 6.527s^{-1}/month [95% CI: (-11.526 -1.527)] more than controls, p=0.011), the left (patients decrease by 6.054 $^{-1}$/month [95% CI: (-11.018 -1.089)] more than controls, p=0.017) and right VLN (patients decrease by 5.156s^{-1}/month [95% CI: (-9.760 -0.552)] more than controls, p=0.028), and the left VPN (patients decrease by 5.185 s^{-1}/month [95%CI: (-10.214 -0.157)] more than controls, p=0.043) showed progressive decreases of myelin-sensitive R1, which levelled-off over time in all structures except the VPN (left VAN: 0.193 s^{-1}/$month^2$, 95%CI: (0.032 0.354), p=0.019; left VLN: 0.173 s^{-1}/$month^2$, 95%CI: (0.0131 0.333), p=0.034; right VLN: 0.159 s^{-1}/$month^2$, 95%CI: (0.011 0.307), p=0.036).

In the striatum, we observed a greater rate of linear decrease of myelin-sensitive MT in the left (patients decrease by 0.020^{-1}/month [95% CI: (-0.039 -0.001)] more than controls, p=0.047) and right ventral striatum (patients decrease by 0.017s^{-1}/month [95% CI: (-0.033 -0.001)] more than controls, p=0.037), and in the left pre-comissural caudate (patients decrease 0.020s^{-1}/month [95% CI: (0.038 -0.003)] more than controls, p=0.021) in patients compared to controls. In addition, myelin-sensitive R1 decreased within the left pre-commisural caudate (patients decrease by 4.598s^{-1} per month [95% CI: (-8.887 -0.308)] more than controls, p=0.036), and levelled-off over time (0.164 s^{-1}/$month^2$, 95%CI: (0.025 0.303), p=0.021). The left post-comissural caudate showed greater rate of linear decreases in iron-sensitive R2* in patients compared to control (patients decrease by 0.001s^{-1}/month [95% CI: (-0.001 -0.001)] more than controls, p=0.034).

Patients had a significantly greater rate of linear change of myelin-sensitive R1 in the left (patients decrease by 5.570s^{-1}/month [95% CI: -10.728 -0.411] more than controls, p=0.034) and right globus pallidus (patients decrease by -5.674s^{-1} per month [95% CI: -10.763 -0.585] more than controls, p=0.029), which levelled-off over time (left: 0.178 s^{-1} /$month^2$, 95%CI: 0.013 0.343, p=0.034; right: 0.187s^{-1}/$month^2$, 95%CI: 0.024 0.350, p=0.024).

5.4.4 Relationship of 1-month macro- and microstructural parameters and outcome

Significant relationships between local surface area of the basal ganglia at 1-month and 24-month clinical outcome were observed in the left and right striatum. Increased surface area expansions within the central caudate and the lateral central-posterior putamen at 1-month were associated with better lower extremity motor score at 24-months. This relationship persisted even when corrected for 1-month lower extremity motor score (Fig. 21A).

Higher iron-sensitive R2* levels within the left and right pulvinar nuclei were associated with lower 24-month pin-prick score (left: p=0.036, R^2=0.57, 95%CI: (-8946.01 -385.67); right: p=0.02, R^2=0.58, 95%CI: (-11298.95 -776.50)) (Fig. 21B). When adjusted for baseline clinical score, this relationship did not sustain.

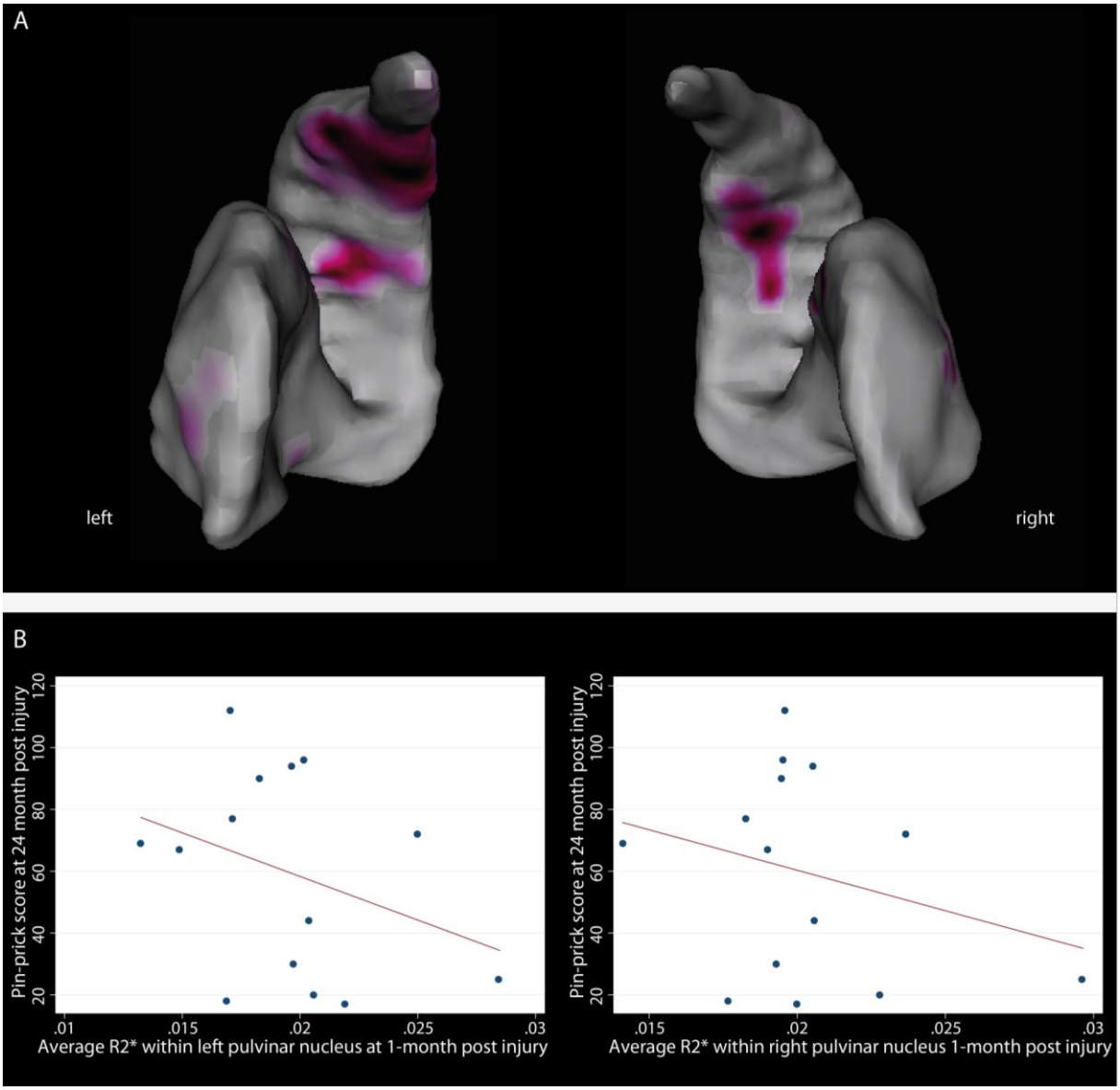

Figure 21: Relationship between 1-month structural and microstructural parameters and outcome. A) Local morphological features of the striatum (motor region) at 1-month post injury predicted 24-month lower extremity motor score, adjusted for age, gender and appropriate baseline clinical score. Red blobs indicate surface area expansions (reflecting compensatory plasticity) – patients with increased surface area at 1-month presented better 24-month lower extremity motor score. B) Higher R2* values at 1-month, indicating higher iron levels, predicted 24-month pin-prick score. When corrected for appropriate baseline score, this association did not persist.

5.6 Discussion

In this study, patients showed a distinct pattern of structural changes in the extrapyramidal system comprising the thalamus, striatum and globus pallidus within the first 2 years after SCI. Over time, we observed both surface contractions and extensions, along with underlying changes in microstructural parameters indicative of demyelination and iron changes. At 1-month such changes within the motor caudate were predictive of 24-month lower extremity motor score, even when adjusted for clinical baseline score.

5.6.1 Time course of surface area and microstructural changes

Previous studies have described anatomical and functional changes within the thalamus after SCI (Pattany *et al.* , 2002, Grabher *et al.* , 2015, Jutzeler *et al.* , 2016). We provide new evidence by showing which sub-regions of the latter structures are most affected. Specifically, patients showed bilateral surface area expansions over time in the superior aspects of the VAN, VLN and VPN compared to controls, and surface area contractions in the inferior parts of the VAN and the VLN, paralleled by decreases in myelin-sensitive R1. The VAN and the VLN are two nuclei of the motor thalamus, with the VAN mainly receiving input from the globus pallidus and projecting to the premotor cortex, and the VLN receiving afferents from the substantia nigra, globus pallidus and the cerebellum and projecting to both primary motor cortex and premotor cortex (Nambu, 2011). The VPN on the other hand, is the thalamic principal somatosensory nucleus receiving input from the lemniscus medialis (transmitting light touch, vibration, and proprioception) and from the spinothalamic tract (transmitting pain and heat sensation), and projecting to the premotor cortex. As within the primary motor and sensory cortices, the sensorimotor thalamic nuclei are also organized somatotopically (Nambu, 2011) with distal muscles being represented dorsal to those for proximal limb portions; and more cranial representations were found more anterior (Asanuma and Hunsperger, 1975, Strick, 1976, Asanuma *et al.* , 1983, Vitek *et al.* , 1994, Schmid *et al.* , 2016). As the sensorimotor thalamus is well conserved across vertebrates, it is likely that the somatotopy is also conserved in humans (Bosch-Bouju *et al.* , 2013). We therefore interpret our observed contractions of surface area in the motor thalamus as local changes within the distal parts of the limbs, in particular in leg areas, and our observed surface area expansion within the sensorimotor thalamus as changes within proximal part of the limbs, in particular in hand areas. Based on animal studies, possible mechanisms for local volume decreases (i.e. surface area contractions) might include changes in the amount of neurons induced by trans-synaptic degeneration, neuronal death, demyelination, synaptic pruning, or changes in the amount of glial cells (Hains *et al.* , 2003, Kim *et al.* , 2006). On the other hand, axonal sprouting and activity-dependent plasticity (Lee *et al.* , 2004) might account for volume increases (i.e. surface area expansions). In particular, compensatory use of the upper limbs might drive expansion of cortical M1 hand area into output-deprived leg area (Ghosh

et al. , 2010) as a consequence of the rewiring of axotomized hind limb neurons onto cervical motor circuits (Ghosh *et al.* , 2010); the same mechanism might also be reflected in the basal ganglia. As such observed surface area changes are not specific to any single pathological process, R1 complement such readouts as they are reflective of demyelination (Lutti *et al.* , 2014), increases in proton density (Gelman *et al.* , 2001, Rooney *et al.* , 2007, Harkins *et al.*, 2015), or decreases in lipid content indicative of degeneration (Stanisz *et al.* , 2005). Overall, demyelinating processes seem to be present within the sensorimotor nuclei of the thalamus.

In addition to sensorimotor nuclei in the thalamus, the lateral and medial pulvinar nuclei showed surface area contraction over time. They are involved in visual attention regulation, and also link visual stimuli with contex- specific motor responses (Petersen *et al.* , 1987). Furthermore, the medial pulvinar also integrates multimodal sensory inputs with limbic influence and coordinates such sensory input with its corresponding motor response (Cappe *et al.* , 2009). As most SCI patients have motor and sensory deficits, it seems likely that the coordination between these two modalities is also altered. In addition, both animals and humans show altered visual activity and connectivity between the visual cortex and other regions after SCI, (Hawasli *et al.* , 2018), maybe because they rely stronger on their visual input in order to coordinate limb movements

Similarly, in the striatum, we observed surface area contractions in patients compared to controls in regions involved in cognition, sensorimotor and emotional processing and surface area expansions were observed in regions involved in cognition, emotion and reward processing (Arsalidou *et al.* , 2013). These changes were paralleled by decreases in myelin-sensitive R1 and MT (Helms *et al.* , 2008, Helms and Dechent, 2009). Interestingly, we observed bilateral surface area contraction within thin the medial and lateral dorsal part of the motor putamen, and as the putamen consists of two sets of somatotopic representation (Tokuno *et al.* , 1999), this indicates loss of afferents from both the primary motor cortex and the supplementary motor area. This is in line with previous studies, showing that both of these structures show altered function and structure (Bruehlmeier *et al.* , 1998, Wrigley *et al.* , 2009a, Freund *et al.* , 2013ab, Hou *et al.* , 2014, Jutzeler *et al.* , 2016). In addition, whereas most studies show elevated iron levels in neurodegenerative diseases (Andersen *et al.* , 2014), we found decreased R2* in the left post-comissural caudate over time in patients compared to controls. R2* maps (=1/T2*) are linearly correlated with tissue iron concentration (Yao *et al.* , 2009). Interestingly, this is the region processing sensorimotor function and showing most prominent surface area contractions. In healthy controls, iron enters the brain via the blood system bound to transferrin and is afterwards presumably taken up by oligodendrocytes and to a less extend by pericytes (Gerber and Connor, 1989) to prevent the environment of the toxic effect of iron and its generated free radicals. In neurodegenerative disorders, it is thought that glial cells are not able to

fully take up iron and therefore iron accumulation appears within disease-specific regions affected by neurodegeneration (Andersen *et al.* , 2014). Possible mechanism for our observed changes might involve chronic neuroinflammation, which is characterized by the invasion of astrocytes and microglia. It was previously shown that iron uptake persists in the central nervous system even in the absence of normal oligodendrocytes and myelin, with astrocytes and microglia sequestering iron via phagocytosis (Connor and Menzies, 1990).

Last, the globus pallidus did not exhibit any surface area changes in patients over time, but we observed decreases in myelin-sensitive R1 in the absence of macrostructural changes pointing at the increased sensitivity of MPM protocols.

5.6.2 Relationship of 1-month macro- and microstructural parameters and outcome

In the present study, we revealed that at 1-month, surface area expansions within the motor striatum were predictive of 24-month lower extremity motor score and R2* within the pulvinar nuclei predicted 24-month pinprick score. Previous studies showed that volume changes within the first 12 months after injury within the right internal capsule, which also encompasses the corticospinal tract, were associated with total motor score at 12-months (Freund *et al.* , 2013a). In addition, volume changes within the corticospinal tract (at the level of the medullary pyramid) and the pons, as well as MT changes within the sensorimotor cortex within the first 6 month after injury were predictive of 24-month lower extremity motor outcome (Ziegler *et al.* , 2018). Changes of R2* within the first 6-month in the right cerebellum and ACC were predictive of 24-month pin-prick score (Ziegler *et al.* , 2018).

It might appear rather surprising at first, that the basal ganglia predict outcome earlier than the primary motor cortex and the corticospinal tract, as the latter are directly involved in execution of movements, whereas the basal ganglia are rather orchestrating and fine-tuning motor commands. However, the mechanisms of reorganization might be fundamentally different. After SCI, the motor system undergoes degenerative changes in grey and white matter, relating to neuronal degeneration, demyelination, shrinkage of somata of pyramidal neurons (Wannier *et al.* , 2005) and apoptotic cell death in a proportion of axotomized cortical motor neurons (Hains *et al.* , 2003). Characterizing the temporal evolution of Wallerian degeneration and distinguishing this effect from other mechanisms (e.g. volume changes associated with changes glia cells) is challenging in humans and has so far not fully been characterized. In animals, degenerative changes within the primary motor cortex have been observed within the first weeks after injury (Hains *et al.* , 2003, Kato *et al.* , 1997). However, as the distance from lesion to cortical areas is much smaller than in humans and MRI methods are less sensitive than histological analysis, it seems rationale that this process cannot be observed at the earliest stages after human injury. In addition, clinical motor scores solely

measures strength of different muscles, but the primary motor cortex represents movement, defined as coordinated motions about joints, rather than single muscle strength. We speculate that this might be reasons, that early markers within the motor system are not predictive of long-term clinical outcome.

Within the basal ganglia, early surface area expansions within motor regions of the striatum predicted lower extremity motor score. In contrast to the motor system, this speaks for compensatory plasticity – a phenomena also known in Multiple sclerosis (Hier and Wang, 2007) and Parkinson's disease (Worker *et al.* , 2014). After SCI, the transection of corticospinal axons causes a decrease of target-derived trophic support of the cell bodies, which leads to a decreased regional blood flow along with decreased activation in the motor cortex in the early phase after injury (Cermik *et al.* ,2006; Jurkiewicz *et al.* , 2007), accompanied by increased activation in associated sensorimotor regions. Specifically, increased intra-hemispheric functional interaction within the primary motor cortex, premotor cortex, SMA, thalamus and cerebellum was observed (Hou *et al.* , 2014). In line, Min et al. (2015) showed increased function connectivity between the secondary somatosensory cortex and the basal ganglia, suggesting that the basal ganglia affects movement by gating sensory inputs in motor areas (Lidsky *et al.* , 1985). In functional imaging studies in monkeys, an increased activity of the ventral striatum was shown during a reach- and grasp task in association with the primary motor cortex (M1) when the animals were recovering from an incomplete SCI (Nishimura *et al.* , 2007, Nishimura *et al.* , 2011); the amount of activity being associated with the extent of recovery. Pharmacologically inactivating the ventral striatum early after injury led to a reduced activity in the sensorimotor cortex which was accompanied by a diminished recovery of the dexterous finger movements during rehabilitation (Sawada *et al.* , 2015). This suggests that the striatum plays a direct role in finger movement control. We therefore speculate that early structural changes within the motor striatum may reflect activity-dependent plasticity, leading to increased functional activity helping to compensate for the motor dysfunction. Our data suggests that establishing novel structural substrates (e.g. axonal sprouting, myelination) within the extrapyramidal system helps in recovery after SCI.

5.6.3 Limitation

This study had a number of limitations. First, the applied MPM protocol, consisting of MT, R1 and R2* measures, are sensitive to demyelination, degeneration and iron content, but not specific to them as they are indirect markers of such processes. Therefore, we cannot certainly identify the exact underlying pathological process. Second, although we identified the gross location of changes within the striatum and the globus pallidus, we currently lack a histology-based atlas of the striatum and the globus pallidus. Second, although our groups did not significantly differ in age or gender; the mean age was on average higher and there were less women in the patients group, which could potentially

affect the analysis. We therefore adjusted for age and gender as potential confounders of no interest in all analyses. Last, in future studies we hope to better understand underlying mechanisms driving basal ganglia changes by investigating the relationship of structural changes between motor and sensory cortex, their associated regions, and the basal ganglia. Such studies of structural connectome will help to better understand the structure and function of complex brain networks and their role after SCI.

5.7 Conclusion

In summary, this study provides evidence for progressive extrapyramidal macro- and microstructural changes after SCI, indicating large scale, transneuronal complex remodeling of primarily unaffected brain regions. We observed surface area contractions and expansion in the thalamus and the striatum, with a remarkable somatotopic reorganization pattern with its sensorimotor regions, along with microstructural changes. In particular, foot representative regions showing sign of degeneration, demyelination and/or neuroinflammation, whereas hand representative areas exhibited local surface area increases, indicative of ongoing compensatory mechanism (axonal sprouting and activity-dependent plasticity). Importantly, increased compensatory reorganization within the motor caudate at 1-month were predictive of 24-month lower extremity motor score, adjusted for baseline clinical status. This study therefore provides unbiased, quantitative readouts of nuclei-specific changes relating to clinical readouts, which might serve as future biomarkers.

6 Literature Review

Tracking trauma-induced structural and functional changes above the level of spinal cord injury

Eveline Huber, Armin Curt, Patrick Freund

This orginal article is published in Current Opinion in Neurology.

Literature research was conducted by E.H. EH., A.C. and P.F. wrote the manuscript. All authors reviewed the manuscript.

6.1 Abstract

Purpose of review: This review will highlight the latest findings from neuroimaging studies that track structural and functional changes within the central nervous system at both the brain and spinal cord levels following acute human spinal cord injury (SCI). The putative, underlying biological mechanisms of structural change (e.g. degradation of neural tissue) rostral to the lesion site will be discussed in relation to animal models of SCI and their potential value in clinical studies of human SCI.

Recent findings: Recent prospective studies in human acute SCI have begun to reveal the time-course, spatial distribution and extent of structural changes following an acute SCI and their relation to functional outcome. Adaptive changes in sensory and motor pathways above the level of the lesion have prognostic value and complement clinical readouts.

Summary: The introduction of sensitive neuroimaging biomarkers will be an essential step forward in the implementation of interventional trials in which proof-of-concept is currently limited to clinical readouts, but more responsive measures are required to improve the sensitivity of clinical trials.

6.2 Introduction

Key points

- Innovative new multimodal MR protocols allow for the quantification of trauma-induced white and gray matter changes in the spinal cord and the brain above the level of SCI.
- Longitudinal studies in both animals and humans are key to understand the course of structural and functional changes from the acute to the chronic stage of SCI, as well as the prediction of early structural changes and their relation to clinical outcomes.
- Translation between experimental animal models of SCI and clinical (human) SCI will be essential to provide information about the comparability of these models and their ability to distinguish specific disease stages such as how to define the transition from acute to chronic SCI, the dynamic stages of secondary axonal and/or myelin degeneration and training or treatment-induced effects of repair and neural plasticity.

Spinal cord injury (SCI) is a devastating life event affecting mostly the young (mean age at injury: 33 years) and is 3.8 times more prevalent in men than in women (Wyndaele and Wyndaele, 2006). Worldwide, about 23 cases per million occur annually (Cripps *et al.* , 2011) with tetraplegia slightly more common than paraplegia (Wyndaele and Wyndaele, 2006). In the majority of instances, patients are left with profound and persistent functional impairments such as immediate paralysis, sensory disturbance and the emergence of neuropathic pain at or below the level of injury as a secondary complication (Siddall and Loeser, 2001, Siddall *et al.* , 2004). A main reason for the limited degree of recovery following SCI relates to failure of the interrupted nerve fiber tracts to regenerate across the lesion site in the adult central nervous system (CNS) of mammals and humans (Schwab, 2004). Important impediments that form the basis of this phenomenon are proteins expressed in CNS myelin (e.g. Nogo-A), which inhibit neurite growth, and the formation of a glial scar that contains extracellular matrix molecules such as chondroitin sulphate proteoglycans (Kwok *et al.* , 2014). Apart from the failure to regenerate, plastic 'hardware' changes in the adult CNS of mammals and humans are restricted. Experimental treatments against these impediments have resulted in first-in-man phase-I trials for human SCI including anti-Nogo-A antibody treatments (Starkey and Schwab, 2012), stem cell transplantation (HuCNS-SC: NCT01321333 identified in ClinicalTrials.gov) and drug administration (Riluzole: NCT00876889 identified in ClinicalTrials.gov; Minocycline: identified as NCT00559494 in ClinicalTrials.gov; for a review, see Nagoshi and Fehling, 2015). Although much has been learned from these trials, they suffer from a lack of adequate outcome assessments and sensitive biomarkers with the potential to stratify the highly diverse patients into homogenous

cohorts and validate the efficacy of drugs (Tanadini *et al.* , 2014, Velstra *et al.* , 2014). To enable efficient translation, these interventions require biomarkers that can be used as surrogate makers of safety and efficacy of agents in a timely and economical manner (Cadotte and Fehlings, 2013).

This review addresses the structural and functional plasticity (i.e. secondary, rostral and degenerative structural changes) in both the spinal cord and the brain after SCI against the background of current advances in the field, their relation to clinical outcomes as well as challenges and future avenues in clinical SCI research.

6.3 Human spinal cord injury: non-invasive tracking of trauma-induced changes

Conventional magnetic resonance imaging (MRI) remains the gold standard for identifying the localization and the extent of an SCI (Dietz and Curt, 2006, Fehlings *et al.* , 2011) but does not allow for the quantification of trauma-induced disruption to the microstructure of the spinal cord and supraspinal changes. Novel quantitative MRI protocols of the spinal cord and brain have the potential to measure neural changes at the microstructural level. This is because the degree of myelination, iron content and neuronal microstructure are reflected in MR relaxation times, magnetization transfer and diffusion-weighted images which can be measured at high resolution (Mohammadi *et al.* , 2013b, Callaghan *et al.* , 2014, Mohammadi *et al.* , 2014). These novel quantitative MR methods include multiparametric mapping (Draganski *et al.* , 2011, Weiskopf *et al.* , 2011, Dick *et al.* , 2012, Weiskopf *et al.* , 2013, Lutti *et al.* , 2014) and diffusion tensor imaging (Le Bihan *et al.* , 2012) next to volumetric measures (i.e. voxel-based morphometry (Ashburner, 2009) and voxel-based cortical thickness (Hutton *et al.* ,2009).

6.3.1 Structural changes

By means of computational anatomy, trauma-induced structural changes have been revealed across the entire neuroaxis. In chronic SCI patients, cervical cross-sectional cord area, rostral to the site of injury, was reduced by up to 30% and white matter integrity within the corticospinal tracts altered (Cohen-Adad *et al.* , 2011, Freund *et al.* , 2011a, Petersen *et al.* , 2012). Further upstream, structural changes in terms of volume and microstructure within the white matter of the pyramids and internal capsule paralleled those of the spinal cord (Freund *et al.* , 2012a). At the cortical level, the primary sensorimotor cortices were atrophied (Jurkiewicz *et al.* , 2006, Wrigley *et al.* , 2009a, Freund *et al.* , 2011a). The question of the temporal evolution and spatial specificity of these atrophic changes was addressed in a recent longitudinal study in acute SCI patients ((Freund *et al.* , 2013a),; see Fig. 22). Extensive upstream structural changes appeared already within the first months after injury as reflected by a decrease in cervical spinal cord area (see Fig. 22AB), white matter volume of the corticospinal tracts at the level of internal capsule and right cerebral peduncle and gray matter

volume in M1 (see Fig. 22CD). Importantly, clinically eloquent relationships between structural spinal and brain changes of the sensorimotor system have been demonstrated. Specifically, the amount of motor and sensory disability, as assessed by the international standards for the neurological classification of SPI protocol (Kirshblum *et al.* , 2011), was directly associated with the degree of spinal (Cohen-Adad *et al.* , 2011, Lundell *et al.* , 2011, Freund *et al.* , 2012b) and brain atrophy (Jurkiewicz *et al.* , 2006, Freund *et al.* , 2011b). Moreover, a decrease in the left-right diameter of the cervical cord area correlated with the motor score and the anterior-posterior diameter with the sensory score (Lundell *et al.* , 2011), indicating tract-specific atrophy. These clinically eloquent structural changes along the neuroaxis are suggestive of axonal degeneration and demyelination of the corticospinal tracts and the volume reduction at the cortical level reflect soma shrinkage of injured corticomotor neurons (Lemon, 2008).

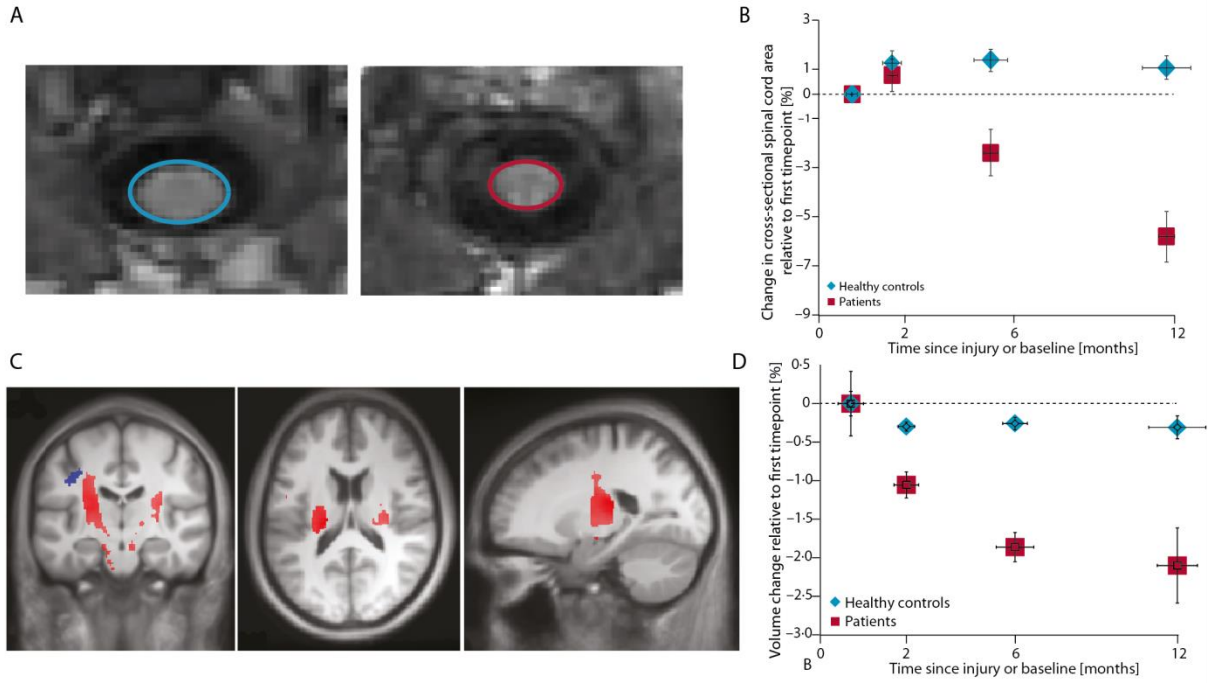

Figure 22: (a)/(b) Progressive structural changes of the acute injured spinal cord. (a) Representative example of a healthy control (spinal cord area highlighted in blue) and a chronic SCI patient (spinal cord area highlighted in red). (b) Change in cross-sectional spinal cord area differed significantly between patients and controls. Error bars show the standard errors of the scan intervals (horizontal) and of the percentage change in cross-sectional spinal cord area (vertical). (c)/(d) Longitudinal changes in local brain volume as revealed by tensor-based morphometry. (c) Statistical parametric map including the cranial corticospinal tract and the bilateral sensorimotor cortex (uncorrected P<0_001, shown for descriptive purposes). Regions of volume changes are highlighted in blue (gray matter) and red (white matter). (d) Changes in white matter volume in the corticospinal tracts, at the level of the left internal capsule, in patients and healthy controls over time. Error bars show the standard errors of the scan intervals (horizontal) and of the percentage change in spinal cord area (vertical). Adapted from Freund *et al.* , 2013.

6.3.2 Functional changes

Next to trauma-induced structural changes, brain (neural) activity in SCI – revealed by functional MRI – has shown motor task-related activation in the primary motor cortex (M1) and associated cortical motor areas in the subacute phase of SCI (Jurkiewicz *et al.* , 2007). In the transition from acute to chronic SCI, the area of M1 activation increased, whereas associated sensorimotor areas (e.g. supplementary motor areas) showed a progressive decrease in activation (Jurkiewicz *et al.* , 2007). Studies in chronic SCI patients indicate that the deafferented M1 regions remain hyperexcitable during motor stimulation (Freund *et al.* , 2013b). Loss of motor input was shown to induce an expansion of the M1 hand area of paraplegic and tetraplegic patients into the output-deprived M1 leg area (Bruehlmeier *et al.* , 1998, Curt *et al.* , 2002, Freund *et al.* ,2011a). However, whether these changes translate into functional output is questionable as stimulations of corticomotor neurons by transcranial magnetic stimulation (TMS) above the M1 leg area did not elicit hand/arm muscle activation (Freund *et al.* , 2011b).

Interestingly, a recent study showed in incomplete paraplegics patients that performance improvements through intensive virtual reality augmented coordination and balance training of foot and leg movements were directly linked to local volume increases in cortical and subcortical areas associated with learning and motor performance (Villiger *et al.* , 2015).

Brain reorganization may not only be related to functional recovery, but could also be associated with sensory disturbances as there is increasing evidence relating thalamic and cortical changes to the generation and/or maintenance of neuropathic pain below the level of injury (Wrigley *et al.* , 2009b, Gustin *et al.* , 2012). Functional and structural alteration in terms of decreased activity in the atrophied thalamus (Jurkiewicz *et al.* , 2006), as well as decreased cortical activity in frontal areas and possibly increased subcortical activity have been related to pain (Jensen *et al.* , 2013, Yoon *et al.* , 2013, Moxon *et al.* , 2014, Vuckovic *et al.* , 2014; for a review, see Pascoal-Faria *et al.* , 2014).

Although the underlying mechanisms are uncertain, Qiu et al. (2014) described that repetitive TMS treatment over M1 leads to a substantial pain relief in a patient who suffered from deafferentation pain for more than 20 years. Interestingly, glucose metabolism was significantly reduced at the contralateral anterior cingulate cortex, insula and caudate nucleus after treatment, which might indicate some type of short-term plasticity induction (Qiu *et al.* , 2014). As treatment over M1 was also shown to be effective for other chronic pain states (Lechaufeur *et al.* , 2008, Leung *et al.* , 2009, Galhardoni *et al.* , 2014) this treatment might be promising for future clinical applications. However, double-blinded studies with larger sample sizes are needed to understand the functional changes at brain level and their effect on pain (Nardone *et al.* , 2014).

6.3.4 Summary

In conclusion, these new findings from neuroimaging studies in human SCI indicate progressive long-distance fiber degeneration along the sensorimotor system, structural cortical reorganization with a typical temporal and spatial course and a close relationship between the degree of structural and functional changes to clinical measures of impairment and outcome.

6.4 Animal models of spinal cord injury: Invasive tracking of trauma-induced changes

Although neuroimaging outcome measures can track trauma-induced structural changes and functional reorganization in human SCI, they cannot reveal the biological processes underlying these changes (i.e. degeneration/demyelination vs. regeneration/remyelination and cortical reorganization). The pathological processes underlying these changes are not fully resolved, but in principal underlying mechanisms of spinal cord damage and regeneration/repair are assumed to be rather similar between animal models of SCI and human SCI (Edgerton and Roy, 2002). Both are characterized by remote axonal damage and demyelination of white matter tracts (Buss and Schwab, 2003), the evolution of the lesion area (i.e. cyst formation) (Miyanji *et al.* , 2007), cortical reorganization (Freund *et al.* , 2013a) and the inherent low capacity of repair (Cregg *et al.* , 2014). In particular, rodent and primate models of SCI have demonstrated progressive axonal anterograde and retrograde degeneration of spinal pathways with subsequent neuronal changes at multiple levels (Beaud *et al.* , 2012, Nardone *et al.* , 2013, Nielson *et al.* , 2014).

When investigating acute stages of SCI, not only the spinal cord circuitries react immediately to the injury (Yague *et al.* , 2011), but also cortical reorganization occurs as early as hours after thoracic hemisection in responses to electrical stimuli to the intact forepaw (Yague *et al.* , 2011, Sydekum *et al.* , 2014), previously only shown in chronic SCI rodents (Aguilar *et al.* , 2010, Dutta *et al.* ,2014). This enlargement of cortical S1 area appeared as early as 3 days after injury (Humanes-Valera *et al.* , 2013, Sydekum *et al.* , 2014), and 7 days after injury the performance of tested animals was proportional to the reorganization at 1 day after injury (Sydekum *et al.* , 2014) (see Fig. 23, Yague *et al.* , 2011). In accordance, resting-state functional MRI showed alterations in spontaneous neuronal activity in several brain regions in monkeys (Rao *et al.* , 2014) as well as in rats (Yague *et al.* , 2011) with a thoracic hemisection. These observations might further help to understand the pathophysiological mechanisms behind these changes.

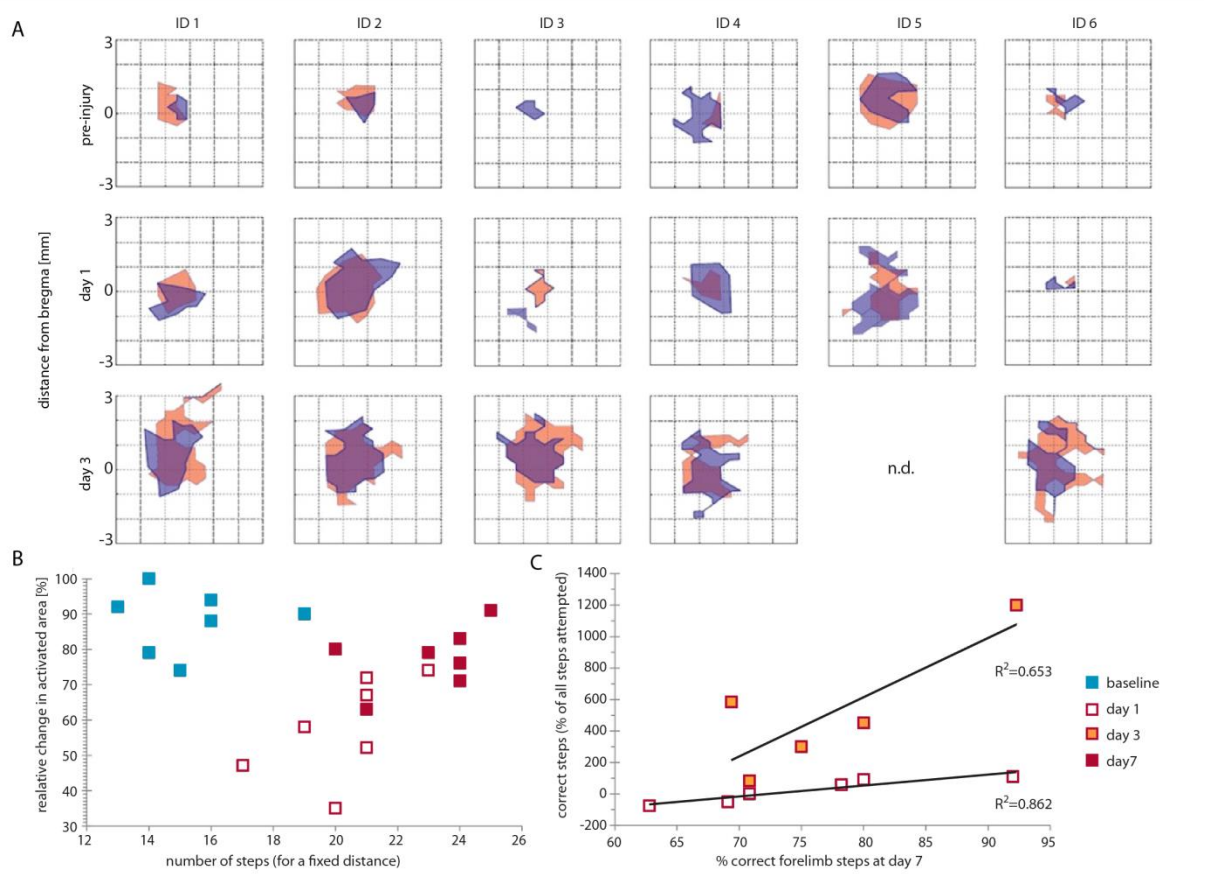

Figure 23: (a) Individual task-related brain activity maps within the forelimb representations for intact animals and SCI animals over time. BOLD-fMRI maps of forelimb representations in the sensory-motor cortex, intact and after injury for six individual rats monitored. Maps (upper: red, lower: blue) are displayed at uniform intensity levels and semitransparent to visualize overlaps. Maps are displayed for the 1.6mA (intact, 1, 3, 7 days postinjury) stimulation strength. In the coordinate space, x-axis denotes lateral distance from the midline (in mm) and y-axis: distance from bregma (in mm). (b)/(c) Effects on spinal cord injury (thoracic level T8) on skilled forelimb function. (b) Success rate quantified as percentage of correct steps among all of the attempted steps while crossing the horizontal ladder as a function of the number of steps required for a fixed distance. Symbols represent values measured as baseline (blue squares), 1 (open squares) and 7 days following SCI (red squares). (c) Success rate in forelimb use at day 7 as a function of change in activation area as derived from BOLD fMRI signal on day 1 (open squares) and days 3 (red squares with orange filling) with respect to baseline values. The correlation coefficients are indicated in the figure. Adapted from (Yague *et al.* , 2011).

Furthermore, recent longitudinal studies showed that disintegration of the spinal cord spreads rostrally and caudally with a tendency to reduced spinal cord diameters 12 weeks after injury as shown in Fig. 24 (Rao *et al.* , 2013, Rao *et al.* , 2014), as in human SCI (Freund *et al.* , 2011a, Lundell *et al.* , 2011). In addition, cortical reorganization of S1 increased over time and correlated with the rostral, anterio-posterior diameter of the spinal cord indicating that a more severe SCI leads to greater cortical reorganization. This is in line with Yang et al. (2014) who showed that not only the severity of injury correlated with the extent of early cortical plasticity in the sensory cortices, but also to the severity of late behavioral deficits. The investigation of cortical activation after electrical forepaw stimulation represents one reliable method for tracking the cortical reorganization. As somatosensory evoked potentials (SSEPs) are already routinely used in patients, Bazley et al. (2014) showed that SSEPs are able to detect significant enhancements in activation of forelimb sensory pathways in rats with SCI at the thorax level, indicating that this method might also be useful for assessing treatments that modulate plasticity after SCI. Moreover, Sydekum et al. (2014) showed a significant latency difference at the ipsilateral S1 cortex on day 7. This might predict, at least in rats, the time at which the brain undergoes the most adaptions which might be a promising time window for therapeutic strategies such as rehabilitation (Bazley *et al.* , 2014).

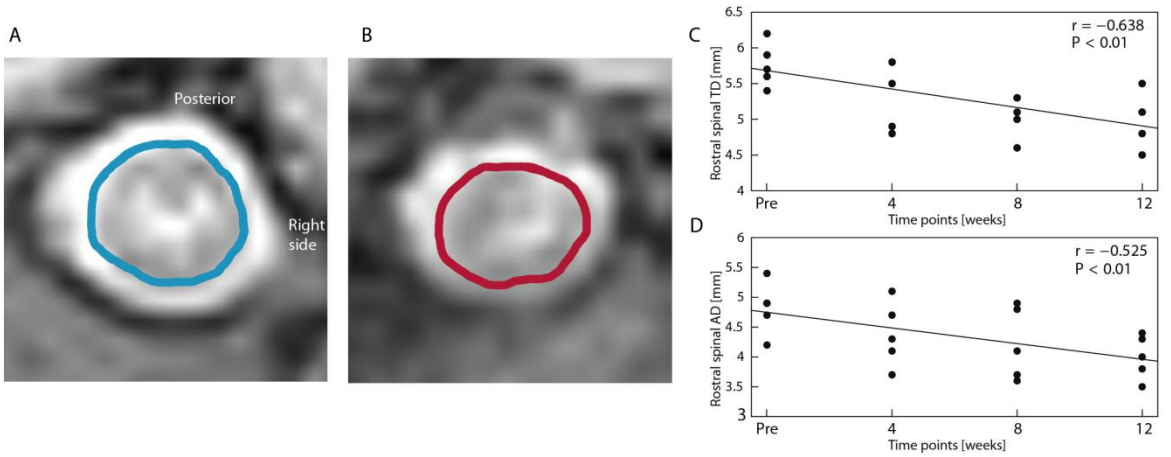

Figure 24: (a)/(b) Progressive structural changes of the injured spinal cord. (a) Representative example of a healthy nonhuman primate (spinal cord area highlighted in blue) at thoracic level. (b) MRI of the injured region in a nonhuman primate model of spinal cord injury (thoracic level T7_T9). Cross-sectional rostral spinal cord area (highlighted in red) assessed 2 cm above the lesion at 12 weeks after SCI. (c)/(d) Correlations among the rostral transverse (TD) and anteriorposterior diameter (AD) of the spinal cord at different time points after lesion. The y-axis in each diagram indicates the measured diameter of the spinal cord at different locations, and the x-axis is the time point. The correlation coefficients areindicated in the figure. Adapted from (Rao *et al.* , 2014).

6.5 Conclusion

At present, neuroimaging biomarkers are still not used routinely in human SCI to assess the efficacy of interventions (physical therapies or drugs) and how they relate to compensatory neuronal processes at the spinal cord and brain level. The proposed neuroimaging biomarkers have shown their potential to provide novel insights specifically wherein clinical measures might be insensitive to reveal subtle changes of spinal cord and brain function. However, these subtle changes ultimately may become valued as a proof-of-concept in which an amplification of the effectiveness eventually may translate into clinically meaningful changes of functional outcomes. The establishment of quantifiable and specific surrogate markers in animal models and human SCI will be essential to inform about the comparability of these models in the sense of disease stage (what indicate the transition from an acute to a chronic SCI, what stages of chronic SCI can be distinguished), extent of axonal/myelin damage and effects of repair/neural plasticity. Ultimately, quantitative and functional MRI in longitudinal multicenter assessments in acute SCI are required that measure central spinal and brain sequels simultaneously (Kong *et al.* , 2014) and their impact on cortical reorganization as SCI patients recover. This should allow the identification of the most sensitive imaging markers and their applicability in clinical trials.

6.5.1 Future directions

From a clinical perspective, the relationships between the extent of the spinal cord lesion, the amount of cortical reorganization and the recovery of behavior need to be further investigated in serial studies (Wu *et al.* , 2015). Animal models will help us understand not only the influence and ensuing consequences of different lesions, but also which neuroimaging outcome measures have predictive value. The continuous developments in the rapidly evolving field of spinal cord MRI at high resolution will help in detecting and understanding the structural changes below, within and above a SCI. Novel, improved MRI sequences and automated image processing methods (Finsterbusch *et al.* , 2012, Mohammadi *et al.* , 2012, Finsterbusch *et al.* , 2013, Fonov *et al.* , 2014) have shown the potential to accurately distinguish (separate) gray and white matter at the spinal level and assess spinal activation patterns (Sprenger *et al.* , 2012). These advances will help us to better define the lesion level, extent of the injury and tracts affected.

Current work in our laboratory is focusing on improving the MR sequences and postprocessing pipelines. The primary aim will be to extend our existing brain image segmentation approach to use atlas data from both head and neck (Fonov *et al.* , 2014). This would allow clinicians to better assess MRI data of patients with SCI and patients with neurological diseases involving the spinal cord. Moreover, anatomical MRI scans of the head and neck, collected at multiple time points following a spinal incidence such as trauma, allow longitudinal changes in terms of both rates of change (i.e. velocity) and its acceleration or deceleration (e.g. atrophy rates and possible recovery) to be

determined more accurately via longitudinal image registration procedures (Ashburner and Ridgway, 2012).

7 General discussion

The overall objective of this thesis was to increase our understanding of trauma-induced structural changes at different levels of the neuraxis and their relationship to clinical outcome. Within each of the specific studies conducted within this thesis, we hoped to gain novel insights into degenerative mechanisms leading to, or manifesting in sensorimotor impairments, as well as understanding compensatory mechanisms during the course of clinical recovery. With this obtained knowledge, we hope to contribute to the development of biomarkers within the SCI field to 1) improve patient selection and stratification into homogenous subgroups for therapeutical interventions and clinical trials, and 2) identify biomarkers which can potentially be used as surrogate markers to improve safety and efficacy determination in early stages of new intervention and clinical trials.

In this thesis, we used a combination of conventional (T1-/T2-weighted images at spinal cord and brain) and advanced imaging modalities (MEDIC, DWI, MRS, quantitative MRI), together with different clinical methods (neurological and neurophysiological assessments, questionnaires). The imaging modalities were analyzed with different post-processing techniques (spinal DTI, spinal VBM, different segmentation techniques, fitting of spectroscopy data in frequency domain, vertex-wise surface area analysis). This enabled us to comprehensively investigate different mechanisms occurring after traumatic SCI. In particular, we assessed the temporal and spatial pattern of macrostructural changes at the lesion site (**chapter 2**), investigated remote macro- and microstructural changes (**chapter 3**), as well as remote cellular and molecular alterations (**chapter 4**) at the cervical cord above the level of lesion, and evaluated the temporal pattern and spatial extent of macro- and microstructural changes within the extrapyramidal system after acute SCI (**chapter 5**).

As the findings of each individual study have been discussed within the specific sections, this general discussion serves as a summary of how each study increases our understanding of trauma-induced structural changes and their ability to serve as a future neuroimaging biomarker. Findings are discussed in conjunction to each other and set in relation to relevant literature. First, structural changes at the lesion site, remote structural changes above the level of lesion and potential mechanisms of such changes will be briefly discussed. Next, associations of structural changes with clinical outcome will be explained, and their potential as a biomarker set into context of current clinical trials. After outlining the limitations and the conclusion, next steps towards improving our understanding of structural changes and the development of neuroimaging biomarkers will be discussed.

7.1 Structural changes at the site of trauma

As MRI is the gold standard to determine the extent of intramedullary changes at the injury site and damage of adjacent structures (e.g. bones), it is usually acquired within the first 48 hours after injury. Therefore, several groups investigated the predictive ability of such acute MRI parameters. In particular, neuroimaging assessments of the acutely injured spinal cord have identified relationships between macro-structural intramedullary changes (e.g. extent of hemorrhage (Boldin *et al.* , *2006)*, lesion length (Arabi *et al.* , 2011, Arabi *et al.* , 2012, Le *et al.* , 2015), maximal spinal canal compromise/compression (Miyanji *et al.* , 2007) and clinical impairment at admission (Miyanji *et al.* , 2007, Flanders *et al.* , 1999, Furlan *et al.* , 2011) or early discharge (Mabray *et al.* , 2016). Although the lesion measures possess information about the extent and location of primary and secondary damage, regenerative treatments aiming at the repair of the injured spinal cord will likely depend on tissue bridges as it provides a bridge (or conduit) for axonal regeneration and or sprouting (Freund et al. , 2006, Krishna *et al.* , 2014).

In this thesis (**chapter 2**), we investigated the dynamics of midsagittal tissue bridges at the lesion site and observed that at 1-month post injury, the lesion was well demarcated and allowed for reliable identification of ventral and dorsal tissue brides and their temporal evolution. In particular, the size of total tissue bridges remained stable within the first year after injury, was paralleled by recordable electrophysiological information flow and predictive of clinical outcome at 12-month.

In chronic SCI, the lesion cavity is surrounded by a rim of spared fibers (Bunge *et al.* , 1993, Hill *et al.* , 2001). As SCI can lead to necrosis at the lesion site, the lesion cavity often contains multilocular cavities which are separated by glial trabeculae, and surrounded by astrocytic fibers and collagenous scar tissue (Bunge *et al.* , 1993, Scholtes *et al.* , 2006). Interestingly, in the majority of functionally complete patients, tissue bridges were evident at the lesion site, a phenomenon also described as discomplete (Kakulas, 1999). In addition, in incomplete SCI, demyelination is also present in intact fibers adjacent to the lesion epicenter (Guest *et al* , 2005). It was therefore debated, whether the size of tissue bridges actually is able to represent the clinical status of a patient. However, we show, that at 1-month post injury, complete patients have much smaller tissue bridges than incomplete patients, and that the size of the tissue bridges is predictive of functional outcome.

This is the first prospective longitudinal study characterizing the spatial and temporal evolution of MRI parameters specific of macrostructural-anatomical changes occurring at the lesion site and linking those to clinical outcome in cervical SCI patients. The sensitivity to change and accuracy for clinical outcome shows the potential of these neuroimaging biomarkers to be used in clinical routine and clinical trials in both acute and chronic SCI.

7.2 Large-scale remodeling above the level of lesion

Plasticity of the CNS is a concept that arose first when long-term potentiation as a form of synaptic plasticity was shown to modulate learning (Raisman, 1969, Teyler and DiScenna, 1987, Bliss and Collingridge, 1993). Before that, researchers regarded the brain as being developed within a critical period in natal and prenatal phase (Pascual-Leone *et al.* , 2005). This ability of the brain to constantly adapt the environments need is of high relevance in daily life, but also important when the fragile CNS gets damaged. As regeneration is very limited in the adult CNS (Ba and Bonhoeffer, 1994), next to functional compensation (Alstermark *et al.* , 1987), CNS plasticity might compensate for loss of function by regenerative axonal growth and sprouting (Weidner *et al.* , 2001), myelin repair (McDonald and Belegu, 2006) , synaptic strengthening (Cooke and Bliss, 2006) and the use of detour pathways (Courtine *et al.* , 2008, Filli *et al.* , 2014) (see also chapter 1.5). In healthy subjects, Draganski *et al.* (2004) first showed that brain plasticity can be captured not only by functional MRI but also by structural MRI. Soon, the idea arose within the neuroscience community that, degenerative and maladaptive processes after CNS injury, in addition to neuronal mechanisms of repair could also potentially be captured by using MRI. One example of CNS injury is traumatic SCI. Specifically, understanding the sequence of structural changes after SCI and their relationship to outcome by means of MRI, might serve as a solution for the pressing need for in-vivo biomarkers in the field, helping to develop evidence-based rehabilitation strategies (Freund *et al.* , 2013a, Huber *et al.* , 2015).

In SCI, one of these first ideas included the observation that directly damaged corticospinal axons degenerate and lead to shrinkage and partially apoptosis of the appropriate cell body in layer IV due to loss of trophic support (Kalil & Schneider, 1975). Although many studies have confirmed apoptosis and shrinkage of appropriate cell bodies in response to corticospinal tract damage (McBride et al. , 1989, Hains *et al.* , 2003, Tang *et al.* , 2004), there is also a body of evidence that is contradictory with this result (Barron *et al.* , 1988, Nielson *et al.* ,2010), possibly resulting from differences in methodologies (e.g. time of injury, injury location) (Oudega and Perez, 2012). Nevertheless, such changes might translate into volume changes at the spinal cord, and possibly also within appropriate brain regions (e.g. primary motor cortex), trackable by means of MRI.

At the spinal level, first studies using structural MRI remote from the lesion site showed decreases in SCA (Freund *et al.* , 2011a) above the level of injury, along with indicators of demyelination and altered white matter integrity (Cohen-Adad *et al.* , 2011, Petersen *et al.* , 2012).
Within this thesis (**chapter 3**), we extended this knowledge and showed that not only white matter atrophies and undergoes demyelination and neurodegeneration, but also grey matter changes contribute to the overall observed remote spinal atrophy. As changes within the grey matter were

associated with lesion severity and the clinical status of the patient, this is suggestive of trans-synaptic neurodegeneration of neuronal circuits within the spinal cord far above the level of injury. Indeed, different preclinical studies show reorganization of intraspinal circuits (Bareyre *et al.* , 2004, Vavrek *et al.* , 2006, Courtine *et al.* , 2008). Similar effects have also been observed in patients with cervical spondylotic myelopathy (Grabher *et al.* , 2016, Grabher *et al.* , 2017), whose cord became progressively compressed, mainly caused by chronic cervical disc degeneration (Crandall and Batzdorf, 1966).

In a next step (**chapter 4**), we investigated underlying cellular and molecular changes in areas of atrophy above the level of lesion and found metabolic alterations related to neurodegeneration and demyelination, which were driven by lesion severity, supporting our findings from **chapter 3**. In addition, we found indicators of chronic neuroinflammation, which were associated with greater clinical impairment. After initial damage to the cord, there is an initial inflammatory response originating in the cord, primarily by activation of microglia. Microglia produce cytokines, like L-1β, TNF-α, proteases, and other cytotoxic factors (Nesic et al. , 2001). As spinal cord trauma leads to degeneration and demyelination of injured axons as well as glial apoptosis, a secondary inflammatory response follows (Dumont *et al.* , 2001). This neuroinflammatory response is poorly understood and can persist months to years after the initial trauma (Norenberg e*t al.* , 2004, Fleming et al. , 2006, Felix *et al.* , 2012). However, inflammatory responses are complex as they exert both beneficial (plasticity enhancing) and detrimental (glial- and neurodegenerative) effects (Schwab, 2014). For example, animal studies showed that even 180 days after injury, inflammation persists. However, blocking the late C5a-mediated inflammatory response (>14 days post injury) leads to reduced locomotor recovery, suggesting a multiphasic response with the late component possibly serving as reparative function (Beck *et al.* , 2010). On the other hand, selective inhibition of transcription factors nuclear factor kB of astrocytes leads to an improvement in recovery (Brambilla *et al.* , 2005). Such persisting inflammatory responses are not a unique feature of SCI – several acute and chronic brain diseases show persisting brain inflammatory responses (Lyman *et al.* , 2014) which might arise from an increased metabolic demand of the CNS when undergoing increased plastic changes (Xanthos and Sandkuehler, 2014). Such responses may also become maladaptive - in humans studies, there is evidence of inflammatory brain changes after SCI related to pain (Pattany *et al.* , 2002, Widerström-Noga *et al.* , 2013), but also to cognitive decline (Wu *et al.* , 2014). Understanding the temporal cascade of spinal neuroinflammatory responses as described in **chapter 4**, and their relationship to structural changes (i.e. ventral and dorsal horn changes, microstructural changes) as described in **chapter 3,** the emergence of neuropathic pain and cognitive function will enhance our understanding of SCI pathophysiology.

At the cortical level, previous studies showed that the brain exhibited volumetric decreases, paralleled by demyelination within the corticospinal tract and in the primary motor cortex (Wrigley *et al.* , 2008, Freund *et al.* , 2011ab, Freund *et al.* , 2013a, Ziegler *et al.* , 2018), and in sensory and limbic system (Jurkiewicz *et al.* , 2006, Hou *et al.* , 2014, Grabher *et al.* , 2015). The extent of such structural changes was also related to the occurrence and amount of neuropathic pain within the motor and sensory system (Gustin *et al.* , 2009, Wrigley *et al.* , 2009b, Yoon *et al. , 2013,* Jutzeler *et al.* , 2016). In addition, our last study (**chapter 5**) shows progressive morphometric somatotopic changes (increases and decreases of surface area) within the basal ganglia, paralleld by decreases in myelin-sensitive paramters. Even tough it remains controversial, under which circumstances directly injured corticospinal neurons lead to atrophy of cell bodies within the motor cortex (Oudega and Perez, 2012), we show clear evidence that even networks not being directly injured undergo structural changes after SCI. Brain networks are topologically organized and consist of different interconnected elements, which transfer information between each other (Bulmore and Sporns, 2012). In terms of structure, this topological organization is critically related the function of each element (Barbarasi *et al.* , 2004, Li *et al.* , 2004). From this perspective, it seems reasonable that damage to one element of this integrated network will lead to alterations in connected elements. Studying the brain as an integrated, hierarchical network (Bullmore and Sporns, 2009) might therefore be a new powerful tool for better understanding brain function and structure, and its alterations after damage to the CNS in both human and animal studies.

Taken together, SCI does not only result in changes at the primary lesion site (**chapter 2**) and in reduced white matter integrity of main sensorimotor tracts (**chapter 3)**, we also found spinal grey matter changes (**chapter 3**) and an altered biochemical environment (**chapter 4**) above the level of lesion, as well as cortical reorganization of primarily unaffected brain regions (**chapter 5**), indicating that SCI leads to a large scale, transneuronal remodeling and wide-spread structural changes throughout the CNS.

7.3 Potential of these neuroimaging biomarkers to serve as surrogate markers

In this thesis, we showed that several of our applied MR sequences exhibited localized trauma-induced changes which were predictive of clinical outcome. These biomarkers might serve as future surrogate markers in interventional studies and clinical trials. Such surrogate markers have the potential to identify potential responders to a certain treatment, and determine safety and efficacy of new treatments in early phases of clinical trials, which will result in reduced developmental, but also ease socioeconomical costs (see also chapter 1.6).

At the lesion site, we revealed that as early as 1-month after injury, the lesion extent but also the size of tissue bridges were predictive of 12-month sensory and motor scores, as well as of daily-life independence (**chapter 2**). These associations were not specific to sensory or motor scores, but rather represented the overall damage, respectively preservation, of function as an approximation of the amount of spared fibers. In preclinical models, there is evidence that tissue bridges are actually responsive to treatment and represent the sensorimotor status of the animal. In particular, the amount of tissue sparing at the lesion center was associated with locomotor recovery in rats with cord contusion (Basso *et al.* , 1996). When comparing two groups of mice receiving different type of treatments, Boato *et al.* (2013) showed that worsened outcome is associated with an increase in lesion width along with a reduced number of spared corticospinal tract fibers. In line, Calderon-Vallejo et al. (2015) showed that pharmacological treatment can increase the number and caliber of nerve axons which leads to significant higher spared tissues. For treatments aiming at the repair of the lesion site, MR biomarkers could help to reproduce preclinical findings and possibly identify efficacy of treatment in a timely manner prior to functional improvements. At the moment, several such clinical trials are conducted in subacute (Schwann cells: NCT01739023 identified in clinical-trials.gov, Collagen scaffolds: NCT02510365 identified in clinical-trials.gov, HuCNS-SC: NCT01321333 identified in clinical-trials.gov) and chronic patients (Schwann cells: NCT02354625 identified in clinical-trials.gov, Scaffolds seeded with stem cells: NCT02688049 identified in clinical-trials.gov), which potentially could profit from these established measures. In particular tissue bridges' responsiveness to treatment will be evaluated within a phase II clinical trial of Anti-Nogo A antibody, a multi-center investigator initiated clinical trial with the Balgrist University Hospital as the lead center.

In the atrophied cervical cord above the level of lesion, molecular levels of NAA/mI and Cho/mI ratios were associated with daily-life independence and sensorimotor scores (**chapter 4**). This indicates that patients with lower N-acetylaspartate and choline, indicative of neuronal degeneration (Bjartmar *et al.* , 2000) and reduced mitochondrial metabolism (Bates *et al.* , 1996) and higher myo-Inositol levels, suggestive of neuroinflammation (Rust and Kaiser, 2017), have worse outcomes. Although MRS measurements are sensitive and specific to absolute concentrations of certain molecules, none of these molecules are involved in a single biological process, making the underlying cause for change conjecturable. However, as we showed that spinal MRS is sensitive to detect trauma-induced changes, such measures might help to detect subtle changes early in pathological processes. In particular, taken the example of neurodegeneration, which results in the breakdown of the cell membrane, this leads to an immediate increase of choline, detectable by MRS. Volumetric changes attributed to neurodegeneration are likely to arise only after the removal of cell debris, which allows the detection of this process only at a later time when using morphometric measures. Future studies

need to assess whether MRS actually holds the potential to detect trauma-induced changes earlier than morphometric measures. As novel therapeutical approaches will most likely have best efficacy when applied earliest after injury, biomarkers able to timely predict outcome of the patients are urgently needed in order to detect treatment effects. Within the last years, a variety of new interventions have been investigated in very acute SCI patients, who could benefit from such early surrogate markers (e.g. Neuro-spinal scaffolds: NCT02138110 identified in clinical-trials.gov, Anti-Nogo-A (ATI355): NCT00406016 identified in clinical-trials.gov, Magnesium-Chloride infusion (AC105): NCT01750684 identified in clinical-trials.gov, Riluzole: NCT01597518 identified in clinical-trials.gov).

In contrast to the measures from study 1 and 3 (**chapter 2/4**), our study 2 and 4 (**chapter 3/5**) showed specific associations of structural changes above the level of injury with outcome. In particular, at the cervical cord, dorsal horn atrophy and microstructural changes within the dorsal column were associated with sensory outcome, while the size of ventral horns was associated with motor outcome (**chapter 3**). Within the basal ganglia, we found that at 1-month after injury, surface area changes within the motor caudate were predictive of 24-month lower extremity motor score (**chapter 5**). As a next step, future studies should longitudinally assess the temporal evolution of such measures and identify the earliest time point for prediction to validate their potential as a surrogate marker.

7.4 Limitation and Considerations

Strengths and limitations of each study were discussed in the specific chapters separately. Here, general limitations and considerations of this thesis are discussed.

All studies were conducted prospectively and included a control group when required. This allowed us to carefully select patients and healthy subjects, minimizes effects not related to the variables of interest and enabled interpretation about the magnitude of our observed effects. In study 2-4 (**chapter 3-5**), structural MRI sequences with high resolution were acquired, which have the potential to detect subtle and small changes. The knowledge gained within this thesis complements previous findings and brings us another step closer towards the development of in-vivo MRI bio- and surrogate markers within the SCI field.

One limitation of this study is that most of our readouts from the different imaging modalities show rather high inter-subject variability. This might be partially due to influencing factors which were not all properly controlled in this study, like lesion level, extent of lesion, time since injury, genetics, and neuroanatomical differences leading to subtle differences in registration and normalization procedures. However, we controlled for age in all of the studies, as previous studies have shown an

age-dependent decline in axonal growth after CNS injury, limiting the potential of repair in the elderly SCI population (Geoffroy *et al.* , 2016). For predicting functional outcome after SCI, it is important that the experimental and biologic variability in the quantified metabolite is smaller than their changes caused by the injury (Öz *et al.* , 2014). For future (multi-center) studies, it is therefore of particular importance to show robustness of MR biomarkers (Raunig, 2015). In particular, reproducibility and reliability need to be assessed for all measures, and eventually improved. In particular, measures of R2* and T1-weighted images show rather low reproducibility between sites (coefficient of variation > 15%) (Weiskopf *et al.*, 2013), which highlights the need for prospective studies to improve the reproducibility of MR imaging-derived metrics.

Next, our studies 2 and 3 (**chapter 3 and 4**) were cross-sectional studies, which does not allow for understanding the temporal relationship between cervical structural changes and outcome. As measures of the cervical cord above the level of injury hold the potential to serve as surrogate markers, longitudinal studies are warranted to close this gap of knowledge.

A further limitation of this thesis involves the fact that all of our applied MR measures are not specific not any biological process (e.g. demyelination, neurodegeneration or inflammation). Morphometric measures (e.g. surface area analysis, VBM, TBM, cortical thickness) allow detecting morphological differences (i.e. volume and surface area) between patients and controls, and tracking them over time. However, they are not specific to any pathological processes occurring after SCI like atrophy, demyelination, or changes in the amount or shape of different cell types. Although quantitative MRI is sensitive, and MRS is sensitive and specific for molecular changes, they remain indirect markers of demyelination and neurodegeneration. Nevertheless, in our studies we show that these MR measures are indeed sensitive to trauma-induced changes.

7.5 Concluding remarks

The present thesis extensively investigated trauma-induced structural changes at and above the level of injury after SCI by applying standard and advanced imaging and post-processing techniques and associating them with neurological and neurophysiological outcome of the patient. Previous studies showed cervical atrophy and cortical changes within the sensorimotor and limbic system occurring after SCI. We now characterized changes at the lesion site and showed degeneration and demyelination in directly injured white matter tracts above the level of injury. In addition, primarily unaffected spinal and brain regions like the dorsal and ventral horns above the level of lesion or the basal ganglia system, also undergo structural and microstructural changes and are predictive of outcome. We conclude that SCI does not only lead to structural changes of directly affected networks, but also results in large scale, transneuronal reorganization. In addition, our findings indicate that chronic neuroinflammation might be present after SCI, relating or contributing to

ongoing degenerative changes within the CNS, and therefore also possibly being associated to clinical outcome. In conclusion, quantitatively analyzed conventional as well as innovative multimodal MR protocols allowed for the quantification of trauma-induced changes. The present findings deepen our understanding of spinal and supraspinal structural changes occurring after SCI and highlight their potential to serve as a future surrogate marker.

7.6 Future directions

7.6.1 The role of tissue bridges and their responsiveness to treatment

The assessment of tissue bridges might be in particular important for all clinical trial investigating treatments aiming at repair at the lesion site (e.g. scaffold implanation, stem cell treatment, Anti-Nogo-A antibody infusion). Before assessing the responsiveness of tissue bridges in future clinical trials, it is important to understand whether preserved dorsal (i.e. representing the dorsal column) and ventral (i.e. representing the anterior corticospinal tract) midsagittal tissue bridges encode tract-specific electrophysiological properties and whether they are specific in predicting appropriate functional outcome. This will enhance our understanding of the specificity and sensitivity of tissue bridges.

Next, as most clinical trials in SCI patients are including paraplegic patients in their Phase I due to safety reasons, an extension of our established measurements from tetraplegic patients to paraplegic patients is highly needed. Generally, injury morphology (e.g. compression, burst, rotation, translation, flexion, hyperextension) differs between tetra- and paraplegic patients as the cervical cord is much more vulnerable to hyper-/hypoflexion injuries. Therefore, the spatial extent and the evolution of lesions in paraplegic patients might fundamentally differ in SCI patients, which should be investigated in future studies. Once developed, measures of tissue bridges could be applied within clinical trials in both tetra- and paraplegic patients.

7.6.2 Disentangle structural correlates of neuropathic pain from neurodegenerative changes

We showed that SCI leads to widespread changes at and above the level of injury (**chapter 2-5**). However, as a large proportion of SCI patients (>80%) develop chronic pain refractory to treatment (Siddall *et al.* , 1999, Siddall *et al.* , 2003, Cruz-Almeida *et al.* , 2005, Finnerup *et al.* , 2014), it is important to disentangle causes and effects of persisting pain from neurodegenerative changes. Previous studies suggest, that patients with neuropathic pain show a less pronounced somatotopic reorganization in the brain (Jutzeler *et al.* , 2015), and less pronounced atrophy in the spinal cord (Jutzeler *et al.* , 2015), but the process of pain development remains incompletely understood.

In patients suffering from chronic pain, but not of SCI, increases in cortical thickness within the primary somatosensory cortex were detected and consistent across different etiologies (Kayris *et al.* ,

2015, DaSilva *et al.* , 2008). In line, preclinical neuropathic pain models showed that localized S1 astrocyte activation in the early phase of developing pain (Kim *et al.* , 2017) led to increased dendritic spine turnover of the pyramidal cells present in the layer V (Kim and Nabekura 2011) and increased spine motility (Kim and Moalem-Taylor, 2011), suggesting that astrocytes are a key trigger for S1 synaptic rewiring (Kim *et al.* , 2017), resulting in S1 hyperexcitability. This in turn might affect also a variety of other regions connected to S1 like the ACC, thalamus and the insula, prefrontal cortex – regions which are also known to be altered after SCI.

For our SCI population, patients suffering from neuropathic pain might exhibit different mechanisms in parallel, which possibly compete against each other. On the one hand, damage to the sensorimotor tracts leads to pronounced atrophy and microstructural changes of the somatosensory cortex. However, when developing pain, mechanism seem to exist which also lead to the opposite effect within the same regions. Whether these mechanisms exist in parallel, are a consequence of each other, or are competing against each other, leading to the development of neuropathic pain, needs to be investigated. In particular, we need to understand causes and effects of neuropathic pain, and how this is translated into structural and microstructural changes as measurable by means of MRI. Longitudinal MRI studies in concordance with neurophysiological recording targeting the somatosensory system are needed to link hyperexcitability states to structural changes. Given the fact that early structural changes leading to neuropathic pain in preclinical models, it is of high importance that such measures (e.g. functional and structural MRI) are applied as close to the injury as possible with close follow-ups in the acute and sub-acute phase.

7.6.3 The role of neuroinflammation in recovering from a spinal cord injury

We investigated cellular and molecular changes within the atrophied cervical cord above the level of injury using MRS (**chapter 4**) in chronic SCI patients, and found indicators of neuroinflammation. The amount of neuroinflammation was related to lesion severity and outcome. To further investigate neuroinflammation after SCI, we need to better understand whether neuroinflammation is globally present throughout the whole CNS, or whether it affects certain regions with the CNS. Future studies should characterize the temporal and spatial evolution of neuroinflammatory markers. In particular, as the neuroimflammatory response consist of a variety of altered processes, combining different imaging methods might be in particular beneficial. Such techniques include MRS to track levels of myo-Inositol (an osmolyte regulating astrocyte cell volume), contrast-enhanced MRI using gadolinium to study blood-brain-barrier alterations (Rebeles *et al.* , 2006), and dynamic contrast-enhanced MRI with appropriate modeling techniques to study cerebral blood flow and blood-brain-barrier permeability (Heye *et al.* , 2014). It is important to note however, that pain should also be

carefully tracked, as pain itself might also be associated with inflammatory responses in a variety of brain regions (Widerström-Noga *et al.* , 2015).

7.6.4 The role of neuroinflammation after spinal cord injury and the risk of developing dementia

Several human studies showed persisting signs of neuroinflammation after CNS injury, including ours (**chapter 4**). Apart from the role of neuroinflammation in recovery after CNS damage, increased risk of dementia after traumatic brain injury possibly mediated by neuroinflammation has lately received widespread attention (Faden *et al.* , 2016). Huang *et al.* , (2017) recently conducted a large epidemiological study and reported that patients with SCI are at higher risk of dementia than age- and sex-matched controls. In line, chronic neuroinflammation is present in mice with SCI and results in impaired neurogenesis within the dentate gyrus of the hippocampus (Wu *et al.* , 2016) along with decreased BDNF levels (Felix *et al.* , 2012, Gommez-Pinilla *et al.* , 2012), depending on initial lesion severity. These mice also showed cognitive impairments in a variety of tests including spatial navigation, object recognition and memory function (Wu *et al.* , 2016). To date, structural changes of the hippocampus after SCI have not been considered yet. Future studies should address if and when structural changes within the hippocampus occur after human SCI. In particular, morphometric and microstructural changes of hippocampal subfields, as recently provided by Chakravarty *et al.* (2013), are of particular interest, as well as their relationship to late cognitive outcome.

7.6.5 Understanding trauma-induced changes in spinal and cortical networks

It has not been that long ago, as the brain organization was considered to consist of different cell types, whereof neurons form a complicated structural network (y Cajal, 1995, Swanson, 2012). As understanding the network organization within the brain in healthy controls is a challenge per se, the Human Connectome Project (HCP) was launched in 2010 with a total of 38.5 million spent over five years to identify and map networks (connectome), shedding light on functional and structural connectivity. This body of research, along with recent advances in graph theory of brain networks (Bullmore and Sporns, 2009) will facilitate the understanding in network changes after SCI. So far, our group focused on understanding structural changes within specific regions of the brain or within several regions belonging to a network (e.g. basal ganglia), and their relationship to lesion severity using simple correlation analysis. It would be of particular interest to unravel the temporal sequence of structural changes, their relationship to each other and to changes at the lesion site. By such means, we could also disentangle primary effects induced by the lesion itself (e.g. degeneration of damaged tracts) from secondary effects not directly related to the lesion (e.g. changes emotional status).

7.6.6 Translational research: Improving transfer from bench to bedside and from bedside back to bench

An important step towards clinically reliable bio- and surrogate markers is the development of comparable methods between animal and human SCI to identify correlations between MRI metrics and pathophysiological processes. Recent studies have already started to assess relationships between DTI (Kozlowski *et al.* , 2008, Kelley *et al.* , 2014), myelin water imaging (Kozlowski *et al.* , 2014), magnetization transfer (Wang *et al.* , 2015, Wang *et al.* , 2016), susceptibility-weighted imaging (Wang *et al.* , 2011) and clinical histological parameters in several animal models of SCI. Most of such MRI studies in animals have focused on changes of the lesion site rather than remote changes above the level of injury. However, novel imaging measures are more prone for metal artefacts caused by instrumentation in the spine, making the application of quantitative MR protocols at the lesion site in humans challenging. Therefore, future animal studies should focus on longitudinal characterization of comparable quantitative MR parameters above the level of injury, assess their predictive ability for clinical outcome, and their relationship to histological changes.

7.6.7 Towards the development of surrogate markers: Next steps

As highlighted in the introduction (chapter 1.6.3), after having found biomarker candidates which provide clinically relevant information about the actual or future status of the patient, we need to validate the biomarker's effectiveness or utility as a surrogate endpoint before we can clinically apply it.

Within this thesis, a prospective, longitudinal training study was conducted, investigating training-induced structural changes after SCI. To date, the only effective treatment leading to a limited extent of functional recovery is by means of intensive neurorehabilitation. We therefore designed an interventional study, where we investigated whether intensive feedback-guided sensorimotor training is reflected by structural changes in learning associated brain areas and /or can induce rebound effects within areas of atrophy in chronic SCI patients. For this aim, during the last 3 years, 18 controls (age: 37.5 ±12.5 years) and 17 incomplete SCI patients (age: 46.1 ± 15.6 years), divided into two equal subgroups for lower and upper limb training, received feedback-guided training during 4 weeks (4 x 30 minutes per week). A further control group consisting of 9 healthy controls (age: 41.1 ± 12.2 years), not receiving training, was additionally included. Participants were assessed weekly and at 84 day follow-up. For those having received the training, improvements and retention in training success, attentional networks, lower extremities reaction and movement time, and 3D gait analysis were assessed next to a comprehensive neurological examination (Fig. 25). Computational morphometry will assess structural correlates (volumetric and myelin changes) of performance improvements in the spinal cord and brain using repeat MRI (n=5 scans per subject).

We are optimistic, that our novel neuroimaging measures of dynamic structural central changes in response to training hold significant potential to elucidate neuronal changes associated with learning vs. clinical recovery. We are optimistic that the sensitive and accurate MRI biomarkers so developed can be applied as surrogate endpoints in clinical trials and to personalize the care of patients with SCI.

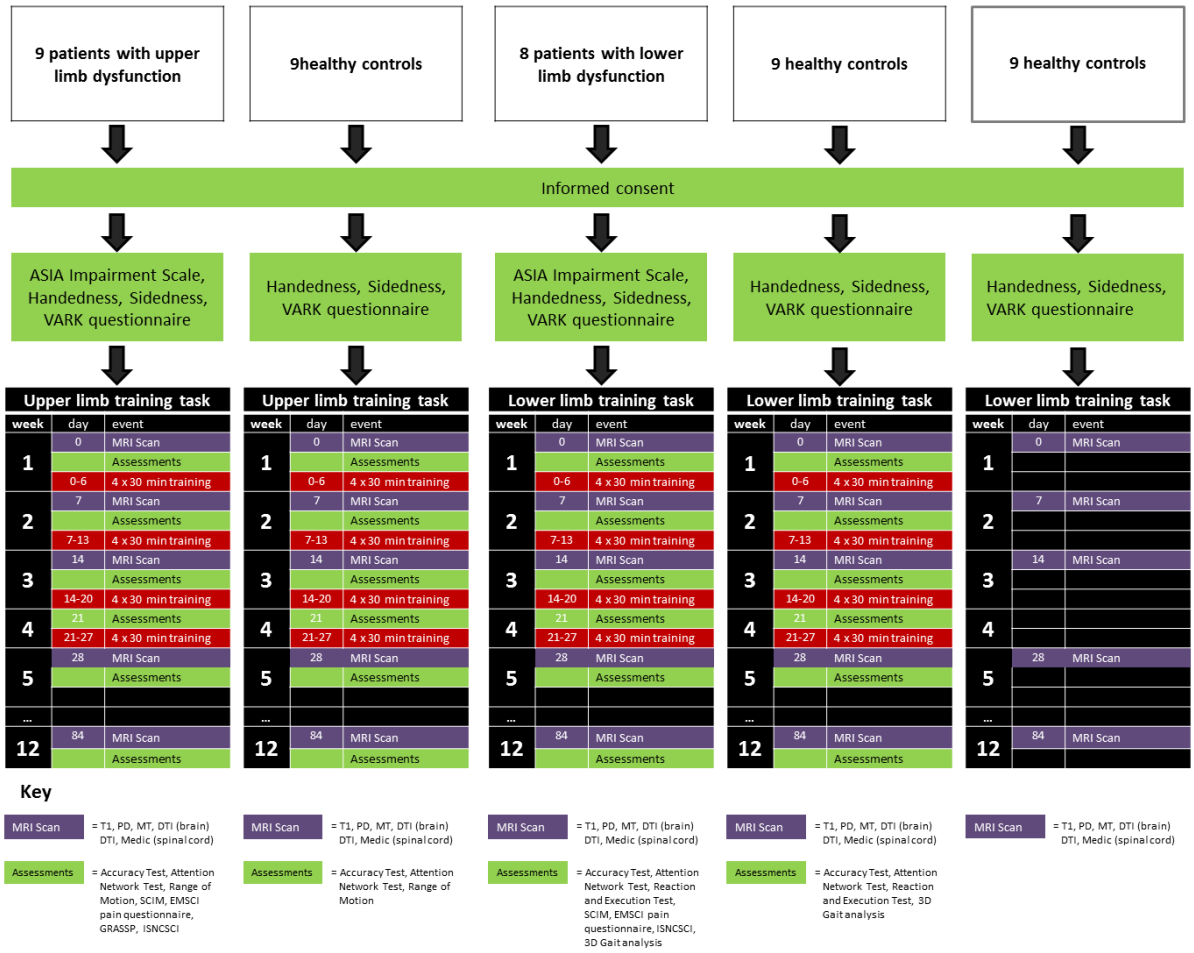

Figure 25: Training and assessment paradigm

8 References

Aarabi B, Alexander M, Mirvis SE, Shanmuganathan K, Chesler D, Maulucci C, et al. Predictors of outcome in acute traumatic central cord syndrome due to spinal stenosis. J Neurosurgery Spine. 2011;14:122-30.

Aarabi B, Simard JM, Kufera JA, Alexander M, Zacherl KM, Mirvis SE et al. Intramedullary lesion expansion on magnetic resonance imaging in patients with motor complete cervical spinal cord injury. J Neurosurgery Spine. 2012;17:243-50.

Abdel-Aziz K, Schneider T, Solanky BS, Yiannakas MC, Altmann DR, Wheeler-Kingshott CA, et al. Evidence for early neurodegeneration in the cervical cord of patients with primary progressive multiple sclerosis. Brain. 2015;138(6):1568-82.

Aguilar J, Humanes-Valera D, Alonso-Calvino E, Yague JG, Moxon KA, Oliviero A, et al. Spinal cord injury immediately changes the state of the brain. J Neurosci. 2010;30(22):7528-37.

Alstermark B, Lundberg A, Pettersson LG, Tantisira B, Walkowska M. Motor recovery after serial spinal cord lesions of defined descending pathways in cats. Neuroscience research. 1987;5(1):68-73.

Andersen HH, Johnsen KB, Moos T. Iron deposits in the chronically inflamed central nervous system and contributes to neurodegeneration. Cell Mol Life Sci. 2014;71(9):1607-22.

Arima H, Hanada M, Hayasaka T, Masaki N, Omura T, Xu D, et al. Blockade of IL-6 signaling by MR16-1 inhibits reduction of docosahexaenoic acid-containing phosphatidylcholine levels in a mouse model of spinal cord injury. Neurosci. 2014;269:1-10.

Ariyannur PS, Moffett JR, Manickam P, Pattabiraman N, Arun P, Nitta A, et al. Methamphetamine-induced neuronal protein NAT8L is the NAA biosynthetic enzyme: implications for specialized acetyl coenzyme A metabolism in the CNS. Brain Res. 2010;1335:1-13.

Arsalidou M, Duerden EG, Taylor MJ. The centre of the brain: topographical model of motor, cognitive, affective, and somatosensory functions of the basal ganglia. Hum Brain Mapp. 2013;34(11):3031-54.

Asanuma C, Thach WT, Jones EG. Cytoarchitectonic delineation of the ventral lateral thalamic region in the monkey. Brain research. 1983;286(3):219-35.

Asanuma H, Hunsperger RW. Functional significance of projection from the cerebellar nuclei to the motor cortex in the cat. Brain research. 1975;98(1):73-92.

Ashburner J, Friston KJ. Voxel-based morphometry--the methods. Neuroimage. 2000;11:805-21.

Ashburner J, Ridgway GR. Symmetric diffeomorphic modeling of longitudinal structural MRI. Front Neurosci. 2012;6:197.

Ashburner J. Computational anatomy with the SPM software. Magn Reson Med. 2009;27(8):1163-74.

Ba M, Bonhoeffer F. Perspectives on axonal regeneration in the mammalian CNS. Trends Neurosci. 1994;17(11):473-479.

Bagory M, Durand-Dubief F, Ibarrola D, Comte JC, Cotton F, Confavreux C, et al. Implementation of an absolute brain 1H-MRS quantification method to assess different tissue alterations in multiple sclerosis. IEEE Trans Biomed Eng. 2012;59(10):2687-94.

Ballermann M, Fouad K. Spontaneous locomotor recovery in spinal cord injured rats is accompanied by anatomical plasticity of reticulospinal fibers. Eur J Neurosci. 2006;23(8):1988-96.

Barabasi AL, Oltvai ZN. Network biology: understanding the cell's functional organization. Nat Rev Genet, 2004;5(2):101.

Bareyre FM, Schwab ME. Inflammation, degeneration and regeneration in the injured spinal cord: insights from DNA microarrays. Trends Neurosci. 2003;26:555-63.

Bareyre FM, Kerschensteiner M, Raineteau O, Mettenleiter TC, Weinmann O, Schwab ME. The injured spinal cord spontaneously forms a new intraspinal circuit in adult rats. Nat Neurosci. 2004;7(3):269-77.

Barron KD, Dentinger MP, Popp AJ, Mankes R. Neurons of layer Vb of rat sensorimotor cortex atrophy but do not die after thoracic cord transection. J Neuropathol Exp Neurol. 1988;47:62–74.

Basso DM, Beattie MS, Bresnahan JC. Graded histological and locomotor outcomes after spinal cord contusion using the NYU weight-drop device versus transection. Exp. Neurol. 1996;139:244-56.

Bates TE, Strangward M, Keelan J, Davey GP, Munro PM, Clark JB. Inhibition of N-acetylaspartate production: implications for 1H MRS studies in vivo. Neuroreport. 1996;7(8):1397-400.

Bazley FA, Maybhate A, Tan CS, Thakor NV, Kerr C, All AH. Enhancement of bilateral cortical somatosensory evoked potentials to intact forelimb stimulation following thoracic contusion spinal cord injury in rats. IEEE Trans Neural Syst Rehabil Eng. 2014;22(5):953-64.

Beaud ML, Rouiller EM, Bloch J, Mir A, Schwab ME, Wannier T, et al. Invasion of lesion territory by regenerating fibers after spinal cord injury in adult macaque monkeys. Neurosci. 2012;227:271-82.

Beck KD, Nguyen HX, Galvan MD, Salazar DL, Woodruff TM, Anderson AJ. Quantitative analysis of cellular inflammation after traumatic spinal cord injury: evidence for a multiphasic inflammatory response in the acute to chronic environment. Brain. 2010;133:433-47.

Belhaj-Saif A, Cheney PD. Plasticity in the distribution of the red nucleus output to forearm muscles after unilateral lesions of the pyramidal tract. Journal of neurophysiology. 2000;83(5):3147-53.

Bellenberg B, Busch M, Trampe N, Gold R, Chan A, Lukas C. 1H-magnetic resonance spectroscopy in diffuse and focal cervical cord lesions in multiple sclerosis. Eur Radiol. 2013;23(12):3379-92.

Berry M. Post-injury myelin-breakdown products inhibit axonal growth: an hypothesis to explain the failure of axonal regeneration in the mammalian central nervous system. Bibl Anat. 1982(23):1-11.

Biomarkers Definitions Working Group. Biomarkers and surrogate endpoints: preferred definitions and conceptual framework. Clin Pharmacol Ther. 2001;69(3):89-95.

Bjartmar C, Kidd G, Mork S, Rudick R, Trapp BD. Neurological disability correlates with spinal cord axonal loss and reduced N-acetyl aspartate in chronic multiple sclerosis patients. Ann Neurol. 2000;48(6): 893-901.

Blamire AM, Cader S, Lee M, Palace J, Matthews PM. Axonal damage in the spinal cord of multiple sclerosis patients detected by magnetic resonance spectroscopy. Magn Reson Med. 2007;58(5):880-5.

Blesch A, Tuszynski MH. Spinal cord injury: plasticity, regeneration and the challenge of translational drug development. Trends Neurosci. 2009;32(1):41-7.

Bliss TV, Collingridge GL. A synaptic model of memory: long-term potentiation in the hippocampus. Nature. 1993;361(6407):31.

Boato F, Rosenberger K, Nelissen S, Geboes L, Peter EM, Nitsch R, Hendrix S. Absence of IL-1beta positively affects neurological outcome, lesion development and axonal plasticity after spinal cord injury. J Neuroinflammation. 2013;10:6.

Boldin C, Raith J, Fankhauser F, et al. Predicting neurologic recovery in cervical spinal cord injury with postoperative MR imaging. Spine. 2006;31:554-9.

Bosch-Bouju C, Hyland BI, Parr-Brownlie LC. Motor thalamus integration of cortical, cerebellar and basal ganglia information: implications for normal and parkinsonian conditions. Front Comput Neurosci. 2013;7:163.

Bracken, MB, Holford, TR. Neurological and functional status 1 year after acute spinal cord injury: estimates of functional recovery in National Acute Spinal Cord Injury Study II from results modeled in National Acute Spinal Cord Injury Study III. J Neurosurg. 2002;96(3):259-266.

Bradbury EJ, Moon LD, Popat RJ, King VR, Bennett GS, Patel PN, et al. Chondroitinase ABC promotes functional recovery after spinal cord injury. Nature. 2002;416(6881):636-40.

Brambilla R, Bracchi-Ricard V, Hu WH, Frydel B, Bramwell A, Karmally S, et al. Inhibition of astroglial nuclear factor κB reduces inflammation and improves functional recovery after spinal cord injury. J. Exp. Med. 2005;202(1):145-156.

Brand A, Richter-Landsberg C, Leibfritz D. Multinuclear NMR studies on the energy metabolism of glial and neuronal cells. Dev Neurosci. 1993;15(3-5):289-98.

Bregman BS, Broude E, McAtee M, Kelley MS. Transplants and neurotrophic factors prevent atrophy of mature CNS neurons after spinal cord injury. Exp. Neurol. 1998;149(1):13-27.

Bregman BS, Coumans JV, Dai HN, Kuhn PL, Lynskey J, McAtee M, Sandhu F. Transplants and neurotrophic factors increase regeneration and recovery of function after spinal cord injury. Prog Brain Res. 2002;137:257-73.

Brennan FH, Cowin GJ, Kurniawan ND, Ruitenberg MJ. Longitudinal assessment of white matter pathology in the injured mouse spinal cord through ultra-high field (16.4 T) in vivo diffusion tensor imaging. Neuroimage. 2013;82:574-85.

Brodmann K. Neue Ergebnisse über die vergleichende histologische Lokalisation der Grosshirnrinde mit besonderer Berücksichtigung des Stirnhirns. Anatomischer Anzeiger. 1912;41(Suppl):157-216.

Brown AG. Organization in the spinal cord: the anatomy and physiology of identified neurons. Springer Science & Business Media; 2012.

Bruehlmeier M, Dietz V, Leenders KL, Roelcke U, Missimer J, Curt A. How does the human brain deal with a spinal cord injury? Eur. J. Neurosci. 1998;10(12):3918-22.

Bullmore E, Sporns O. Complex brain networks: graph theoretical analysis of structural and functional systems. Nat Rev Neurosci. 2009;10(3):186.

Bullmore E, Sporns O. The economy of brain network organization. Nat Rev Neurosci. 2012;13(5):336.

Bunge RP, Puckett WR, Becerra JL, Marcillo A, Quencer RM. Observations on the pathology of human spinal cord injury. A review and classification of 22 new cases with details from a case of chronic cord compression with extensive focal demyelination. Advances Neurol, 1993;59:75.

Bunge MB. Book review: bridging areas of injury in the spinal cord. The Neuroscientist. 2001;7(4):325-39.

Buss A, Brook GA, Kakulas B, Martin D, Franzen R, Schoenen J, et al.Gradual loss of myelin and formation of an astrocytic scar during Wallerian degeneration in the human spinal cord. Brain. 2004;127(1):34-44.

Buss A, Pech K, Merkler D, Kakulas BA, Martin D, Schoenen J, et al. Sequential loss of myelin proteins during Wallerian degeneration in the human spinal cord. Brain. 2005;128(2):356-64.

Cadotte DW, Fehlings MG. Will imaging biomarkers transform spinal cord injury trials? Lancet Neurol. 2013;12(9):843-4.

Calabrese M, Magliozzi R, Ciccarelli O, Geurts JJ, Reynolds R, Martin R. Exploring the origins of grey matter damage in multiple sclerosis. Nat Rev Neurosci. 2015;16:147-58.

Calderón-Vallejo D, Quintanar-Stephano A, Hernández-Jasso I, Jiménez-Hernández V, Ruiz-Ornelas J, Jiménez I, et al. Functional and structural recovery of the injured spinal cord in rats treated with gonadotropin-releasing hormone. Neurochem Research, 2015;40(3):455-462.

Callaghan MF, Freund P, Draganski B, Anderson E, Cappelletti M, Chowdhury R, et al. Widespread age-related differences in the human brain microstructure revealed by quantitative magnetic resonance imaging. Neurobiol Aging. 2014;35(8):1862-72.

Cao Y, Zhou Y, Ni S, Wu T, Li P, Liao S, et al. Three Dimensional Quantification of Microarchitecture and Vessel Regeneration by Synchrotron Radiation Microcomputed Tomography in a Rat Model of Spinal Cord Injury. J Neurotrauma. 2017;34(6):1187-99.

Cappe C, Morel A, Barone P, Rouiller EM. The thalamocortical projection systems in primate: an anatomical support for multisensory and sensorimotor interplay. Cerebral cortex. 2009;19(9):2025-37.

Carew JD, Nair G, Pineda-Alonso N, Usher S, Hu X, Benatar M. Magnetic resonance spectroscopy of the cervical cord in amyotrophic lateral sclerosis. Amyotroph Lateral Scler. 2011;12(3):185-91.

Caroni P, Schwab ME. Antibody against myelin associated inhibitor of neurite growth neutralizes nonpermissive substrate properties of CNS white matter. Neuron. 1988;1(1):85-96.

Chakraborty G, Mekala P, Yahya D, Wu G, Ledeen RW. Intraneuronal N-acetylaspartate supplies acetyl groups for myelin lipid synthesis: evidence for myelin-associated aspartoacylase. J Neurochem. 2001;78(4):736-45.

Chakravarty MM, Bertrand G, Hodge CP, Sadikot AF, Collins DL. The creation of a brain atlas for image guided neurosurgery using serial histological data. Neuroimage. 2006;30(2):359-76.

Chakravarty MM, Sadikot AF, Germann J, Bertrand G, Collins DL. Towards a validation of atlas warping techniques. Med Image Anal. 2008;12(6):713-26.

Chakravarty MM, Rosa-Neto P, Broadbent S, Evans AC, Collins DL. Robust S1, S2, and thalamic activations in individual subjects with vibrotactile stimulation at 1.5 and 3.0 T. Hum Brain Mapp. 2009a;30(4):1328-37.

Chakravarty MM, Sadikot AF, Germann J, Hellier P, Bertrand G, Collins DL. Comparison of piece-wise linear, linear, and nonlinear atlas-to-patient warping techniques: analysis of the labeling of subcortical nuclei for functional neurosurgical applications. Hum Brain Mapp. 2009b;30(11):3574-95.

Chakravarty MM, Steadman P, van Eede MC, Calcott RD, Gu V, Shaw P, et al. Performing label-fusion-based segmentation using multiple automatically generated templates. Hum Brain Mapp. 2013;34(10):2635-54.

Chandra J, Sheerin F, Lopez de Heredia L, Meagher T, King D, Belci M, et al. MRI in acute and subacute post-traumatic spinal cord injury: pictorial review. Spinal Cord. 2012;50(1):2-7.

Chen AC, Niddam DM, Arendt-Nielsen L. Contact heat evoked potentials as a valid means to study nociceptive pathways in human subjects. Neurosci Lett. 2001;316(2):79-82.

Chinthu R, Anju TR, Paulose CS. Cholinergic receptor alterations in the cerebral cortex of spinal cord injured rat. Biochem Biophys Rep. 2017;10:46-51.

Cermik TF, Tuna H, Kaya M, Tuna F, Gultekin A, Yigitbasi ON, et al. Assessment of regional blood flow in cerebral motor and sensory areas in patients with spinal cord injury. Brain Res. 2006;1109(1):54-9.

Ciccarelli O, Altmann DR, McLean MA, Wheeler-Kingshott CA, Wimpey K, Miller DH, et al. Spinal cord repair in MS: does mitochondrial metabolism play a role? Neurology. 2010;74(9):721-7.

Ciccarelli O, Wheeler-Kingshott CA, McLean MA, Cercignani M, Wimpey K, Miller DH, et al. Spinal cord spectroscopy and diffusion-based tractography to assess acute disability in multiple sclerosis. Brain. 2007;130(8):2220-31.

C.M.R International. 2006/7 Pharmaceutical R&D Factbook. CMR International. 2006.

Cockcroft S. The diverse functions of phosphatidylinositol transfer proteins. Curr Top Microbiol Immunol. 2012;362:185-208.

Cohen-Adad J, El Mendili MM, Lehericy S, Pradat PF, Blancho S, Rossignol S, et al. Demyelination and degeneration in the injured human spinal cord detected with diffusion and magnetization transfer MRI. Neuroimage. 2011;55(3):1024-33.

Cooke SF, Bliss TV. Plasticity in the human central nervous system. Brain. 2006;129(7):1659-73.

Collins DL, Pruessner JC. Towards accurate, automatic segmentation of the hippocampus and amygdala from MRI by augmenting ANIMAL with a template library and label fusion. Neuroimage. 2010;52(4):1355-66.

Connor JR, Menzies SL. Altered cellular distribution of iron in the central nervous system of myelin deficient rats. Neurosci. 1990;34(1):265-71.

Courtine G, Song B, Roy RR, Zhong H, Herrmann JE, Ao Y, et al. Recovery of supraspinal control of stepping via indirect propriospinal relay connections after spinal cord injury. Nature Med. 2008;14(1):69-74.

Courtine G, Gerasimenko Y, Van Den Brand R, Yew A, Musienko P, Zhong H, et al.. Transformation of nonfunctional spinal circuits into functional states after the loss of brain input. Nat. Neurosci. 2009;12(10):1333.

Cramer SC, Lastra L, Lacourse MG, Cohen MJ. Brain motor system function after chronic, complete spinal cord injury. Brain. 2005;128(12):2941-50.

Crandall PH, Batzdorf U. Cervical spondylotic myelopathy. J Nneurosurg. 1966;25(1):57-66.

Cregg JM, DePaul MA, Filous AR, Lang BT, Tran A, Silver J. Functional regeneration beyond the glial scar. Exp. Neurol. 2014;253:197-207.

Cripps RA, Lee BB, Wing P, Weerts E, Mackay J, Brown D. A global map for traumatic spinal cord injury epidemiology: towards a living data repository for injury prevention. Spinal Cord. 2011;49(4):493-501.

Crowe MJ, Bresnahan JC, Shuman SL, Masters JN, Beattie MS. Apoptosis and delayed degeneration after spinal cord injury in rats and monkeys. Nat Med. 1997;3:73-6.

Cruz-Almeida Y, Martinez-Arizala A, Widerström-Noga EG. Chronicity of pain associated with spinal cord injury: A longitudinal analysis. J. Rehabil. Res. Dev. 2005;42(5):585.

Curt A, Bruehlmeier M, Leenders KL, Roelcke U, Dietz V. Differential effect of spinal cord injury and functional impairment on human brain activation. J Neurotrauma. 2002;19(1):43-51.

Curt A, Van Hedel HJ, Klaus D, Dietz V. Recovery from a spinal cord injury: significance of compensation, neural plasticity, and repair. J Neurotrauma. 2008;25:677-685.

DaSilva AF, Becerra L, Pendse G, Chizh B, Tully S, Borsook D. Colocalized structural and functional changes in the cortex of patients with trigeminal neuropathic pain. PLoS One, 2008;3(10):e3396.

David G, Freund P, Mohammadi S. The efficiency of retrospective artifact correction methods in improving the statistical power of between-group differences in spinal cord DTI. Neuroimage. 2017;158:296-307.

Davies SJ, Fitch MT, Memberg SP, Hall AK, Raisman G, Silver J. Regeneration of adult axons in white matter tracts of the central nervous system. Nature. 1997;390(6661):680.

Dawson GD. Cerebral responses to electrical stimulation of peripheral nerve in man. J Neurol Neurosurg Psychiatry. 1947;10(3):134.

De Gruttola VG, Clax P, DeMets DL, Downing GJ, Ellenberg SS, Friedman L, et al. Considerations in the evaluation of surrogate endpoints in clinical trials: summary of a National Institutes of Health workshop. Contemp Clin Trials, 2001;22(5):485-502.

De Leener B, Lévy S, Dupont SM, Fonov VS, Stikov N, Collins DL, et al. SCT: Spinal Cord Toolbox, an open-source software for processing spinal cord MRI data. Neuroimage. 2017;145:24-43.

Dick F, Tierney AT, Lutti A, Josephs O, Sereno MI, Weiskopf N. In vivo functional and myeloarchitectonic mapping of human primary auditory areas. J Neurosci. 2012;32(46):16095-105.

Dietz V, Curt A. Neurological aspects of spinal-cord repair: promises and challenges. Lancet Neurol. 2006;5(8):688-94.

Dittuno PL, Ditunno JF, Jr. Walking index for spinal cord injury (WISCI II): scale revision. Spinal Cord. 2001;39:654-6.

Draganski B, Gaser C, Busch V, Schuierer G, Bogdahn U, May A. Neuroplasticity: changes in grey matter induced by training. Nature. 2004;427(6972):311-2.

Draganski B, Ashburner J, Hutton C, Kherif F, Frackowiak RS, Helms G, et al. Regional specificity of MRI contrast parameter changes in normal ageing revealed by voxel-based quantification (VBQ). Neuroimage. 2011;55(4):1423-34.

Dryden DM, Saunders LD, Jacobs P, Schopflocher DP, Rowe BH, May LA, et al. Direct health care costs after traumatic spinal cord injury. J Trauma Acute Care Surg. 2005;59(2):441-7.

Dula AN, Gochberg DF, Valentine HL, Valentine WM, Does MD. Multiexponential T2, magnetization transfer, and quantitative histology in white matter tracts of rat spinal cord. Magn Reson Med. 2010;63(4):902-9.

Dumont RJ, Okonkwo DO, Verma S, Hurlbert RJ, Boulos PT, Ellegala DB, Dumont AS. Acute spinal cord injury, part I: pathophysiologic mechanisms. Clin Neuropharmacol. 2001;24(5):254-64.

Dutta A, Kambi N, Raghunathan P, Khushu S, Jain N. Large-scale reorganization of the somatosensory cortex of adult macaque monkeys revealed by fMRI. Brain Struct Funct. 2014;219(4):1305-20.

Edden RA, Schar M, Hillis AE, Barker PB. Optimized detection of lactate at high fields using inner volume saturation. Magn Reson Med. 2006;56(4):912-7.

Edgerton VR, Roy RR. Paralysis recovery in humans and model systems. Curr Opin Neurobiol. 2002;12(6):658-67.

Ellaway PH, Kuppuswamy A, Balasubramaniam AV, Maksimovic R, Gall A, Craggs MD, et al. Development of quantitative and sensitive assessments of physiological and functional outcome during recovery from spinal cord injury: a clinical initiative. Brain Res Bull. 2011;84:343-57.

Evercooren ABV, Avellana-Adalid V, Lachapelle F, Liblau R. Schwann cell transplantation and myelin repair of the CNS. Mult. Scler. J. 1997;3(2):157-161.

Faden AI, Wu J, Stoica BA, Loane DJ. Progressive inflammation-mediated neurodegeneration after traumatic brain or spinal cord injury. Br J Pharmacol. 2016;173(4):681-91.

Faulkner JR, Herrmann JE, Woo MJ, Tansey KE, Doan NB, Sofroniew MV. Reactive astrocytes protect tissue and preserve function after spinal cord injury. J Neurosci. 2004;24(9):2143-55.

Fawcett JW, Keynes RJ. Peripheral nerve regeneration. Annu Rev Neurosci. 1990;13(1):43-60.

Fawcett JW, Asher RA. The glial scar and central nervous system repair. Brain Res. Bull. 1999;49(6):377-91.

Fawcett, JW, Curt, A, Steeves, JD. Guidelines for the conduct of clinical trials for spinal cord injury as developed by the ICCP panel: spontaneous recovery after spinal cord injury and statistical power needed for therapeutic clinical trials. Spinal Cord. 2006;45:190-205.

Fehlings MG, Theodore N, Harrop J, Maurais G, Kuntz C, Shaffrey CI, et al. A phase I/IIa clinical trial of a recombinant Rho protein antagonist in acute spinal cord injury. J Neurotrauma. 2011;28(5):787-96.

Felix MS, Popa N, Djelloul M, Boucraut J, Gauthier P, Bauer S, et al. Alteration of forebrain neurogenesis after cervical spinal cord injury in the adult rat. Front Neurosci, 2012;6:45.

Fleming JC, Norenberg MD, Ramsay DA, Dekaban GA, Marcillo AE, Saenz AD, et al. The cellular inflammatory response in human spinal cords after injury. Brain. 2006;129(12):3249-69.

Finnerup NB, Norrbrink C, Trok K, Piehl F, Johannesen IL, Sørensen JC et al. Phenotypes and predictors of pain following traumatic spinal cord injury: a prospective study. J Pain. 2014;15(1):40-48.

Filli L, Engmann AK, Zörner B, Weinmann O, Moraitis T, Gullo M, et al. Bridging the gap: a reticulo-propriospinal detour bypassing an incomplete spinal cord injury. J Neurosci. 2014;34(40):13399-410.

Filli L, Schwab ME. Structural and functional reorganization of propriospinal connections promotes functional recovery after spinal cord injury. Neural Regen Res. 2015;10:509-13.

Finsterbusch J. Improving the performance of diffusion-weighted inner field-of-view echo-planar imaging based on 2D-selective radiofrequency excitations by tilting the excitation plane. J Magn Reson Imaging. 2012;35(4):984-92.

Finsterbusch J, Busch MG, Larson PE. Signal scaling improves the signal-to-noise ratio of measurements with segmented 2D-selective radiofrequency excitations. Magn Reson Med. 2013;70(6):1491-9.

Flanders AE, Spettell CM, Friedman DP, Marino RJ, Herbison GJ. The relationship between the functional abilities of patients with cervical spinal cord injury and the severity of damage revealed by MR imaging. AJNR Am J Neuroradiol. 1999;20:926-34.

Flynn JR, Graham BA, Galea MP,Callister RJ. The role of propriospinal interneurons in recovery from spinal cord injury. Neuropharmacology. 2011;60:809-822.

Fonov VS, Le Troter A, Taso M, De Leener B, Leveque G, Benhamou M, et al. Framework for integrated MRI average of the spinal cord white and gray matter: the MNI-Poly-AMU template. Neuroimage. 2014;102(2):817-27.

Fouad K, Klusman I, Schwab ME. Regenerating corticospinal fibers in the Marmoset (Callitrix jacchus) after spinal cord lesion and treatment with the anti-Nogo-A antibody IN-1. Eur J Neurosci. 2004;20(9):2479-82.

Freund P, Schmidlin E, Wannier T, Bloch J, Mir A, Schwab ME, et al. Nogo-A-specific antibody treatment enhances sprouting and functional recovery after cervical lesion in adult primates. Nat Med. 2006;12:790-2.

Freund P, Wannier T, Schmidlin E, Bloch J, Mir A, Schwab ME, Rouiller EM. Anti-Nogo-A antibody treatment enhances sprouting of corticospinal axons rostral to a unilateral cervical spinal cord lesion in adult macaque monkey. J. Comp. Neurol. 2007;502(4):644-59.

Freund P, Weiskopf N, Ward NS, Hutton C, Gall A, Ciccarelli O, et al. Disability, atrophy and cortical reorganization following spinal cord injury. Brain. 2011a;134(6):1610-22.

Freund P, Rothwell J, Craggs M, Thompson AJ, Bestmann S. Corticomotor representation to a human forearm muscle changes following cervical spinal cord injury. Eur J Neurosci. 2011b;34(11):1839-46.

Freund P, Wheeler-Kingshott CA, Nagy Z, Gorgoraptis N, Weiskopf N, Friston K, et al. Axonal integrity predicts cortical reorganisation following cervical injury. J Neurol Neurosurg Psychiatry. 2012a;83(6):629-37.

Freund P, Schneider T, Nagy Z, Hutton C, Weiskopf N, Friston K, et al. Degeneration of the injured cervical cord is associated with remote changes in corticospinal tract integrity and upper limb impairment. PLoS One. 2012b;7(12):e51729.

Freund P, Weiskopf N, Ashburner J, Wolf K, Sutter R, Altmann DR, et al. MRI investigation of the sensorimotor cortex and the corticospinal tract after acute spinal cord injury: a prospective longitudinal study. Lancet Neurol. 2013a;12:873-81.

Freund P, Curt A, Friston K, Thompson A. Tracking changes following spinal cord injury: insights from neuroimaging. Neuroscientist. 2013b;19(2):116-28.

Freund P, Friston K, Thompson AJ, Stephan KE, Ashburner J, Bach DR, et al. Embodied neurology: an integrative framework for neurological disorders. Brain. 2016;139:1855-61.

Frey S, Pandya DN, Chakravarty MM, Bailey L, Petrides M, Collins DL. An MRI based average macaque monkey stereotaxic atlas and space (MNI monkey space). Neuroimage. 2011;55(4):1435-42.

Furlan JC, Kailaya-Vasan A, Aarabi B, Fehlings MG. A novel approach to quantitatively assess posttraumatic cervical spinal canal compromise and spinal cord compression: a multicenter responsiveness study. Spine. 2011;36:784-93.

Galhardoni R, Correia GS, Araujo H, Yeng LT, Fernandes DT, Kaziyama HH, et al. Repetitive transcranial magnetic stimulation in chronic pain: a review of the literature. Arch Phys Med Rehabil. 2015;96(4):156-72.

Gasparovic C, Song T, Devier D, Bockholt HJ, Caprihan A, Mullins PG, et al. Use of tissue water as a concentration reference for proton spectroscopic imaging. Magn Reson Med. 2006;55(6):1219-26.

Gelman N, Ewing JR, Gorell JM, Spickler EM, Solomon EG. Interregional variation of longitudinal relaxation rates in human brain at 3.0 T: relation to estimated iron and water contents. Magn Reson Med. 2001;45(1):71-9.

Genovese CR, Lazar NA, Nichols T. Thresholding of statistical maps in functional neuroimaging using the false discovery rate. Neuroimage. 2002;15(4):870-8.

Geoffroy CG, Meves JM, Zheng B. The age factor in axonal repair after spinal cord injury: A focus on neuron-intrinsic mechanisms. Neurosci Lett. 2016.

Gerber MR, Connor JR. Do oligodendrocytes mediate iron regulation in the human brain? Ann. Neurol. 1989;26(1):95-8.

Ghosh A, Haiss F, Sydekum E, Schneider R, Gullo M, Wyss MT, et al. Rewiring of hindlimb corticospinal neurons after spinal cord injury. Nat. Neurosci. 2010;13(1):97-104.

Gomez-Pinilla F, Ying Z, Zhuang Y. Brain and spinal cord interaction: protective effects of exercise prior to spinal cord injury. PLoS On. 2012;7(2):e32298.

Goshgarian H. Development, Anatomy, and Function of the Spinal Cord. Spinal Cord Medicine: Principles and Practice. 2010.

Grabher P, Callaghan MF, Ashburner J, Weiskopf N, Thompson AJ, Curt A, et al. Tracking sensory system atrophy and outcome prediction in spinal cord injury. Ann Neurol. 2015;78(5):751-61.

Grabher P, Mohammadi S, Trachsler A, Friedl S, David G, Sutter R, et al. Voxel-based analysis of grey and white matter degeneration in cervical spondylotic myelopathy. Sci Rep. 2016;6:24636.

Grabher P, Mohammadi S, David G, Freund P. Neurodegeneration in the spinal ventral horn prior to motor impairment in cervical spondylotic myelopathy. J Neurotrauma .2017;34(15):2329-34.

Grill R, Murai K, Blesch A, Gage FH, Tuszynski MH. Cellular delivery of neurotrophin-3 promotes corticospinal axonal growth and partial functional recovery after spinal cord injury. J Neurosci. 1997;17(14):5560-72.

Gruetter R. Automatic, localized in vivo adjustment of all first- and second-order shim coils. Magn Reson Med. 1993;29(6):804-11.

Grumbles RM, Thomas CK. Motoneuron death after human spinal cord injury. J Neurotrauma. 2017;34(3):581-90.

Guest JD, Rao A, Olson L, Bunge MB, Bunge RP. The ability of human Schwann cell grafts to promote regeneration in the transected nude rat spinal cord. Exp. Neurol. 1997;148(2):502-22.

Guest JD, Hiester ED, Bunge RP. Demyelination and Schwann cell responses adjacent to injury epicenter cavities following chronic human spinal cord injury. Exp. Neurol. 2005;192(2):384-93.

Guleria S, Gupta RK, Saksena S, Chandra A, Srivastava RN, Husain M et al. Retrograde Wallerian degeneration of cranial corticospinal tracts in cervical spinal cord injury patients using diffusion tensor imaging. J. Neurosci. Res. 2008;86(10): 2271-2280.

Gustin SM, Wrigley PJ, Siddall PJ, Henderson LA. Brain anatomy changes associated with persistent neuropathic pain following spinal cord injury. Cereb Cortex. 2009;20(6):1409-19.

Gustin SM, Peck CC, Cheney LB, Macey PM, Murray GM, Henderson LA. Pain and plasticity: is chronic pain always associated with somatosensory cortex activity and reorganization? J. Neurosci. 2012;32(43):14874-84.

Gwak YS, Hulsebosch CE, Leem JW. Neuronal-Glial Interactions Maintain Chronic Neuropathic Pain after Spinal Cord Injury. Neural Plasticity. 2017;2017:14.

Hains BC, Black JA, Waxman SG. Primary cortical motor neurons undergo apoptosis after axotomizing spinal cord injury. J Comp Neurol. 2003;462(3):328-41.

Hankins JS, McCarville MB, Loeffler RB, Smeltzer MP, Onciu M, Hoffer FA, et al. R2* magnetic resonance imaging of the liver in patients with iron overload. Blood. 2009;113(20):4853-5.

Harkema S, Gerasimenko Y, Hodes J, Burdick J, Angeli C, Chen Y, et al. Effect of epidural stimulation of the lumbosacral spinal cord on voluntary movement, standing, and assisted stepping after motor complete paraplegia: a case study. The Lancet. 2011;377(9781):1938-47.

Harkins KD, Xu J, Dula AN, Li K, Valentine WM, Gochberg DF, et al. The microstructural correlates of T1 in white matter. Magn Reson Med. 2016;75(3):1341-5.

Hawasli AH, Rutlin J, Roland JL, Murphy RK, Song SK, Leuthardt EC, et al. Spinal Cord Injury Disrupts Resting-State Networks in the Human Brain. J Neurotrauma. 2018.

Henry P-G, Deelchand D, Iltis I, Hutter D, Bushara KO, Oz G, et al. MRS and diffusion MRI of the spinal cord in Friedreich's Ataxia. In: Proc Intl Soc Magn Reson Med. 2014:571.

Helms G, Dathe H, Kallenberg K, Dechent P. High-resolution maps of magnetization transfer with inherent correction for RF inhomogeneity and T1 relaxation obtained from 3D FLASH MRI. Magn Reson Med. 2008;60(6):1396-407.

Helms G, Dechent P. Increased SNR and reduced distortions by averaging multiple gradient echo signals in 3D FLASH imaging of the human brain at 3T. J Magn Reson Imaging. 2009;29(1):198-204.

Heye AK, Culling RD, Hernández MD, Thrippleton MJ, Wardlaw JM. Assessment of blood–brain barrier disruption using dynamic contrast-enhanced MRI. A systematic review. Neuroimage Clin. 2014;6:262-74.

Hier DB, Wang J. Reduced cortical surface area in multiple sclerosis. Neurol Res. 2007;29(3):231-2.

Hill CE, Beattie MS, Bresnahan JC. Degeneration and sprouting of identified descending supraspinal axons after contusive spinal cord injury in the rat. Exp. Neurol. 2001;171(1):153-169.

Hock A, Fuchs A, Boesiger P, Kollias SS, Henning A. Electrocardiogram-triggered, higher order, projection-based B(0) shimming allows for fast and reproducible shim convergence in spinal cord (1)H MRS. NMR Biomed. 2013a;26(3):329-35.

Hock A, Henning A, Boesiger P, Kollias SS. (1)H-MR spectroscopy in the human spinal cord. Am J Neuroradiol. 2013b;34(9):1682-9.

Hock A, MacMillan EL, Fuchs A, Kreis R, Boesiger P, Kollias SS, et al. Non-water-suppressed proton MR spectroscopy improves spectral quality in the human spinal cord. Magn Reson Med. 2013c;69(5):1253-60.

Holly LT, Freitas B, McArthur DL, Salamon N. Proton magnetic resonance spectroscopy to evaluate spinal cord axonal injury in cervical spondylotic myelopathy. J Neurosurg Spine. 2009;10(3):194-200.

Holmes CJ, Hoge R, Collins L, Woods R, Toga AW, Evans AC. Enhancement of MR images using registration for signal averaging. J Comput Assist Tomogr. 1998;22(2):324-33.

Hou JM, Yan RB, Xiang ZM, Zhang H, Liu J, Wu YT, et al. Brain sensorimotor system atrophy during the early stage of spinal cord injury in humans. Neurosci. 2014;266:208-15.

Hou J, Xiang Z, Yan R, Zhao M, Wu Y, Zhong J, et al. Motor recovery at 6 months after admission is related to structural and functional reorganization of the spine and brain in patients with spinal cord injury. Hum. Brain Mapp. 2016;37(6):2195-2209.

Holub BJ. The nutritional significance, metabolism, and function of myo-inositol and phosphatidylinositol in health and disease. Adv Nutr Res. 1982;4:107-41.

Horsfield MA, Sala S, Neema M, Absinta M, Bakshi A, Sormani MP, et al. Rapid semi-automatic segmentation of the spinal cord from magnetic resonance images: application in multiple sclerosis. Neuroimage. 2010;50(2):446-55.

Howe FA, Opstad KS. 1H MR spectroscopy of brain tumours and masses. NMR Biomed. 2003;16(3):123-31.

Huang JK, Phillips GR, Roth AD, Pedraza L, Shan W, Belkaid W, et al. Glial membranes at the node of Ranvier prevent neurite outgrowth. Science. 2005;310(5755):1813-7.

Huang SW, Wang WT, Chou LC, Liou TH, Lin HW. Risk of dementia in patients with spinal cord injury: A nationwide population-based cohort study. J Neurotrauma. 2017;34(3):615-22.

Huang WL, George KJ, Ibba V, Liu MC, Averill S, Quartu M, et al. The characteristics of neuronal injury in a static compression model of spinal cord injury in adult rats. Eur J Neurosci. 2007;25:362-72.

Huber E, Curt A, Freund P. Tracking trauma-induced structural and functional changes above the level of spinal cord injury. Curr Opin Neurol. 2015;28(4):365-72.

Huber E, Lachappelle P, Sutter R, Curt A, Freund P. Are midsagittal tissue bridges predictive of outcome after cervical spinal cord injury? Ann Neurol. 2017;81(5):740-8.

Huber E, David G, Thompson A, Weiskopf N, Mohammadi S, Freund P. Dorsal and ventral horn atrophy is associated with clinical outcome after spinal cord injury. Neurology. 2018. In press.

Humanes-Valera D, Aguilar J, Foffani G. Reorganization of the intact somatosensory cortex immediately after spinal cord injury. PLoS One. 2013;8(7):e69655.

Husted CA, Matson GB, Adams DA, Goodin DS, Weiner MW. In vivo detection of myelin phospholipids in multiple sclerosis with phosphorus magnetic resonance spectroscopic imaging. Ann. Neurol. 1994;36(2):239-41.

Huston JP, Steiner H, Weiler HT, Morgan S, Schwarting RK. The basal ganglia-orofacial system: studies on neurobehavioral plasticity and sensory-motor tuning. Neurosci Biobehav Rev. 1990;14(4):433-46.

Hutton C, Draganski B, Ashburner J, Weiskopf N. A comparison between voxel-based cortical thickness and voxel-based morphometry in normal aging. Neuroimage. 2009;48(2):371-80.

Isaacks RE, Bender AS, Kim CY, Prieto NM, Norenberg MD. Osmotic regulation of myo-inositol uptake in primary astrocyte cultures. Neurochem Res. 1994;19(3):331-8.

Itzkovich M, Gelernter I, Biering-Sorensen F, Weeks C, Laramee MT, Craven BC, et al. The Spinal Cord Independence Measure (SCIM) version III: reliability and validity in a multi-center international study. Disabil Rehabil. 2007;29(24):1926-33.

Jensen MP, Sherlin LH, Gertz KJ, Braden AL, Kupper AE, Gianas A, et al. Brain EEG activity correlates of chronic pain in persons with spinal cord injury: clinical implications. Spinal Cord. 2013;51(1):55-8.

Jirjis MB, Vedantam A, Budde MD, Kalinosky B, Kurpad SN, Schmit BD. Severity of spinal cord injury influences diffusion tensor imaging of the brain. J Magn Reson Imaging. 2016;43(1):63-74.

Jung JK, Oh CH, Yoon SH, Ha Y, Park S, Choi B. Outcome evaluation with signal activation of functional MRI in spinal cord injury. J Korean Neurosurg Soc. 2011;50(3):209-15.

Jurkiewicz MT, Crawley AP, Verrier MC, Fehlings MG, Mikulis DJ. Somatosensory cortical atrophy after spinal cord injury: a voxel-based morphometry study. Neurology. 2006;66(5):762-4.

Jurkiewicz MT, Mikulis DJ, McIlroy WE, Fehlings MG, Verrier MC. Sensorimotor cortical plasticity during recovery following spinal cord injury: a longitudinal fMRI study. Neurorehabil Neural Repair. 2007;21(6):527-38.

Jutzeler CR, Freund P, Huber E, Curt A, Kramer JL. Neuropathic pain and functional reorganization in the primary sensorimotor cortex after spinal cord injury. J Pain, 2015;16(12):1256-1267.

Jutzeler CR, Huber E, Callaghan MF, Luechinger R, Curt A, Kramer JL, et al. Association of pain and CNS structural changes after spinal cord injury. Sci Rep. 2016;6:18534.

Kakulas AB. Pathology of spinal injuries. Central Nervous System Trauma. 1984;1(2):117-126.

Kakulas AB, Lorimer RL, Gubbay AD. In Spinal Cord Monitoring. Basic Principles, Regeneration, Pathophysiology and Clinical Aspects (eds Stalberg E., Sharma HR, Olsson Y) Ch. 395–407, (Springer Vienna, 1998).

Kakulas AB. A review of the neuropathology of human spinal cord injury with emphasis on special features. J Spinal Cord Med. 1999;22(2):119-24.

Kalat JW. Biological Psychology . Pacific Grove: Brooks. 1998.

Kalil K, Schneider GE. Retrograde cortical and axonal changes following lesions of the pyramidal tract. Brain research. 1975;89(1):15-27.

Kalsi-Ryan S, Curt A, Verrier MC, Fehlings MG. Development of the Graded Redefined Assessment of Strength, Sensibility and Prehension (GRASSP): reviewing measurement specific to the upper limb in tetraplegia. J Neurosurg Spine. 2012a; 17(1): 65-76.

Kalsi-Ryan S, Beaton D, Curt A, Duff S, Popovic MR, Rudhe C, et al. The Graded Redefined Assessment of Strength Sensibility and Prehension: reliability and validity. J Neurotrauma. 2012b;29:905-14.

Kamble RB, Venkataramana NK, Naik AL, Rao SV. Diffusion tensor imaging in spinal cord injury. Indian J Radiol Imaging. 2011;21:221-4.

Kato H, Kanellopoulos GK, Matsuo S, Wu YJ, Jacquin MF, Hsu CY, et al. Neuronal apoptosis and necrosis following spinal cord ischemia in the rat. Exp. Neurol. 1997;148(2):464-74.

Kaul R, Gao GP, Balamurugan K, Matalon R. Cloning of the human aspartoacylase cDNA and a common missense mutation in Canavan disease. Nat Genet. 1993;5(2):118-23.

Kairys AE, Schmidt-Wilcke T, Puiu T, Ichesco E, Labus JS, Martucci K, et al. Increased brain gray matter in the primary somatosensory cortex is associated with increased pain and mood disturbance in patients with interstitial cystitis/painful bladder syndrome. J Urol. 2015;193(1):131-137.

Kelley BJ, Harel NY, Kim CY, Papademetris X, Coman D, Wang X, et al. Diffusion tensor imaging as a predictor of locomotor function after experimental spinal cord injury and recovery. J Neurotrauma. 2014;31(15):1362-73.

Kendi AT, Tan FU, Kendi M, Yilmaz S, Huvaj S, Tellioglu S. MR spectroscopy of cervical spinal cord in patients with multiple sclerosis. Neuroradiology. 2004;46(9):764-9.

Kennedy P, Lude P, Taylor N. Quality of life, social participation, appraisals and coping post spinal cord injury: a review of four community samples. Spinal cord. 2006;44(2):95-105.

Kerschensteiner M, Schwab ME, Lichtman JW, Misgeld T. In vivo imaging of axonal degeneration and regeneration in the injured spinal cord. Nat Med. 2005;11:572-7.

Kim BG, Dai HN, McAtee M, Vicini S, Bregman BS. Remodeling of synaptic structures in the motor cortex following spinal cord injury. Exp. Neurol. 2006;198(2):401-15.

Kim CF, Moalem-Taylor G. Interleukin-17 contributes to neuroinflammation and neuropathic pain following peripheral nerve injury in mice. J Pain. 2011;12(3):370-383.

Kim SK, Nabekura J. Rapid synaptic remodeling in the adult somatosensory cortex following peripheral nerve injury and its association with neuropathic pain. J Neurosci. 2011;31(14):5477-5482.

Kim SK, Nabekura J, Koizumi S. Astrocyte mediated synapse remodeling in the pathological brain. Glia. 2017.

Kim W, Kim SK, Nabekura J. Functional and structural plasticity in the primary somatosensory cortex associated with chronic pain. J Neurochem. 2017.

Kim Y, Park YK, Cho HY, Kim J, Yoon YW. Long-term changes in expressions of spinal glutamate transporters after spinal cord injury. Brain Res. 2011;1389:194-9.

Kimura J. Principles and pitfalls of nerve conduction studies. Ann Neurol. 1984;16(4):415-29.

Kirov, II, Tal A, Babb JS, Herbert J, Gonen O. Serial proton MR spectroscopy of gray and white matter in relapsing-remitting MS. Neurology. 2013;80(1): 39-46.

Kirshblum SC, Burns SP, Biering-Sorensen F, Donovan W, Graves DE, Jha A, et al. International standards for neurological classification of spinal cord injury (revised 2011). J Spinal Cord Med. 2011;34(6): 535-46.

Kola I, Landis J. Can the pharmaceutical industry reduce attrition rates? Nat. Rev. Drug Discov. 2004;3(8):711.

Kong Y, Eippert F, Beckmann CF, Andersson J, Finsterbusch J, Buchel C, et al. Intrinsically organized resting state networks in the human spinal cord. Proc. Natl. Acad. Sci. U.S.A. 2014;111(50):18067-72.

Koskinen E, Brander A, Hakulinen U, Luoto T, Helminen M, Ylinen A, et al. Assessing the state of chronic spinal cord injury using diffusion tensor imaging. J Neurotrauma. 2013;30:1587-95.

Kozlowski P, Raj D, Liu J, Lam C, Yung AC, Tetzlaff W. Characterizing white matter damage in rat spinal cord with quantitative MRI and histology. J Neurotrauma. 2008;25(6):653-76.

Kozlowski P, Rosicka P, Liu J, Yung AC, Tetzlaff W. In vivo longitudinal Myelin Water Imaging in rat spinal cord following dorsal column transection injury. Magn Reson Imaging. 2014;32(3):250-8.

Kramer JL, Moss AJ, Taylor P, Curt A. Assessment of posterior spinal cord function with electrical perception threshold in spinal cord injury. J Neurotrauma. 2008;25(8):1019-1026.

Kramer JL, Taylor P, Haefeli J, Blum J, Zariffa J, Curt A, Steeves J. Test–retest reliability of contact heat-evoked potentials from cervical dermatomes. J Clin Neurophysiol. 2012;29(1):70-5.

Kramer JL, Haefeli J, Jutzeler CR, Steeves JD, Curt A. Improving the acquisition of nociceptive evoked potentials without causing more pain. Pain. 2013:154(2):235-241.

Kreis R. The trouble with quality filtering based on relative Cramer-Rao lower bounds. Magn Reson Med. 2016;75(1):15-8.

Krishna V, Andrews H, Varma A, Mintzer J, Kindy MS, Guest J. Spinal cord injury: how can we improve the classification and quantification of its severity and prognosis? J Neurotrauma. 2014;31:215-27.

Kucera P, Goldenberg Z, Kurca E. Sympathetic skin response: review of the method and its clinical use. Bratisl Med J. 2004;105(3):108-16.

Kuypers HG. The descending pathways to the spinal cord, their anatomy and function. Progress in brain research. 1964;11:178-202.

Kwok JC, Heller JP, Zhao RR, Fawcett JW. Targeting inhibitory chondroitin sulphate proteoglycans to promote plasticity after injury. Methods Mol Biol. 2014;1162:127-38.

Lamb AH. The projection patterns of the ventral horn to the hind limb during development. Dev Biol. 1976;54(1):82-99.

Lammertse D, Tuszynski MH, Steeves JD, Curt A, Fawcett JW, Rask C, et al. Guidelines for the conduct of clinical trials for spinal cord injury as developed by the ICCP panel: clinical trial design. Spinal cord. 2007;45(3):232.

Lawrence DG, Kuypers HG. The functional organization of the motor system in the monkey. I. The effects of bilateral pyramidal lesions. Brain. 1968;91(1):1-14.

Le E, Aarabi B, Hersh DS, Shanmuganathan K, Diaz C, Massetti J, et al. Predictors of intramedullary lesion expansion rate on MR images of patients with subaxial spinal cord injury. J Neurosurgery Spine. 2015;22:611-21.

Le Bihan D, Johansen-Berg H. Diffusion MRI at 25: exploring brain tissue structure and function. Neuroimage. 2012;61(2):324-41.

Lee BH, Lee KH, Kim UJ, Yoon DH, Sohn JH, Choi SS, et al. Injury in the spinal cord may produce cell death in the brain. Brain research. 2004;1020(1-2):37-44.

Lee TT, Green BA, Dietrich WD,Yezierski RP. Neuroprotective effects of basic fibroblast growth factor following spinal cord contusion injury in the rat. J Neurotrauma, 1999;16(5):347-356.

Lefaucheur JP, Antal A, Ahdab R, Ciampi de Andrade D, Fregni F, Khedr EM, et al. The use of repetitive transcranial magnetic stimulation (rTMS) and transcranial direct current stimulation (tDCS) to relieve pain. Brain Stimul. 2008;1(4):337-44.

Lemasson B, Valable S, Farion R, Krainik A, Rémy C, Barbier EL. In vivo imaging of vessel diameter, size, and density: a comparative study between MRI and histology. Magn Reson Med. 2013;69(1):18-26.

Lemon RN, Griffiths J. Comparing the function of the corticospinal system in different species: organizational differences for motor specialization? Muscle Nerve. 2005;32:261-79.

Lemon RN. Descending pathways in motor control. Annu Rev Neurosci. 2008;31:195-218.

Lenglet C, Joers J, Pisharady P, Deelchand D, Hutter D, Bushara KO, et al. Cross-sectional and longitudinal diffusion MRI and MRS of the spinal cord in Friedreich's Ataxia. In: Proc of the Hum Brain Mapp. 2016:1245.

Lerch JP, Carroll JB, Spring S, Bertram LN, Schwab C, Hayden MR, et al. Automated deformation analysis in the YAC128 Huntington disease mouse model. Neuroimage. 2008;39(1):32-9.

Leung A, Donohue M, Xu R, Lee R, Lefaucheur JP, Khedr EM, et al. rTMS for suppressing neuropathic pain: a meta-analysis. J Pain. 2009;10(12):1205-16.

Li S, Armstrong CM, Bertin N, Ge H, Milstein S, Boxem M et al. A map of the interactome network of the metazoan C. elegans. Science. 2004;303:540–543.

Li XH, Li JB, He XJ, Wang F, Huang SL, Bai ZL. Timing of diffusion tensor imaging in the acute spinal cord injury of rats. Sci. Rep. 2015;5:12639.

Liebscher T, Schnell L, Schnell D, Scholl J, Schneider R, Gullo M, et al. Nogo-A antibody improves regeneration and locomotion of spinal cord–injured rats. Ann Neurol. 2005;58(5):706-19.

Lindner M, Bell T, Iqbal S, Mullins PG, Christakou A. In vivo functional neurochemistry of human cortical cholinergic function during visuospatial attention. PLoS One. 2017;12(2):e0171338.

Lidsky TI, Manetto C, Schneider JS. A consideration of sensory factors involved in motor functions of the basal ganglia. Brain research. 1985;356(2):133-46.

Liu S, Qu Y, Stewart TJ, Howard MJ, Chakrabortty S, Holekamp TF, McDonald JW. Embryonic stem cells differentiate into oligodendrocytes and myelinate in culture and after spinal cord transplantation. Proc. Natl. Acad. Sci. U.S.A. 2000;97(11):6126-31.

Lorensen WE, Cline HE. Marching cubes: A high resolution 3D surface construction algorithm. ACM Siggraph Computer Graphics. 1987;21:163–169.

Lundell H, Barthelemy D, Skimminge A, Dyrby TB, Biering-Sorensen F, Nielsen JB. Independent spinal cord atrophy measures correlate to motor and sensory deficits in individuals with spinal cord injury. Spinal Cord. 2011;49(1):70-5.

Lutti A, Dick F, Sereno MI, Weiskopf N. Using high-resolution quantitative mapping of R1 as an index of cortical myelination. Neuroimage. 2014;93(2):176-88.

Lyman M, Lloyd DG, Ji X, Vizcaychipi MP, Ma D. Neuroinflammation: the role and consequences. Neuroscience research, 2014;79:1-12.

Mabray MC, Talbott JF, Whetstone WD, Dhall SS, Phillips DB, Pan JZ, et al.. Multidimensional analysis of magnetic resonance imaging predicts early impairment in thoracic and thoracolumbar spinal cord injury. J Neurotrauma. 2016;33(10):954-62.

Manganas LN, Zhang X, Li Y, Hazel RD, Smith SD, Wagshul ME, et al. Magnetic resonance spectroscopy identifies neural progenitor cells in the live human brain. Science. 2007;318(5852):980-5.

Marliani AF, Clementi V, Albini Riccioli L, Agati R, Carpenzano M, Salvi F, et al. Quantitative cervical spinal cord 3T proton MR spectroscopy in multiple sclerosis. Am J Neuroradiol. 2010;31(1):180-4.

Martin AR, Aleksanderek I, Cohen-Adad J, Tarmohamed Z, Tetreault L, Smith N, et al. Translating state-of-the-art spinal cord MRI techniques to clinical use: A systematic review of clinical studies utilizing DTI, MT, MWF, MRS, and fMRI. NeuroImage Clinical. 2016;10:192-238.

Matute C, Alberdi E, Domercq M, Sanchez-Gomez MV, Perez-Samartin A, Rodriguez-Antiguedad A, et al. Excitotoxic damage to white matter. J Anat. 2007;210:693-702.

McBride RL, Feringa ER, Garver MK, Williams JK Jr. Prelabeled red nucleus and sensorimotor cortex neurons of the rat survive 10 and 20 weeks after spinal cord transection. J Neuropathol Exp Neurol 1989;48, 568–576.

McDonald JW, Belegu V. Demyelination and remyelination after spinal cord injury. J Neurotrauma, 2006;23(3-4):345-359.

McDonald JW, Sadowsky C. Spinal-cord injury. Lancet. 2002;359(9304):417-25.

McKeon RJ, Schreiber RC, Rudge JS, Silver J. Reduction of neurite outgrowth in a model of glial scarring following CNS injury is correlated with the expression of inhibitory molecules on reactive astrocytes. J Neurosci. 1991;11(11):3398-411.

Merkler D, Metz GA, Raineteau O, Dietz V, Schwab ME, Fouad K. Locomotor recovery in spinal cord-injured rats treated with an antibody neutralizing the myelin-associated neurite growth inhibitor Nogo-A. J Neurosci. 2001;21(10):3665-73.

Metz GA, Curt A, van de Meent H, Klusman I, Schwab ME, Dietz V. Validation of the weight-drop contusion model in rats: a comparative study of human spinal cord injury. J Neurotrauma. 2000;17:1-17.

Min YS, Park JW, Jin SU, Jang KE, Nam HU, Lee YS, et al. Alteration of Resting-State Brain Sensorimotor Connectivity following Spinal Cord Injury: A Resting-State Functional Magnetic Resonance Imaging Study. J Neurotrauma. 2015;32(18):1422-7.

Miyanji F, Furlan JC, Aarabi B, Arnold PM, Fehlings MG. Acute cervical traumatic spinal cord injury: MR imaging findings correlated with neurologic outcome--prospective study with 100 consecutive patients. Radiology. 2007;243(3):820-7.

Moffett JR, Arun P, Ariyannur PS, Garbern JY, Jacobowitz DM, Namboodiri AM. Extensive aspartoacylase expression in the rat central nervous system. Glia. 2011;59(10):1414-34.

Mohammadi S, Moller HE, Kugel H, Muller DK, Deppe M. Correcting eddy current and motion effects by affine whole-brain registrations: evaluation of three-dimensional distortions and comparison with slicewise correction. Magn Reson Med. 2010;64:1047-56.

Mohammadi S, Nagy Z, Hutton C, Josephs O, Weiskopf N. Correction of vibration artifacts in DTI using phase-encoding reversal (COVIPER). Magn Reson Med. 2012;68(3):882-9.

Mohammadi S, Hutton C, Nagy Z, Josephs O, Weiskopf N. Retrospective correction of physiological noise in DTI using an extended tensor model and peripheral measurements. Magn Reson Med. 2013a; 70: 358-69.

Mohammadi S, Freund P, Feiweier T, Curt A, Weiskopf N. The impact of post-processing on spinal cord diffusion tensor imaging. Neuroimage. 2013b;70:377-85.

Mohammadi S, Tabelow K, Ruthotto L, Feiweier T, Polzehl J, Weiskopf N. High-resolution diffusion kurtosis imaging at 3T enabled by advanced post-processing. Front Neurosci. 2014;8:427.

Morelli JN, Runge VM, Feiweier T, Kirsch JE, Williams KW, Attenberger UI. Evaluation of a modified Stejskal-Tanner diffusion encoding scheme, permitting a marked reduction in TE, in diffusion-weighted imaging of stroke patients at 3 T. Invest Radiol. 2010;45:29-35.

Mottershead JP, Schmierer K, Clemence M, Thornton JS, Scaravilli F, Barker GJ, et al. High field MRI correlates of myelin content and axonal density in multiple sclerosis. J Neurol. 2003;250(11):1293-301.

Moxon KA, Oliviero A, Aguilar J, Foffani G. Cortical reorganization after spinal cord injury: always for good?. Neuroscience. 2014;283:78-94.

Nambu A. Somatotopic organization of the primate Basal Ganglia. Front Neuroanat. 2011;5:26.

Nagamoto-Combs K, McNeal DW, Morecraft RJ, Combs CK. Prolonged microgliosis in the rhesus monkey central nervous system after traumatic brain injury. J Neurotrauma, 2007;24(11):1719-1742.

Nagoshi N, Fehlings MG. Investigational drugs for the treatment of spinal cord injury: review of preclinical studies and evaluation of clinical trials from phase I to II. Expert Opin Investig Drugs. 2015;24:1-14.

Nardone R, Holler Y, Brigo F, Seidl M, Christova M, Bergmann J, et al. Functional brain reorganization after spinal cord injury: systematic review of animal and human studies. Brain Res. 2013;1504:58-73.

Nardone R, Höller Y, Brigo F, Orioli A, Tezzon F, Schwenker K, et al. Descending motor pathways and cortical physiology after spinal cord injury assessed by transcranial magnetic stimulation: a systematic review. Brain Res. 2015;1619:139-54.

Nathan PW, Smith MC, Marion C. The rubrospinal and central tegmental tracts in man. Brain: a J Neurol. 1982;105(2):223-269.

Nathan PW, Smith MC, Marion C, Deacon P. The corticospinal tracts in man: course and location of fibres at different segmental levels. Brain. 1990;113(2):303-324.

Nesic O, Xu GY, McAdoo D, Westlund High K, Hulsebosch C, Perez-Polo R. IL-1 receptor antagonist prevents apoptosis and caspase-3 activation after spinal cord injury. J Neurotrauma. 2001;18(9):947-56.

Nielson JL, Sears-Kraxberger I, Strong MK,Wong JK, Willenberg R, Steward O. Unexpected survival of neurons of origin of the pyramidal tract after spinal cord injury. J Neurosci. 2010;30:11516–11528.

Nielson JL, Haefeli J, Salegio EA, Liu AW, Guandique CF, Stuck ED, et al. Leveraging biomedical informatics for assessing plasticity and repair in primate spinal cord injury. Brain Res. 2015;1619:124-38.

Nishimura Y, Onoe H, Morichika Y, Perfiliev S, Tsukada H, Isa T. Time-dependent central compensatory mechanisms of finger dexterity after spinal cord injury. Science. 2007;318(5853):1150-5.

Nishimura Y, Onoe H, Onoe K, Morichika Y, Tsukada H, Isa T. Neural substrates for the motivational regulation of motor recovery after spinal-cord injury. PLoS One. 2011;6(9):e24854.

Noble LJ, Wrathall JR. Spinal cord contusion in the rat: morphometric analyses of alterations in the spinal cord. Exp. Neurol. 1985;88:135-49.

Nordengen K, Heuser C, Rinholm JE, Matalon R, Gundersen V. Localisation of N-acetylaspartate in oligodendrocytes/myelin. Brain Struct Funct. 2015;220(2):899-917.

Norenberg MD, Smith J, Marcillo A. The pathology of human spinal cord injury: defining the problems. J Neurotrauma. 2004;21(4):429-40.

Oudega M, Perez MA. Corticospinal reorganization after spinal cord injury. J Physiol. 2012;590(16):3647-63.

Orlovsky GN. Activity of vestibulospinal neurons during locomotion. Brain research. 1972;46:85-98.

Öz G, Alger JR, Barker PB, Bartha R, Bizzi A, Boesch C, et al. Clinical proton MR spectroscopy in central nervous system disorders. Radiology. 2014;270(3):658-79.

Paling D, Solanky BS, Riemer F, Tozer DJ, Wheeler-Kingshott CA, Kapoor R, et al. Sodium accumulation is associated with disability and a progressive course in multiple sclerosis. Brain. 2013;136(7):2305-17.

Pascoal-Faria P, Yalcin N, Fregni F. Neural markers of neuropathic pain associated with maladaptive plasticity in spinal cord injury. Pain Practice. 2015;15(4):371-7.

Pascual-Leone A, Amedi A, Fregni F, Merabet LB. The plastic human brain cortex. Annu Rev Neurosci. 2005;28:377–401.

Pattany PM, Yezierski RP, Widerstrom-Noga EG, Bowen BC, Martinez-Arizala A, Garcia BR, et al. Proton magnetic resonance spectroscopy of the thalamus in patients with chronic neuropathic pain after spinal cord injury. Am J Neuroradiol. 2002;23(6):901-5.

Pearse DD, Lo TP, Jr., Cho KS, Lynch MP, Garg MS, Marcillo AE, et al. Histopathological and behavioral characterization of a novel cervical spinal cord displacement contusion injury in the rat. J Neurotrauma. 2005;22:680-702.

Peck RW. Driving earlier clinical attrition: if you want to find the needle, burn down the haystack. Considerations for biomarker development. Drug Discov Today. 2007;12(7):289-94.

Petersen JA, Wilm BJ, von Meyenburg J, Schubert M, Seifert B, Najafi Y, et al. Chronic cervical spinal cord injury: DTI correlates with clinical and electrophysiological measures. J Neurotrauma. 2012;29:1556-66.

Petersen SE, Robinson DL, Morris JD. Contributions of the pulvinar to visual spatial attention. Neuropsychologia. 1987;25(1A):97-105.

Pinheiro JC, Bates DM. Linear Mixed Effects Models. Mixed Effect Models in S and S-Plus. Springer Verlag: New York, 2000.

Pipitone J, Park MT, Winterburn J, Lett TA, Lerch JP, Pruessner JC, et al. Multi-atlas segmentation of the whole hippocampus and subfields using multiple automatically generated templates. Neuroimage. 2014;101:494-512.

Plaud B, Debaene B, Donati F, Marty J. Residual paralysis after emergence from anesthesia. Anesthesiology. 2010;112(4):1013-22.

Posse S, Aue WP. Susceptibility artifacts in spin-echo and gradient-echo imaging. J Magnc Res. 1990;88(3):473-92.

Provencher SW. Estimation of metabolite concentrations from localized in vivo proton NMR spectra. Magn Reson Med. 1993;30(6):672-9.

Qian J, Herrera JJ, Narayana PA. Neuronal and axonal degeneration in experimental spinal cord injury: in vivo proton magnetic resonance spectroscopy and histology. J Neurotrauma. 2010;27(3):599-610.

Qiu YQ, Hua XY, Zuo CT, Li T, Zheng MX, Shen YD, et al. Deactivation of distant pain-related regions induced by 20-day rTMS: a case study of one-week pain relief for long-term intractable deafferentation pain. Pain Physician. 2014;17(1):E99-105.

R Core Team. R: A Language and Environment for Statistical Computing. Vienna, Austria: R Foundation for Statistical Computing; 2016.

Raineteau O, Schwab ME. Plasticity of motor systems after incomplete spinal cord injury. Nat. Rev. Neurosci. 2001;2(4):263-73.

Raisman, G. Neuronal plasticity in the septal nuclei of the adult rat. Brain research. 1969;14(1):25-48.

Rao JS, Manxiu M, Zhao C, Xi Y, Yang ZY, Zuxiang L, et al. Atrophy and primary somatosensory cortical reorganization after unilateral thoracic spinal cord injury: a longitudinal functional magnetic resonance imaging study. Biomed Res Int. 2013;2013:753061.

Rao JS, Ma M, Zhao C, Zhang AF, Yang ZY, Liu Z, et al. Fractional amplitude of low-frequency fluctuation changes in monkeys with spinal cord injury: a resting-state fMRI study. Magn Reson Imaging. 2014;32(5):482-6.

Raunig DL, McShane LM, Pennello G, Gatsonis C, Carson PL, Voyvodic JT, et al. Quantitative imaging biomarkers: a review of statistical methods for technical performance assessment. Stat. Methods Med. Res. 2015;24(1):27-67.

Raznahan A, Shaw PW, Lerch JP, Clasen LS, Greenstein D, Berman R, et al. Longitudinal four-dimensional mapping of subcortical anatomy in human development. Proc. Natl. Acad. Sci. U.S.A. 2014;111(4):1592-7.

Rebeles F, Fink J, Anzai Y, Maravilla KR. Blood-brain barrier imaging and therapeutic potentials. Top Magn Reson Imaging. 2006;17(2):107-16.

Rexed B. The cytoarchitectonic organization of the spinal cord in the cat. J Comp Neurol. 1952;96(3):415-95.

Rexed B. A cytoarchitectonic atlas of the spinal coed in the cat. J Comp Neurol. 1954;100(2):297-379.

Richards TL. Proton MR spectroscopy in multiple sclerosis: value in establishing diagnosis, monitoring progression, and evaluating therapy. Am J Roentgenol. 1991;157(5):1073-8.

Roitbak T, Syková E. Diffusion barriers evoked in the rat cortex by reactive astrogliosis. Glia. 1999;28(1):40-8.

Rolls A, Shechter R, Schwartz M. The bright side of the glial scar in CNS repair. Nat. Rev. Neurosci. 2009;10(3):235.

Rooney WD, Johnson G, Li X, Cohen ER, Kim SG, Ugurbil K, et al. Magnetic field and tissue dependencies of human brain longitudinal 1H2O relaxation in vivo. Magn Reson Med. 2007;57(2):308-18.

Rosenzweig ES, Courtine G, Jindrich DL, Brock JH, Ferguson AR, Strand SC, et al. Extensive spontaneous plasticity of corticospinal projections after primate spinal cord injury. Nat Neurosci. 2010;13(12):1505-10.

Rust R, Kaiser J. Insights into the Dual Role of Inflammation after Spinal Cord Injury. J Neurosci. 2017;37(18):4658-60.

Sawada M, Kato K, Kunieda T, Mikuni N, Miyamoto S, Onoe H, et al. Function of the nucleus accumbens in motor control during recovery after spinal cord injury. Science. 2015;350(6256):98-101.

Schmid AC, Chien JH, Greenspan JD, Garonzik I, Weiss N, Ohara S, et al. Neuronal responses to tactile stimuli and tactile sensations evoked by microstimulation in the human thalamic principal somatic sensory nucleus (ventral caudal). J Neurophysiol. 2016;115(5):2421-33.

Schmid MR, Pfirrmann CW, Koch P, Zanetti M, Kuehn B, Hodler J. Imaging of patellar cartilage with a 2D multiple-echo data image combination sequence. Am J Roentgenol. 2005;184:1744-8.

Schmierer K, Scaravilli F, Altmann DR, Barker GJ, Miller DH. Magnetization transfer ratio and myelin in postmortem multiple sclerosis brain. Ann Neurol. 2004;56(3):407-15.

Schmierer K, Wheeler-Kingshott CA, Tozer DJ, Boulby PA, Parkes HG, Yousry TA, et al. Quantitative magnetic resonance of postmortem multiple sclerosis brain before and after fixation. Magn Reson Med. 2008;59(2):268-77.

Scholtes F, Adriaensens P, Storme L, Buss A, Kakulas AB, Gelan J, et al. Correlation of postmortem 9.4 tesla magnetic resonance imaging and immunohistopathology of the human thoracic spinal cord 7 months after traumatic cervical spine injury. Neurosurgery. 2006;59(3):671-678.

Schulte RF, Henning A, Tsao J, Boesiger P, Pruessmann KP. Design of broadband RF pulses with polynomial-phase response. J Magn Reson. 2007;186(2):167-75.

Schwab ME, Bartholdi D. Degeneration and regeneration of axons in the lesioned spinal cord. Physiol Rev. 1996;76:319-370.

Schwab ME. Repairing the injured spinal cord. Science. 2002;295(5557):1029-31.

Schwab ME. Nogo and axon regeneration. Curr Opin Neurobiol. 2004;14(1):118-24.

Schwab JM, Zhang Y, Kopp MA, Brommer B, Popovich PG. The paradox of chronic neuroinflammation, systemic immune suppression, autoimmunity after traumatic chronic spinal cord injury. Exp. Neurol. 2014;258:121-9.

Schwerdtfeger K, Mautes AE, Bernreuther C, Cui Y, Manville J, Dihne M, et al. Stress-resistant neural stem cells positively influence regional energy metabolism after spinal cord injury in mice. J Mol Neurosci. 2012;46(2):401-9.

Sekhon LH, Fehlings MG. Epidemiology, demographics, and pathophysiology of acute spinal cord injury. Spine. 2001;26(24):2-12.

Shimada K, Tokioka T. Sequential MR studies of cervical cord injury: correlation with neurological damage and clinical outcome. Spinal Cord. 1999;37:410-5.

Siddall PJ, Taylor DA, McClelland JM, Rutkowski SB, Cousins MJ. Pain report and the relationship of pain to physical factors in the first 6 months following spinal cord injury. Pain. 1999;81(1-2): 187-197.

Siddall PJ, Loeser JD. Pain following spinal cord injury. Spinal Cord. 2001;39(2):63-73.

Siddall PJ, McClelland JM, Rutkowski SB, Cousins MJ. A longitudinal study of the prevalence and characteristics of pain in the first 5 years following spinal cord injury. Pain. 2003;103(3):249-57.

Silver J, Miller JH. Regeneration beyond the glial scar. Nat Rev Neurosci. 2004;5(2):146-56.

Solanky BS, De Vita E. Chapter 5.1 - Single Voxel MR Spectroscopy in the Spinal Cord: Technical Challenges and Clinical Applications A2 - Cohen-Adad, Julien. In: Wheeler-Kingshott CAM, editor. Quantitative MRI of the Spinal Cord. San Diego: Academic Press. 2014;267-90.

Solanky BS, Riemer F, Golay X, Wheeler-Kingshott CA. Sodium quantification in the spinal cord at 3T. Magn Reson Med. 2013;69(5):1201-8.

Sprenger C, Eippert F, Finsterbusch J, Bingel U, Rose M, Buchel C. Attention modulates spinal cord responses to pain. Curr Biol. 2012;22(11):1019-22.

Stanisz GJ, Odrobina EE, Pun J, Escaravage M, Graham SJ, Bronskill MJ, et al. T1, T2 relaxation and magnetization transfer in tissue at 3T. Magn Reson Med. 2005;54(3):507-12.

Starkey ML, Schwab ME. Anti-Nogo-A and training: can one plus one equal three? Exp. Neurol. 2012;235(1):53-61.

Strange K, Emma F, Paredes A, Morrison R. Osmoregulatory changes in myo-inositol content and Na+/myo-inositol cotransport in rat cortical astrocytes. Glia. 1994;12(1):35-43.

Strick PL. Activity of ventrolateral thalamic neurons during arm movement. J Neurophysiol. 1976;39(5):1032-44.

Strimbu K, Tavel JA. What are biomarkers?. Curr Opin **HIV AIDS.** 2010;5(6):463.

Stroman PW, Wheeler-Kingshott C, Bacon M, Schwab JM, Bosma R, Brooks J, et al. The current state-of-the-art of spinal cord imaging: methods. Neuroimage. 2014;84:1070-81.

Stüber C, Morawski M, Schäfer A, Labadie C, Wähnert M, Leuze C, et al. Myelin and iron concentration in the human brain: A quantitative study of MRI contrast. Neuroimage. 2014;93:95–106.

Sundberg LM, Herrera JJ, Narayana PA. In vivo longitudinal MRI and behavioral studies in experimental spinal cord injury. J Neurotrauma. 2010;27(10):1753-67.

Swanson LW. Brain architecture: understanding the basic plan. Oxford University Press; 2012.

Sydekum E, Ghosh A, Gullo M, Baltes C, Schwab M, Rudin M. Rapid functional reorganization of the forelimb cortical representation after thoracic spinal cord injury in adult rats. Neuroimage. 2014;87:72-9.

Tanadini LG, Steeves JD, Hothorn T, Abel R, Maier D, Schubert M, et al. Identifying Homogeneous Subgroups in Neurological Disorders: Unbiased Recursive Partitioning in Cervical Complete Spinal Cord Injury. Neurorehabil Neural Repair. 2014;28(6):507-15.

Tang XQ, Wang Y, Huang ZH, Han JS, Wan Y. Adenovirus-mediated delivery of GDNF ameliorates corticospinal neuronal atrophy and motor function deficits in rats with spinal cord injury. Neuroreport. 2004;15:425–429.

Tardif CL, Collins DL, Pike GB. Sensitivity of voxel-based morphometry analysis to choice of imaging protocol at 3 T. Neuroimage. 2009;44(3):827-38.

Teyler TJ, DiScenna P. Long-term potentiation. Annu Rev Neurosci. 1987;10(1):131-61.

Tokuno H, Inase M, Nambu A, Akazawa T, Miyachi S, Takada M. Corticostriatal projections from distal and proximal forelimb representations of the monkey primary motor cortex. Neurosci. Lett. 1999;269(1):33-6.

Tracey DJ. Ascending and descending pathways in the spinal cord. Elsevier Academic Press. 2004.

Truckenmiller ME, Namboodiri MA, Brownstein MJ, Neale JH. N-Acetylation of L-aspartate in the nervous system: differential distribution of a specific enzyme. J Neurochem. 1985;45(5):1658-62.

Tsintou M, Dalamagkas K, Seifalian AM. Advances in regenerative therapies for spinal cord injury: a biomaterials approach. Neural Regen. Res. 2015;10(5):726.

Turati L, Moscatelli M, Mastropietro A, Dowell NG, Zucca I, Erbetta A, et al. In vivo quantitative magnetization transfer imaging correlates with histology during de-and remyelination in cuprizone-treated mice. NMR Biomed. 2015;28(3):327-37.

Vavrek R, Girgis J, Tetzlaff W, Hiebert GW, Fouad K. BDNF promotes connections of corticospinal neurons onto spared descending interneurons in spinal cord injured rats. Brain. 2006;129(6):1534-45.

Velstra IM, Bolliger M, Tanadini LG, Baumberger M, Abel R, Rietman JS, et al. Prediction and stratification of upper limb function and self-care in acute cervical spinal cord injury with the graded redefined assessment of strength, sensibility, and prehension (GRASSP). Neurorehabil Neural Repair. 2014;28(7):632-42.

Villiger M, Grabher P, Hepp-Reymond M, Kiper D, Curt A, Bolliger M, et al. Relationship between structural brainstem and brain plasticity and lower-limb training: a longitudinal pilot study. Front Hum Neurosci. 2015;9:254.

Vitek JL, Ashe J, DeLong MR, Alexander GE. Physiologic properties and somatotopic organization of the primate motor thalamus. J Neurophysiol. 1994;71(4):1498-513.

Vuckovic A, Hasan MA, Fraser M, Conway BA, Nasseroleslami B, Allan DB. Dynamic oscillatory signatures of central neuropathic pain in spinal cord injury. J Pain. 2014;15(6):645-55.

Wang D, Bodley R, Sett P, Gardner B, Frankel H. A clinical magnetic resonance imaging study of the traumatised spinal cord more than 20 years following injury. Paraplegia. 1996;34:65-81.

Wang J, Matalon R, Bhatia G, Wu G, Li H, Liu T, et al. Bimodal occurrence of aspartoacylase in myelin and cytosol of brain. J Neurochem. 2007;101(2):448-57.

Wang F, Qi HX, Zu Z, Mishra A, Tang C, Gore JC, Chen LM. Multiparametric MRI reveals dynamic changes in molecular signatures of injured spinal cord in monkeys. Magn Reson Med. 2015;74(4):1125-37.

Wang F, Li K, Mishra A, Gochberg D, Min Chen L, Gore JC. Longitudinal assessment of spinal cord injuries in nonhuman primates with quantitative magnetization transfer. Magn Reson Med. 2016;75(4):1685-96.

Wang M, Dai Y, Han Y, Haacke EM, Dai J, Shi D. Susceptibility weighted imaging in detecting hemorrhage in acute cervical spinal cord injury. Magn Reson Imaging. 2011;29(3):365-73.

Wang XC, Du XX, Tian Q, Wang JZ. Correlation between choline signal intensity and acetylcholine level in different brain regions of rat. Neurochem Res. 2008;33(5):814-9.

Wannier T, Schmidlin E, Bloch J, Rouiller EM. A unilateral section of the corticospinal tract at cervical level in primate does not lead to measurable cell loss in motor cortex. J Neurotrauma. 2005;22(6):703-17.

Ward RE, Huang W, Kostusiak M, Pallier PN, Michael-Titus AT, Priestley JV. A characterization of white matter pathology following spinal cord compression injury in the rat. Neurosci. 2014;260:227-39.

Weidner N, Ner A, Salimi N, Tuszynski MH. Spontaneous corticospinal axonal plasticity and functional recovery after adult central nervous system injury. Proc. Natl. Acad. Sci. U.S.A. 2001;98(6):3513-8.

Weiskopf N, Lutti A, Helms G, Novak M, Ashburner J, Hutton C. Unified segmentation based correction of R1 brain maps for RF transmit field inhomogeneities (UNICORT). Neuroimage. 2011;54(3):2116-24.

Weiskopf N, Suckling J, Williams G, Correia MM, Inkster B, Tait R, et al. Quantitative multi-parameter mapping of R1, PD(*), MT, and R2(*) at 3T: a multi-center validation. Front Neurosci. 2013;7:95.

Wickham H. ggplot2: Elegant Graphics for Data Analysis: Springer-Verlag New York; 2009.

Widerström-Noga E, Pattany PM, Cruz-Almeida Y, Felix ER, Perez S, Cardenas DD, Martinez-Arizala A. Metabolite concentrations in the anterior cingulate cortex predict high neuropathic pain impact after spinal cord injury. Pain. 2013;154(2):204-12.

Widerström-Noga E, Cruz-Almeida Y, Felix ER, Pattany PM. Somatosensory phenotype is associated with thalamic metabolites and pain intensity after spinal cord injury. Pain. 2015;156(1):166.

Wilm BJ, Svensson J, Henning A, Pruessmann KP, Boesiger P, Kollias SS. Reduced field-of-view MRI using outer volume suppression for spinal cord diffusion imaging. Magn Reson Med. 2007;57(3):625-30.

Wilson JR, Arnold PM, Singh A, Kalsi-Ryan S, Fehlings MG. Clinical prediction model for acute inpatient complications after traumatic cervical spinal cord injury: a subanalysis from the Surgical Timing in Acute Spinal Cord Injury Study. J Neurosurg. 2012;17(Suppl1):46-51.

Worker A, Blain C, Jarosz J, Chaudhuri KR, Barker GJ, Williams SC, et al. Cortical thickness, surface area and volume measures in Parkinson's disease, multiple system atrophy and progressive supranuclear palsy. PLoS One. 2014;9(12):e114167.

Wrigley PJ, Gustin SM, Macey PM, Nash PG, Gandevia SC, Macefield VG, et al. Anatomical changes in human motor cortex and motor pathways following complete thoracic spinal cord injury. Cereb Cortex. 2008;19(1):224-32.

Wrigley PJ, Gustin SM, Macey PM, Nash PG, Gandevia SC, Macefield VG, et al. Anatomical changes in human motor cortex and motor pathways following complete thoracic spinal cord injury. Cereb Cortex. 2009a;19(1):224-32.

Wrigley PJ, Press SR, Gustin SM, Macefield VG, Gandevia SC, Cousins MJ, et al. Neuropathic pain and primary somatosensory cortex reorganization following spinal cord injury. Pain. 2009b;141(1-2):52-9.

Wu J, Zhao Z, Sabirzhanov B, Stoica BA, Kumar A, Luo T, et al. Spinal cord injury causes brain inflammation associated with cognitive and affective changes: role of cell cycle pathways. J Neurosci. 2014;34(33):10989-11006.

Wu J, Zhao Z, Kumar A, Lipinski MM, Loane DJ, Stoica BA, et al. Endoplasmic reticulum stress and disrupted neurogenesis in the brain are associated with cognitive impairment and depressive-like behavior after spinal cord injury. J Neurotrauma, 2016;33(21):1919-1935.

Wu X, Liu J, Tanadini LG, Lammertse DP, Blight AR, Kramer JL, et al. Challenges for defining minimal clinically important difference (MCID) after spinal cord injury. Spinal Cord. 2015;53(2):84-91.

Wyndaele M, Wyndaele JJ. Incidence, prevalence and epidemiology of spinal cord injury: what learns a worldwide literature survey? Spinal Cord. 2006;44(9):523-9.

Xanthos DN, Sandkuehler J. Neurogenic neuroinflammation: inflammatory CNS reactions in response to neuronal activity. Nat Rev Neurosci. 2014;15(1):43-53.

y Cajal SR. Histology of the nervous system of man and vertebrates. Oxford University Press, USA; 1995.

Yague JG, Foffani G, Aguilar J. Cortical hyperexcitability in response to preserved spinothalamic inputs immediately after spinal cord hemisection. Exp Neurol. 2011;227(2):252-63.

Yague JG, Humanes-Valera D, Aguilar J, Foffani G. Functional reorganization of the forepaw cortical representation immediately after thoracic spinal cord hemisection in rats. Exp Neurol. 2014;257:19-24.

Yang L, Blumbergs PC, Jones NR, Manavis J, Sarvestani GT, Ghabriel MN. Early expression and cellular localization of proinflammatory cytokines interleukin-1β, interleukin-6, and tumor necrosis factor-α in human traumatic spinal cord injury. Spine. 2004;29(9):966-971.

Yang PF, Qi HX, Kaas JH, Chen LM. Parallel functional reorganizations of somatosensory areas 3b and 1, and S2 following spinal cord injury in squirrel monkeys. J Neurosci. 2014;34(28):9351-63.

Yao B, Li TQ, Gelderen P, Shmueli K, de Zwart JA, Duyn JH. Susceptibility contrast in high field MRI of human brain as a function of tissue iron content. Neuroimage. 2009;44(4):1259-66.

Yoon EJ, Kim YK, Shin HI, Lee Y, Kim SE. Cortical and white matter alterations in patients with neuropathic pain after spinal cord injury. Brain research. 2013;1540:64-73.

Yu H, Li L, Liu R, Shu B, Chen H, Huang H, et al. Autophagy in long propriospinal neurons is activated after spinal cord injury in adult rats. Neurosci Lett. 2016;634:138-45.

Zaaimi B, Edgley SA, Soteropoulos DS, Baker SN. Changes in descending motor pathway connectivity after corticospinal tract lesion in macaque monkey. Brain. 2012;135(7):2277-89.

Zaitsev M, Maclaren J, Herbst M. Motion artifacts in MRI: a complex problem with many partial solutions. J Magn Reson Imaging. 2015;42(4):887-901.

Ziegler G, Grabher P, Thompson A, Altman D, Hupp M, Ashburner J, Friston K, Weiskopf N, Curt A, Freund P. Progressive neurodegeneration following spinal cord injury: implications for clinical trials. Neurology. 2018: In press.

Zoelch N, Hock A, Heinzer-Schweizer S, Avdievitch N, Henning A. Accurate determination of brain metabolite concentrations using ERETIC as external reference. NMR Biomed 2017.

9 List of Abbreviations

AD	axonal diffusivity
AH	abductor hallucis
AIS	American Spinal Injury Association Impairment Scale
ASIA	American Spinal Injury Association
CHEPs	contact heat evoked potentials
CNS	central nervous system
COV	coefficient of variation
Cr	creatine
CSGP	chondroitin sulphate proteoglycans
DCA	cross-sectional dorsal column area
DHA	cross-sectional dorsal horn area
DTI	diffusion tensor imaging
DWI	diffusion-weighted imaging
FA	fractional anisotropy
FLASH	fast low angle shot
FOV	field of view
GMA	cross-sectional grey matter area
GRASSP	Graded Redefined Assessment of Strength, Sensibility and Prehension
ISNCSCI	International Standards for Neurological Classification of Spinal Cord Injury
LEMS	lower extremity motor score
MEDIC	multiple echo data image combination
mI	myo-Inositol
MD	mean diffusivity
MEPs	motor evoked potentials
MPM	multi-parameter mapping
MRI	magnetic resonance imaging
MRS	magnetic resonance spectroscopy
MT	magnetization transfer
PD	proton density
RD	radial diffusivity
R1	longitudinal relaxation rate
R2*	effective transverse relaxation rate
ROI	region of interest

SCA	cross-sectional spinal cord area
SCI	spinal cord injury
SCIM	spinal cord independence measure
SEPs/ SSEPs	somatosensory evoked potentials
TA	tibialis anterior
TMS	transcranial magnetic stimulation
TNF-α	tumor necrosis factor alpha
tNAA	total N-acetyl-aspartate and N-acetyl-aspartate-glutamate
tCho	phosphocholine and glycerophosphocholine
UEMS	upper extremity motor score
VAN	ventral anterior nucleus
VHA	cross-sectional ventral horn area
VLN	ventral lateral nucleus
VOI	voxel of Interest
VPN	ventral posterior nucleus
WISCI	Walking Index for Spinal Cord Injury
WMA	cross-sectional white matter area

Curriculum vitae

EVELINE HUBER

I am a clinical scientist, with real-world research experience; passionate about bridging the gap between science and industry.

Date of birth: 23.07.1988
Citizen of: Zürich ZH

Rellikonstrasse 11
8124 Maur

Switzerland

+41 79 324 08 01
Mobile

+41 44 510 72 14
Office

eve.s.huber@gmail.com

Outdoor Activities:
Hiking, bivouacking, canoeing, camping.

Art & Creativity:
Poetry slam, painting, sewing.

EDUCATION

2014 – 2018 **PhD in Neuroscience**
University of Zurich, Balgrist University Hospital, Zurich
PhD Thesis: "Tracking structural changes in the spinal cord and brain as biomarkers for interventions after spinal cord injury"

2013 – 2014 **Master of Science in Human Biology**
University of Zurich
Master thesis: "Neuropathic pain and reorganization of dorsal column and spinothalamic tract input after spinal cord injury"
Grade Master thesis: 6
Final grade Master: 5.8

2008 – 2013 **Bachelor of Science in Biology**
University of Zurich

2008 – 2012 **Diploma in Medical Massage Therapy SPA**
Swiss Praevensana Akademie, Rapperswil
Diploma thesis: "Comorbidity of depression und low back pain"

2008 **Exchange semester for language studies**
St Giles College, San Francisco, USA

2007 **Matura (Certificate of university maturity)**
Kantonschule Glattal, Dübendorf

RESEARCH & WORK EXPERIENCE

2011 – present **Scientific Associate**
IT'IS Foundation, Zurich (40%, February-August 2014 100%, since then 10-20%)
Development of 3D whole-body, anatomical, MR-based models for computational life sciences. Responsible for developing a standardized QC management. Automated and manual segmentation of anatomical structures. Supervising collaborators in Greece and India. Conducting trainings in Delhi, India. International customer support tin English.

06/2013 – 09/2013 **Study Nurse Assistant**
Balgrist University Hospital (<20%)
Assisting in a Phase I/II clinical trial of human neural stem cells in chronic spinal cord injury. GCP trainings.

1

11/2009 – 03/2011
Assistant in Occupational Health Management
makora AG, Zurich (50-60%)
Assistance in the implementation of risk assessments into an online check-up. Operational planning of therapists. Compile statistics for employer presentations. Controlling debtors/ creditors. Setting up job advertisements, preselection of candidates, conducting/ evaluating recruitment test, creating contracts.

06/2010 – 11/2010
Internship at the Center for Interdisciplinary Sleep Research
Children's hospital, Zurich, (~50%)
Assistance in the study "Trait-like sleep spindle activity, information processing speed and their association to sleep-dependent performance improvement". Placement of EEG/EOG/EMG/ECG electrodes. Conductance of learning tasks/ wake EEG/ impedance measurements. Sleep surveillance. EEG data processing.

02/2009 – 10/2009
Research Internship in Anthropology
Anthropological Institute & Museum, University of Zurich, (~20%)
Assistance in the study "Prosocial behavior in human infants – the influence of study design and Theory of Mind". Conductance of the socio-cognitive und prosocial tasks in day cares around Zurich.

09/2007 – 12/2007
Backoffice Employee
Helsana Health Insurance, Stettbach, 100%
Processing of notices and proofs of insurance. Adapting training material.

07/2007 – 08/2007
Medical Internship on surgical and medical floor
Hospital Uster (100%)
Patient care. Insight into intensive care unit, surgeries, and daily clinical routines.

03/2006 – 08/2009
Part time employee in a Sport Centre
Sportzentrum Bluepoint, Uster
Responsible for processing of reservations, bar, cafeteria and catering services.

SKILLS

Languages
German
English
- Writing for Neuroscientists (2016)
- Grammar for Academic Purposes (2012)
- Academic Writing (2009)
- Cambridge Advanced Certificate C1 (2008)

French
- Good conversational skills (8 years of education)

Latin
- Elementary knowledge (2 years of education)

Analyzing skills
Statistics
- STATA, R Statistics, SPSS,

MRI analysis
- Matlab, Linux (Shape analysis, DTI)
- SPM, FSL, JIM (VBM, TBM, VBQ, DTI)
- CAD (SemcadX, Sim4Life, Amira, iSEG

EMG/ EEG analysis:
- BrainVision Analyzer
- Soleasy

Methodological skills
MRI safety course, GCP Module 1-3
Writing Ethics applications & amendments
Neurophysiology (SSEPs, CHEPs, TMS)
Immunohistochemistry, Western Blot, PCR

Editing and Graphics
MS Office
RedCap, MS Access
Adobe Illustrator
Endnote, Citavi

2

Publications

9.1 Published Articles

Huber E, David G, Thompson A, Weiskopf N, Mohammadi S, Freund P. Dorsal and ventral horn atrophy is associated with clinical outcome after spinal cord injury. Neurology. 2018: In press.

Huber E, Lachappelle P, Sutter R, Curt A, Freund P. Are tissue bridges predictive of outcome after cervical spinal cord injury? Annals of Neurology. 2017:81(5), 740-748.

Jutzeler CR, **Huber E**, Callaghan MF, Luechinger R, Curt A, Kramer JL, Freund P. Association of pain and CNS structural changes after spinal cord injury. Scientific reports. 2016: 6.

Huber E, Curt A, Freund P. Tracking trauma-induced structural and functional changes above the level of spinal cord injury. Current opinion in neurology.2015: 28(4), 365-372.

Jutzeler CR, Freund P, **Huber E**, Curt A, Kramer JL. Neuropathic pain and functional reorganization in the primary sensorimotor cortex after spinal cord injury. The Journal of Pain. 2015: 16(12), 1256-1267.

Gosselin MC, Neufeld E, Moser H, **Huber E**, Farcito S, Gerber L, Jedensjö M, Hilber I, Di Gennaro F, Lloyd B, Cherubini E, Szczerba D, Kainz W, Kuster N. Development of a new generation of high-resolution anatomical models for medical device evaluation: the Virtual Population 3.0. Physics in medicine and biology. 2014: 59(18), 5287.

9.2 Forthcoming Articles

Huber E, Wyss PO, Curt A, Kollias S, Freund P, Henning A (under review in elife). Spectroscopic Insights into Neuroinflammation and Clinical Impairment in Chronic Spinal Cord Injury

Huber E, Patel R, Chakravarty M, Freund P (soon to be submitted). Somatotopic reorganization of the basal ganglia and their relationship to outcome after spinal cord injury: A longitudinal study.

Gergely D, **Huber E**, Curt A, Weiskopf N, Mohammadi S, Freund P (soon to be submitted). Assessing neurodegeneration after spinal cord injury across the spinal axis using high-resolution MRI.

Vallotton K, **Huber E**, Freund P, Hupp M, Curt A (soon to be submitted). Functionality of sensorimotor pathways depends on the size and location of tissue bridges after spinal cord injury.

Huber E, Chakravarty M, Patel R, Grabher P, Killeen T, Bolliger M, Draganski B, Weiskopf N, Thompson A, Curt A, Freund P (in progress). Revealing training-induced basal ganglia changes in healthy subjects and those with spinal cord injury.

9.3 Conference Proceedings

Huber E, David G, Thompson A, Weiskopf N, Mohammadi S, Freund P. Neurodegeneration above the level of injury predicts tract-specific impairment after spinal cord injury. ZNZ Symposium 2017, Zurich, Switzerland.

Vallotton K, **Huber E**, Freund P, Hupp M, Curt A. Functionality of sensorimotor pathways depends on the size and location of tissue bridges after spinal cord injury. ZNZ Symposium 2017, Zurich, Switzerland.

Huber E, David G, Weiskopf N, Mohammadi S, Freund P. Impact of lesion extent on spinal cord white and grey matter degeneration and disability after SCI. OHBM 2017, Vancouver, Canada.

Wyss P, **Huber E**, Freund P, Beck D, Curt A, Kollias S, Henning A. Cervical spinal cord proton spectroscopy and impairment in spinal cord injury at 3T. OHBM 2017, Vancouver, Canada.

Huber E, David G, Weiskopf N, Mohammadi S, Freund P. Voxel-based analysis of grey and white matter degeneration above the level of injury in cervical spinal cord injury. ISMRM 2017, Honolulu.

Huber E, Lachappelle P Suter R, Curt A, Freund P. Neuroimaging biomarkers of tissue bridges and lesion area are potential outcome predictors after acute spinal cord injury. Swiss Society for Neuroscience Annual Meeting, 2017, Basel, Switzerland.

Huber E, Lachappelle P Suter R, Curt A, Freund P. Spared tissue bridges: A potential biomarker for outcome prediction after acute traumatic cervical spinal cord injury? ZNZ Symposium 2016, Zurich, Switzerland.

Gergely D, **Huber E**, Curt A, Weiskopf N, Mohammadi S, Freund P. Assessing neurodegeneration across the spinal axis using high-resolution MRI. ZNZ Symposium 2016, Zurich, Switzerland.

Baumgartner C, Farcito S, **Huber E**, Neufeld E, Lloyd B, Kuser N. The IT'IS Tissue Properties Database for Computational Modelling. Latsys Symposium 2016, Zurich, Switzerland.

Gergely D, **Huber E**, Curt A, Weiskopf N, Mohammadi S, Freund P. Assessing neurodegeneration across the spinal axis using high-resolution MRI. ISMRM 2016, Singapore.

Huber E, Lachappelle P Suter R, Curt A, Freund P. Spared tissue bridges are predictive of outcome after acute traumatic cervical spinal cord injury. ISCoS Annual Scientific Meeting 2016, Vienna, Austria.

Huber E, Patel R, Curt A, Chakravarty MM, Freund P. Extrapyramidal changes after acute spinal cord injury. Organization for Human Brain Mapping Conference 2016, Geneva, Switzerland.

Huber E, Grabher P, Killeen T, Trachsler A, Kubin T, Lachappelle P, Bolliger M, Draganski B, Weiskopf N, Thompson A, Curt A, Freund P. Tracking structural MRI changes in the spinal cord and brain as surrogate markers for interventions in SCI rehabilitation. ZNZ Symposium 2015, Zurich, Switzerland.

Huber E , Grabher P, Killeen T, Trachsler A, Kubin T, Bolliger M, Draganski B, Weiskopf N, Thompson A, Curt A, Freund. Plasticity of grey and white matter in response to motor skill training in healthy individuals and those with spinal cord injury. Swiss Society for Neuroscience Annual Meeting, 2015, Fribourg, Switzerland.

Huber E, Gerber L, Moser H, Di Gennaro F, Hilber I, Neufeld E, Gosselin MC, Kuster N. The making of the Virtual Population 3.0: Image Segmentation and Surface Reconstruction. 4th International Workshop on Computational Phantoms for Radiation Protection, Imaging and Radiotherapy, 2013, Zurich, Switzerland.

Acknowledgments

Along the way of conducting this thesis, my motivation has resulted from the many dedicated professional individuals and organizators, and I wish to thank the many people who have seen me through this journey.

First and foremost, I thank my supervisor Patrick Freund for his trust, assistance and academic support. Your selfless time and intellectual curiosity inspired me and your maddening attention to detail drove me to learn how to ask the right questions and write manuscripts with clear messages. While your approach to make me think for myself was sometimes challenging, I am grateful for all the lessons learned and thank you for guiding me through this process.

I also thank all my committee members for their support. In particular, I am grateful to Armin Curt for several discussions and critical questions raised that helped me to embed my work in a larger context. Your strong focus on improving patient's life motivated me to keep on going. I also thank Dominik Bach, Martin Schwab, and Bogdan Draganski for their conceptual and administrative help and inputs to my projects.

Next, I am indebted to my collaborators in Montreal from McGill University, in particular Mallar Chakravarty and Raihaan Patel, for their strong technical support. Thank you Mallar for having me over in Montreal, integrating me in your lab and the many social events I could attend. Thank you Rai for always patiently explaining all the different image processing steps and helping me with technical issues. I also thank the whole COBRA team for their creative input, the good times and food (no, not Poutine!) and for instantly having made me feel at home.

My warmest thanks also go to my collaborators from the ETH/ USZ in Zurich, Anke Henning and Patrik Wyss. I absolutely enjoyed our collaboration, and I am in particular thankful to Patrik for his technical assistance and providing me access to his knowledge in MRS. I thank Anke for her valuable input to the study design and our manuscript.

In addition, I also thank my collaborators in Germany, Niklaus Weiskopf from the Max Planck Institute, and Siawoosh Mohammadi, from the Medical Center Hamburg-Eppendorf, for their help in setting up the MR sequences for our studies, and their intellectual input.

Last, I also thank Alan Thompson from the University College London, United Kingdom, for his editorial and linguistic help.

The paralab was a pleasure to work in due to the friendly and supportive environment provided, as well as the great infrastructure within the Campus. I thank all members of the paralab who challenged me, for the numerous discussions and inputs, for analytic eyes and open ears. Many of

you become close friends. In particular, I thank the Neuroimaging Group, Gergely David, Maryam Seif and Michela Azzarito for supplementing my biological background with technical advice, and helping me with running different pipelines. I thank my interns and Master students, that I supervised or co-supervised, for the invaluable support and effort- Aaron Trachler, Tim Kubin, Patrice Lachappelle, Céline Steger, Desiree Beck, Gaia Bonetti, and Kevin Vallonton. I thank Sophie Schneider, Felix Thomas, Christian Meyer, Stephanie van der Lely, Vinc Huyhn, Martina Stefanovic, Lazlo Demko, Fabian Just, Gergely David, Miriam Koschorke, Maryam Seif and Kevin Vallonton for their shared time, Bohemia evenings, workouts, hiking trips, shared apartments, stand-up paddle boarding at 4am to catch the first sunlight at the lake, skiing weekends, Friday Schnaps, brunch and painted faces.

Special thanks go to all my study volunteers and all the patients for participating in my studies, especially those who endured the time-consuming Plastidance study. Thanks to all the patients who help me better understanding the influence of an SCI on their life and environment, the daily challenges they have, and for sharing their wishes and expectations on future research. Many interactions deeply touched me and I was sincerely impressed by the many strong people I met who managed to live a fulfilling life despite all the additional struggles.

This whole thesis would not have been possible without financial support. In particular, I thank Wings for Life, Austria (WFL-CH-007/14) and InVivo Therapeutics (Cambridge, Massachusetts, USA) for providing salary and support for the conduction of studies. I also thank the 'The Oxford McGill ZNZ Partnership in the Neurosciences' which provided a funding for mobility and training in Montreal, Canada. Last, I thank SciNet for usage of Canada's largest supercomputer platform, which is funded by the Canada Foundation for Innovation, NSERC, the Government of Ontario, Fed Dev Ontario, and the University of Toronto.

Finally, numerous others have quietly championed me from afar – my heartfelt thanks go to my family, my friends (in particular Monika Egli, Jana Frei, Peter Gagstätter), dogs, and my love Tian. You helped me to stay on the ground and create a mind of peacefulness and happiness. Thank you.